UNIVERSITY OF CALIFORNIA
RIVERSIDE

Molecular and Mechanistic Study of *Phytophthora* RxLR Effector PSR2 in Arabidopsis

A Dissertation submitted in partial satisfaction
of the requirements for the degree of

Doctor of Philosophy

in

Microbiology

by

Tung Kuan

September 2018

Dissertation Committee:
Dr. Wenbo Ma, Chairperson
Dr. Howard S. Judelson
Dr. Katherine A. Borkovich

The Dissertation of Tung Kuan is approved:

Committee Chairperson

University of California, Riverside

ACKNOWLEDGEMENTS

I would like to thank people from the lab who made contributions to this thesis research. Dr. Wenbo Ma directed and supervised the research. Dr. Yingnan Hou contributed the Northern blotting result in figure 3.26, as well as assisted me in the Northern blotting in figures 3.27 and 3.32. Y.H. also provided technical assistance in BiFC assay and Arabidopsis CRISPR mutant generation. Dr. Duseok Choi and M.S. Shuyi Duan generated PSR2 deletion mutants in pEG100 vector, which were used in this dissertation for co-IP assay in figure 3.30 and plant transformation in figure 3.31. These constructs were subcloned for Y2H analysis in figure 3.29. Dr. Liping Zeng assisted me in generating phylogenetic trees in figures 3.4 and 3.33. Dr. Simon Schwizer provided suggestions on DSI statistical analysis in figures 3.22, 3.24, and 3.25.

I would also like to thank Dr. Qin Xiong for initiating PSR2 IP experiment by constructing pEG100-PSR2 and establishing IP and *Phytophthora capsici* infection protocols. I thank Dr. Yi Zhai for constructing pRSF-PSR2 and pGEX-RCN1; Dr. Yongli Qiao for constructing pGBKT7-PSR2; Dr. Shushu Jiang for providing pEG100-HopZ1a^{C216A}; and Dr. Yao Zhao, Kelley Clark and Eva Hawara for providing negative control constructs in the pull-down assay. I thank undergrad volunteers, Brandon Duong and Reno Truong, for their assistance in screening transgenic plants and mutants.

Additionally, I thank Dr. Songqin Pan of IIGB Proteomics Core at UC Riverside for his service on mass spec analysis; Dr. Cyril Zipfel at the Sainsbury Laboratory for providing *pp2a c1-c5* mutant seeds; Dr. Xuemei Chen at UC Riverside and her postdoc

Dr. Bailong Zhang for sharing Y2H constructs of various AGO1 domains; and Dr. Jinbiao Ma at Fudan University for providing unpublished crystal structure of PSR2.

Finally, I would especially like to thank my P.I. Dr. Wenbo Ma for her support and guidance over the past five years. Thank you to my committee, Dr. Howard Judelson, Dr. Katherine Borkovich, and Dr. Xuemei Chen (former) for the useful discussions and advice on my dissertation. I would also like to thank my master P.I. Dr. Hsin-Hung Yeh and future postdoc P.I. Dr. Anand Ray for their encouragement, and thank my husband David Chen for reading and giving overall comments on my thesis. Additionally, I would like to thank Taiwan Ministry of Education for awarding me a two-year Studying Abroad Fellowship. Most importantly, I thank my family and my friends for their love, encouragement, and support.

ABSTRACT OF THE DISSERTATION

Molecular and Mechanistic study of *Phytophthora* RxLR Effector PSR2 in Arabidopsis

by

Tung Kuan

Doctor of Philosophy, Graduate Program in Microbiology
University of California, Riverside, September 2018
Dr. Wenbo Ma, Chairperson

Phytophthora belong to a group of fungus-like and zoospore-forming microorganisms, which are important plant pathogens that cause diseases on a broad range of crop and tree species worldwide. However, the control of *Phytophthora* diseases remains challenging due to the lack of understanding of their pathogenesis. *Phytophthora* are successful plant pathogens since they encode hundreds of effectors to suppress plant immune responses. Among them, the PSR2 family effectors are evolutionarily conserved among several *Phytophthora* species. Both PSR2 (encoded by *Phytophthora sojae*) and PiPSR2 (encoded by *Phytophthora infestans*) function as RNA silencing suppressors and are able to promote *Phytophthora* infection in plants.

To understand the molecular mechanisms by which PSR2 suppresses RNA silencing and increase disease susceptibility in plants, I identified serine/threonine protein phosphatase 2A (PP2A) as a PSR2-associating protein in plants. PP2A is a heterotrimeric enzyme consisting of scaffold A, regulatory B, and catalytic C subunits, where each subunit is encoded by gene families with multiple members. PSR2 has stronger

associations with A subunits, weaker associations with C subunits, and no association with B subunits.

Arabidopsis transgenic plant expressing PSR2 showed reduced production of phasiRNAs, which might be one of the underlying mechanisms suppressing plant immunity. To determine the functional involvement of PP2A subunits in PSR2-mediated RNA silencing suppression, I examined small RNA accumulation in transgenic Arabidopsis with PSR2-expressed in *pp2a* mutation backgrounds. Interestingly, the reduction of the phasiRNAs caused by PSR2 was rescued by the scaffold subunit *rcn1* and *pdf1* mutations, while these *rcn1* and *pdf1* mutants alone did not alter small RNA biogenesis. In addition, PSR2 deletion mutants that had reduced interaction with PP2A partially lost the phasiRNA suppression activity, suggesting the functional involvement of PP2A in PSR2-mediated small RNA suppression.

Lastly, mass spectrometry analyses revealed plenty of PP2A B subunits in RCN1-, but not PSR2-, associated protein complexes. Thus, PSR2 may serve as a regulatory B subunit to modulate the function of PP2A core enzyme (consisting of A and C subunits). This hypothesis was further supported by that PSR2 structurally mimicked PP2A B′ family subunits and it also shared similar binding sites to the scaffold with B′ family subunits. Furthermore, PSR2 was able to compete out a B′ subunit from the PP2A by an initial replacement pull-down assay. Together, my thesis research provides novel mechanistic insights into the pathogenesis of *Phytophthora* PSR2 effector by hijacking PP2A core enzyme in plants to suppress plant RNA silencing.

TABLE OF CONTENTS

LIST OF FIGURES

LIST OF TABLES

Chapter I

INTRODUCTION

1.1 Economic importance of Phytophthora diseases

Oomycete are fungus-like eukaryotic organisms living in moist soil or aquatic environments. They were considered to be true fungi until about 1990, when molecular phylogenetic evidence prompted their classification as members of Stramenopila (the Kingdom of diatoms, water molds and brown algae) (Agrios, 2005, Richards & Talbot, 2007). *Phytophthora* form a large genus in oomycete, consisting of more than 100 known species. Many of them are pathogenic to a broad range of economically important crops and wood trees, causing tens of billion US dollars loss worldwide each year (Erwin & Ribeiro, 1996, Haverkort et al., 2008).

The most known *Phytophthora* disease is the potato late blight caused by *Phytophthora infestans* (**Figure 1.1**). This disease unfortunately led to the outbreak of Irish famine in the late 1840s, resulting in death of 1.5 millions of people in Ireland (Agrios, 2005, Kamoun et al., 2015). In 1990s, another species *Phytophthora ramorum* caused the outbreak of sudden oak death and severely damaged woodlands in North America (Grunwald, 2012, Kamoun et al., 2015). *Phytophthora sojae* caused prevalent root/stem rot diseases in most soybean growing regions (Kamoun et al., 2015, Tyler, 2007, Wrather & Koenning, 2006). *Phytophthora capsici*, a species infects peppers and cucurbits, also evolved much more virulent strains in the last decade (Kamoun et al., 2015).

Although *Phytophthora* are great threats to agricultural and natural environments, the controls of these destructive diseases remain challenging due to the lack of understanding on *Phytophthora* pathogenesis, which is more complicated than prokaryotic and viral pathogenesis (Jiang & Tyler, 2012). To develop effective disease control strategies and maintain global food supplies, it is important to understand how these pathogens achieve infection.

1.2 Phytophthora infection cycle

Phytophthora are free-living pathogens that infect both roots and shoots of the host. The infection of *Phytophthora* usually starts with zoospores (**Figure 1.1**) (Judelson & Blanco, 2005). Zoospores are produced asexually and bear flagella so that they can actively move towards host tissue. After the attachment, zoospore forms a germ tube to directly penetrate plant tissue or enters through stomata, and the invasive hyphae grow along intercellular spaces, protruding a specialized infection structure, called haustorium, into the cell (**Figure 1.1 and Figure 1.2A**). *Phytophthora* actively interact with plant cells through haustoria and export virulence factors.

Phytophthora infection eventually promotes tissue discoloration and collapse, and leads to symptoms like leaf blight and root/stem rot (Agrios, 2005, Tyler, 2007). When a mycelium reaches the aerial parts of infected tissues as well as the air spaces underground, it produces sporangiophores bearing zoosporangia. The released zoospores will be dispersed and start a new infection cycle. Alternatively, *Phytophthora* are also able to reproduce sexually and use oospores for infection.

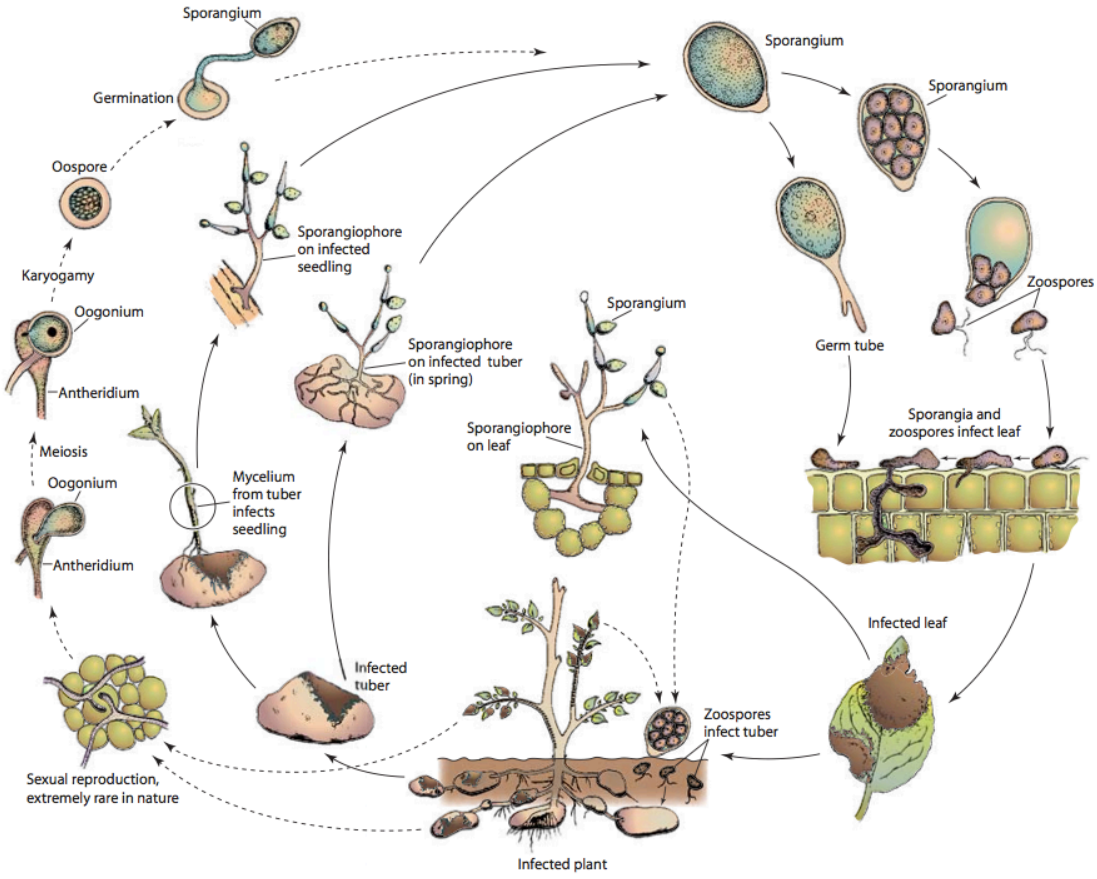

Figure 1.1. Infection cycle of *Phytophthora infestans*, the causal agent of potato late blight. *Phytophthora* infection mainly depends on its flagellated zoospores, which induce leaf blight, root rot, and stem rot diseases [Figure modified from(Agrios, 2005)]

1.3 Phytophthora effectors and pathogenesis

As a group of highly pathogenic pathogens, *Phytophthora* evolved efficient strategies to achieve successful infection. *Phytophthora* are hemibiotrophic, characterized by the exhibition of two distinct infection stages (Lee & Rose, 2010). In the initial biotrophic phase, *Phytophthora* secrete effector proteins through haustoria to subvert plant immunity, allowing the hyphae to spread throughout the tissues (**Figure 1.2A**) (Bos et al., 2010, Jiang & Tyler, 2012, Jones & Dangl, 2006, Kamoun, 2006, Tyler et al., 2006, Fawke et al., 2015). They later enter the necrotrophic phase to destroy the infected tissue (Kamoun, 2006, Lee & Rose, 2010).

Based on the target sites in the host, *Phytophthora* effectors can be divided into apoplastic and cytoplasmic effectors. The former are secreted into the extracellular space to battle with defensive molecules derived from the plant (Doehlemann & Hemetsberger, 2013, Panstruga & Dodds, 2009); while the latter contain "host-targeting motifs" to be delivered into the plant cell to disrupt critical cellular processes and counteract plant immunity. One large family of cytoplasmic effectors, the RxLR family, has been the subject to much research interest in recent years. RxLR effectors contain a conserved N terminal signal peptide (for extracellular secretion) followed by a signature RxLR motif (Arg-X-Leu- Arg, where X is any amino acid), and a variable functional domain at the C termini (for virulence activity) (**Figure 1.2B**) (Boutemy et al., 2011, Kale et al., 2010, Whisson et al., 2007, Win et al., 2007).

To date, as the genome sequences of several *Phytophthora* species have been completed, hundreds to over one thousand of diverse effectors encoded by *Phytophthora*

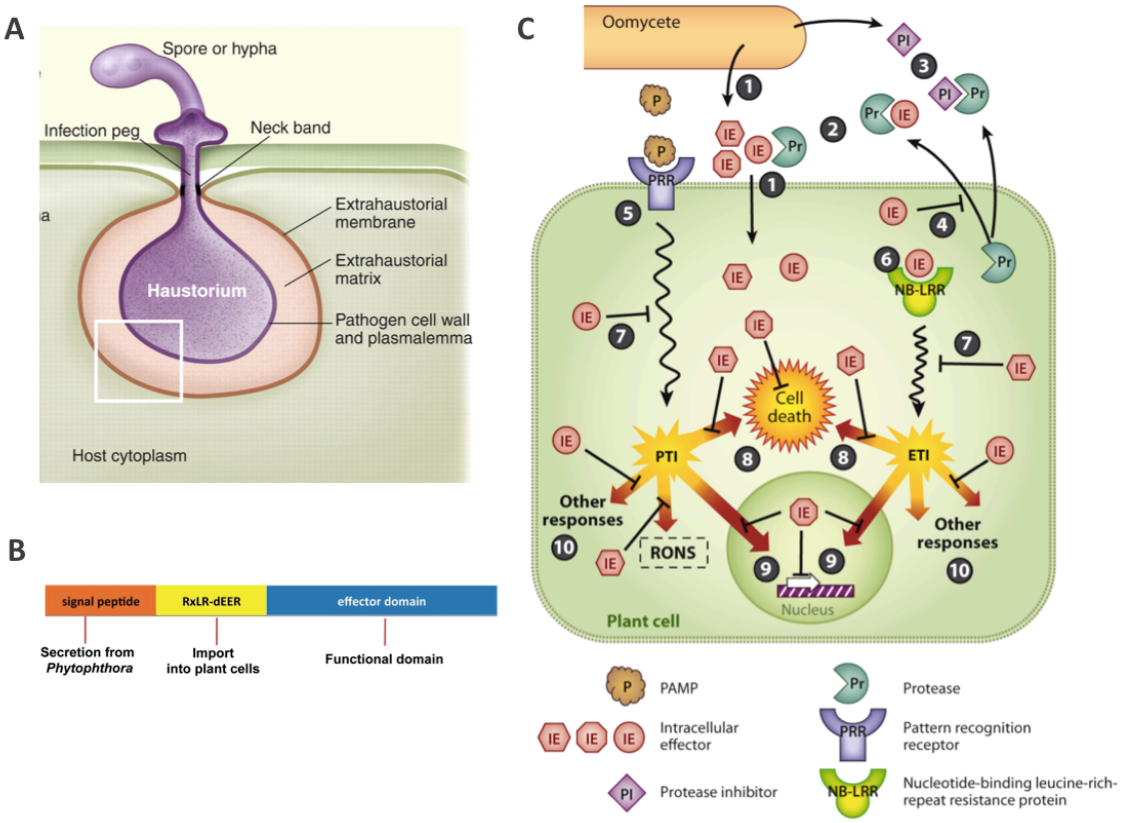

Figure 1.2. *Phytophthora* effectors and pathogenesis. (**A**) Effectors are secreted by haustoria into extrahaustorial matrix and those containing the "host-targeting" motifs will enter the plant cell. (**B**) The schematic diagram of RxLR-effector. (**C**) Interactions between *Phytophthora* effectors and host molecules. [Figure modified from(Jiang & Tyler, 2012, Panstruga & Dodds, 2009); Mauch Lab Website, University of Fribourg]

are revealed from each species (Haas et al., 2009). *Phytophthora sojae* and *Phytophthora infestans* has about 400 and 563 RxLR effectors, respectively (Haas et al., 2009). These extraordinarily large effector repertoires in *Phytophthora* compared to other pathogens (e.g. bacteria only produce 20-50 effectors), suggesting the more sophisticated interactions between host and *Phytophthora* pathogens (Torto-Alalibo et al., 2009).

A fundamental function of pathogen effectors is to suppress the pattern-triggered immunity (PTI) and the effector-triggered immunity (ETI) in plants, and thereby determine the pathogenicity (**Figure 1.2C**) (Jiang & Tyler, 2012, Jones & Dangl, 2006, Thomma et al., 2011). Though their molecular mechanisms are still poorly understood, many of the RxLR effectors are shown to interrupt the defense signaling events such as the mitogen-associated protein kinase (MAPK) signaling (Haas et al., 2009, Jiang & Tyler, 2012, Morgan & Kamoun, 2007, Tyler et al., 2006). Recently, RxLR effectors were also found to regulate plant RNA silencing pathway, suggesting the involvement of RNA silencing in plant-*Phytophthora* interaction (Qiao et al., 2013, Wong et al., 2014).

1.4 RNA silencing: the transcriptional and post-transcriptional gene regulation

Plants do not have immune cells; instead, they develop induced resistance to produce various defense-related substances against insect pests, nematodes, fungi, oomycetes, bacteria, and viruses (Jones & Dangl, 2006). Plant defense is under stringent regulation: it maintains basal or no expression under normal conditions to avoid developmental defect and autoimmune disease; however, it can be rapidly activated upon perception of

pathogens (Li et al., 2015). Therefore, to understand how the plant immune genes are regulated in response to the pathogens gains more insights on plant defense.

One of the central mechanisms of gene expression in eukaryotes is the transcriptional and post-transcriptional gene regulation controlled by small non-coding RNAs called RNA silencing (also known as RNA interference or RNAi). RNA silencing is one of the most important discoveries in 1990s. It is evolutionarily conserved within eukaryotes and is involved in many fundamental biological processes such as development, genome organization, transposition, immunity, and disease development (Katiyar-Agarwal & Jin, 2010, Molnar et al., 2011). Interestingly, the CRISPR (Clustered Regularly Interspaced Short Palindromic Repeats) immune mechanism was also found in bacterial species for protecting themselves form foreign nucleic acids, such as plasmids and bacteriophages (Barrangou et al., 2007).

RNAi is usually induced by long double-stranded RNAs (dsRNA), followed by the generation of small RNAs, and the degradation or translational inhibition of cognate target mRNA. Small RNAs of different origins and functions were subsequently identified in several organisms. There are three main classes of small RNAs in plant systems: 1) microRNAs (miRNAs) derived by endogenous MIR genes; 2) small interfering RNAs (siRNAs) derived from exogenous nucleic acid, endogenous repeats, and transposition sequences; 3) phased secondary siRNAs (phasiRNAs) derived from the PHAS loci, whose biogenesis requires the production of specific miRNAs and the cellular machinery of RDR6, SGS3, DCL4, DRB4, AGO1, and AGO7 (**Figure 1.3**) (Yoshikawa et al., 2005, Fei et al., 2013).

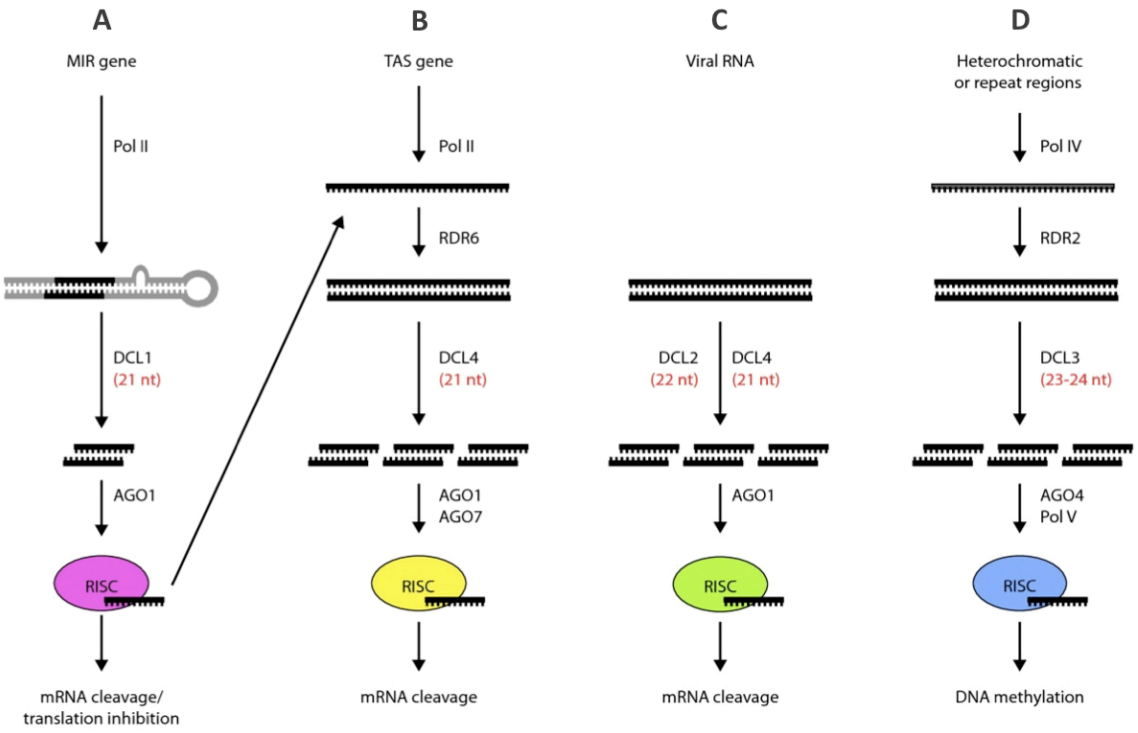

Figure 1.3. Schematic diagram of silencing pathways in plants. An overview of the (A) miRNA, (B) phasiRNA (also known as tasiRNA), (C) virus-induced siRNA, and (D) heterochromatic siRNA (also known as RNA-dependent DNA methylation) pathways.

Small RNA species are used to define different RNAi pathways based on their characteristics, biogenesis, and mode-of- actions for gene silencing; however, they are all common in providing the sequence specificity for RNAi to inhibit the cognate target RNAs (Pumplin & Voinnet, 2013). The precise gene regulation ability makes RNAi a fundamental part in plant defense regulation. In addition, RNAi also regulates transcriptional gene silencing by introducing methylations on target genome sequences. This RNA-dependent DNA methylation (RdDM) was recently found to be involved in plant defense as well (Yu et al., 2013). Dicer-like proteins (DCLs), Argonaute proteins (AGOs) and RNA polymerases (RDRs, Pols) are the key players in all pathways. [Figure modified from (Molnar et al., 2011)]

1.5 RNA silencing as a part of plant immune response

RNAi was firstly recognized as an immune strategy developed to compromise RNA virus infection, since the viral dsRNA replication intermediates serve as the RNAi inducer (Nakahara & Masuta, 2014). siRNA pathway was found to be the main defense mechanism to viral pathogens by directly targeting to the viral genome (Ding, 2010). Later, the virus-activated siRNAs (vasi-RNAs) were also found to silence host genes to confer broad-spectrum antiviral activity (**Figure 1.3C**) (Cao et al., 2014).

The RNAi machinery is also used for regulating the expression of defense genes against other groups of pathogens, e.g. bacteria, oomycetes and true fungi. Many of the plant small RNA species were found to be up- or down-regulated in response to pathogen infection. In general, cellular events such as phytohormone signaling, defense signaling,

and RNAi pathways were the targets of these pathogen-responsive small RNAs (Kuan et al., 2016). For example, Arabidopsis miR393 regulates the PAMP-responsive protein and the receptor-like kinase for anti-bacterial defense (**Figure 1.4A**) (Navarro et al., 2006, Navarro et al., 2008, Zhang et al., 2011). Soybean miR393 enhances soybean resistance during *P. sojae* infection (Wong et al., 2014). Arabidopsis AGO1-dependent RNAi pathway controls MPK1/2 and WAK against fungal pathogen *Botrytis cinerea* (Weiberg et al., 2013).

Cross-kingdom RNAi was recently demonstrated as a part of immune response that hosts employ small RNAs to hijack the pathogen RNAi machinery and silence the pathogen virulence genes (Cai et al., 2018, Zhang et al., 2016). MiR166 and miR159 of cotton plants were found to be exported to the hyphae of fungal pathogen *Verticillium dahlia* for fungal gene silencing (Zhang et al., 2016). In Arabidopsis system, specific exosome-like extracellular vesicles of the plant were identified to deliver plant small RNAs into *B. cinerea* cells to silence pathogenesis-related genes (Cai et al., 2018). Therefore, the small RNAs in hosts are important for regulating the plant immunity against pathogens.

1.6 Pathogen-encoded RNA silencing suppressors against host immunity

From the pathogen's perspective to counteract the plant defense, RNA silencing suppressors have been discovered in several plant pathogens to compromise plant RNAi immunity by targeting either key components in RNA silencing pathways or other cellular proteins that indirectly regulate RNA silencing (**Figure 1.4**). However, majority

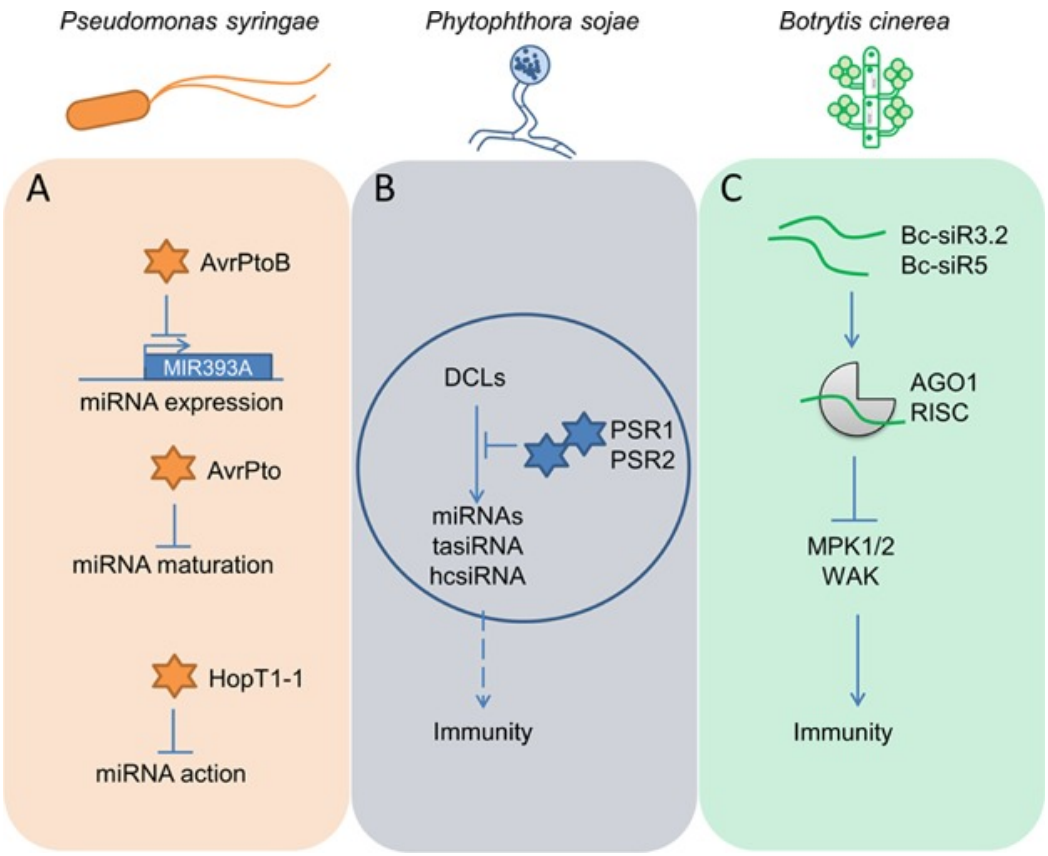

Figure 1.4. Small RNA-mediated defense and its modification by pathogen-derived molecules. (**A, C**) miRNA-mediated defense against bacterial and fungal pathogens, *Pseudomonas* and *Botrytis*; (**B**) miRNA- and phasiRNA (ta-siRNA)-mediated defense against oomycete pathogen, *Phytophthora*. Pathogen virulence has evolved to compromise different steps in small RNA-mediated defense. [Figure adapted from (Yang & Huang, 2014)]

of the silencing suppressors are viral proteins, mainly found in RNA viruses (Katiyar-Agarwal & Jin, 2010, Nakahara & Masuta, 2014, Pumplin & Voinnet, 2013). Without the protection from viral silencing suppressors, RNA viruses are degraded by host RNAi machinery.

Until 2008, the first prokaryote-encoded silencing suppressors were discovered in a plant bacterial pathogen—three *Pseudomonas* effectors, AvrPto, AvrPtoB, HopT1-1, suppressed RNA silencing by interfering the miRNA pathway (**Figure 1.4A**) (Navarro et al., 2008). As the causal agents of ~80% of plant diseases, eukaryotic plant pathogen (fungi and oomycetes) also evolved virulence proteins with RNA silencing suppression activity (Qiao et al., 2013). Two RxLR effectors (PSR1 and PSR2) encoded by *Phytophthora sojae* possess the ability to suppress the transgene-induced gene silencing in *Nicotiana benthamiana* and reduce the biogenesis of particular classes of small RNAs in Arabidopsis (**Figure 1.4B**). The RNAi-based plant-microbe interaction is now an active research field with accumulating research evidence indicating that pathogens have evolved efficient strategies to suppress or hijack host RNAi systems.

1.7 Phytophthora suppressor of RNA silencing 2 (PSR2)

The two RxLR effectors found in *Phytophthora sojae* were named as *Phytophthora* suppressor of RNA silencing 1 and 2 (PSR1 and PSR2). Although both PSR1 and PSR2 exhibit silencing suppression activity in plants, the biological importance of PSR2 is more evident (**Figure 1.5**) based on the following evidence. Previous study showed that overexpressing PSR2 in both Arabidopsis and *Nicotiana benthamian* promotes the

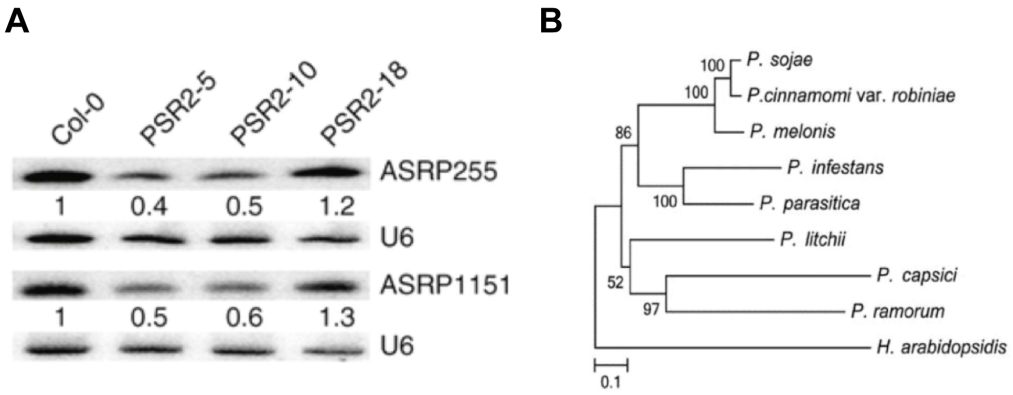

Figure 1.5. PSR2 is biologically important in terms of its regulation of particular small RNA species and evolutionary conservation. (**A**). Reduced accumulation of representative phasiRNAs (ASRP255 from *TAS1* locus, ASRP1151 from *TAS2* locus) in three *PsPSR2*-expressing transgenic *Arabidopsis* lines. (**B**) Phylogenetic analysis showed high conservation of PSR2 throughout *Phytophthora* species. [Figure modified from (Qiao et al., 2013, Xiong et al., 2014)]

disease symptoms of *Phytophthora*, suggesting PSR2 is a virulence factor (Qiao et al., 2013, Xiong et al., 2014). Further characterization of endogenous small RNA species revealed that the biogenesis of tasiRNAs was specifically reduced in the transgenic Arabidopsis overexpressing PSR2 (PSR2-5^{OE} and PSR2-10^{OE}) (Qiao et al., 2013) (**Figure 1.5A**).

In addition, phylogenetic analysis of PSR2 prevalence within different *Phytophthora* species suggested PSR2 is a conserved effector (**Figure 1.5B**). Its homologs were found in other *Phytophthora* species, including *P. sojae*, and *P. cinnamomi*, *P. melonis*, *P. infestans*, and *P. parasitica*. (Xiong et al., 2014). This type of widely distributed "core effectors" across the population of a specific pathogen are considered to have critical contribution to the virulence (Dangl et al., 2013, Bart et al., 2012), which are very different from majority of pathogen effectors that evolve rapidly to overcome resistance. Further characterization of PiPSR2, the PSR2 homolog of *Phytophthora infestans*, also confirmed its silencing suppression and disease promotion activities (Xiong et al., 2014).

1.8 Protein phosphatase 2A is a conserved serine/threonine phosphatase family among eukaryotic cells

Protein phosphatase 2A (PP2A) was found to be one of the plant cellular helper of PSR2 in this thesis research. PP2A is a ubiquitous and conserved serine/threonine phosphatase with broad substrate specificity and diverse cellular functions in eukaryotic organisms. PP2A is a heterotrimeric enzyme consisting of three subunits: a scaffold A subunit, a regulatory B subunit, and a catalytic C subunit (Farkas et al., 2007, Uhrig et al.,

2013). A and C subunits form functional core enzymes, and are remarkably conserved throughout eukaryotes. B subunits are more heterogeneous, controlling the subcellular localization and substrate specificity (Shi, 2009, Farkas et al., 2007). The binding of B subunits to PP2A core enzyme in a variety of combinations allows the core enzyme to regulate diverse cellular pathways.

In addition to cell development and survival, plant PP2A was found to participate in the regulation of ethylene biosynthesis, brassinosteroids (BR) signaling, abiotic and biotic stress responses (He et al., 2004, Segonzac et al., 2014, Zhou et al., 2004). PP2A is also a negative defense regulator which associates with BAK1 immune receptor against bacterial pathogen *Pseudomonas syringe* (Segonzac et al., 2014). However, so far no report specifically indicates PP2A functions in RNA silencing regulation. In the mass spectrometry-based IP proteomic analysis in this thesis, PP2As were identified as the most enriched proteins in the PSR2-associated complexes. All the PP2A hits were annotated as PP2A A or C subunits that themselves can form the PP2A core enzymes.

1.9 Objectives of the study

Evidence from PSR2 family effectors strongly suggests an arms race between plant and *Phytophthora* on plant RNA silencing regulation. However, the molecular mechanisms of PSR2 (silencing suppressor)-based *Phytophthora* pathogenesis is still unclear. In this thesis research, I investigated how *Phytophthora* regulates plant defense by the activity of PSR2. Firstly, I identified the potential cellular targets of PSR2 in plants, where protein phosphatase 2A (PP2A) core enzyme was revealed to strongly

associate with PSR2. Subsequently, the functional requirements of PP2A in the PSR2-mediated phasiRNA biogenesis suppression and immune regulations were examined. I hypothesized that PSR2 may regulate the plant PP2A core enzyme via serving as a regulatory subunit of PP2A to exert its cellular functions in hosts. Finally, the protein association between the PSR2/PP2A complex and Argonaute proteins (AGOa), potential substrates of the PSR2/PP2A complex, were also examined. The five specific aims included in this study are shown below:

a) Identifying the potential targets of PSR2 by mass spectrometry-based immunoprecipitation proteomics.
b) Confirming the interactions between PSR2 and PP2A using protein-protein interaction experiments.
c) Functional analyses of PSR2/PP2A complex in small RNA and immune regulations.
d) Elucidating the mechanism that PSR2 may regulate PP2A core enzyme by acting as a regulatory subunit of PP2A.
e) Screening potential substrates of PSR2/PP2A holoenzyme that regulate RNAi and defense.

Chapter II

MATERIALS AND METHODS

2.1 Microbial strains and construct information

Microbial strains and plasmids used in this thesis research are summarized in **Table 2.1** (*Escherichia coli* strains and plasmids), **Table 2.2** (*Agrobacterium tumefaciens* strains and plasmids), and **Table 2.3** (*Saccharomyces cerevisiae* strain and plasmids).

Specifically, the *E. coli* strains DH5α, Top10, JM109, and NEB10 were used for molecular cloning. *E. coli* strain BL21-RIL and BL21-RosettaII were used for the protein expression for pull-down assays. *A. tumefaciens* strain GV3101 was used for either transiently expressing proteins in plants or generating transgenic plants. Both *E. coli* and *A. tumefaciens* were grown in Luria−Bactani (LB) liquid medium and/or agar at 37°C and 28°C, respectively.

S. cerevisiae yeast strain AH109 was used for the yeast-two-hybrid (Y2H) assay. AH109 was grown in Synthetic Dropout (SD) medium at 28−30°C. The SD medium preparation was described in Y2H user manual (Clontech, PT3247-1).

2.2 Plant materials and growth conditions

Arabidopsis thaliana ecotype Col-0 was used for functional assays in this study. All Arabidopsis mutants used in this thesis research are summarized in **Table 2.4**. *Nicotiana benthamiana* wild-type and the transgenic line 16c that constitutively expresses GFP proteins were used for mass spectrometry-based immunoprecipitations proteomic

analysis, BiFC, and co-IP assays. All plants were maintained in a growth room with controlled temperature (23−25°C) and light (12h light/12h dark). Plants about 4−6 weeks old were used for all experiments.

2.3 Primers, probes, and antibodies used in this thesis research

Molecular cloning primers, sequencing primers, genotyping primers, RT-PCR primers, and probes used in this thesis research are listed in **Table 2.5**. Antibodies used in this thesis research are listed in **Table 2.6**.

Table 2.1 *Escherichia coli* strains and plasmids used in this thesis research.

No.	Plasmid name	Strain	Antibiotics	Purpose/Description
1	pVYNE	DH5α	Kan	BiFC
2	pVYCE	DH5α	Kan	BiFC
3	pVYNE(R)	DH5α	Kan	BiFC
4	pVYCE(R)	DH5α	Kan	BiFC
5	pSCYNE-CBL1	DH5α	Kan	BiFC
6	pVYNE-CBL10	DH5α	Kan	BiFC
7	pSCYCE(R)-CIPK24	DH5α	Kan	BiFC
8	pGADT7-RCN1	DH5α	Amp	Y2H
9	pGADT7-PDF1	DH5α	Amp	Y2H
10	pGADT7-PDF2 (At1g13320.2)	DH5α	Amp	Y2H
11	pGADT7-AtAGO1	DH5α	Amp	Y2H
12	pGBKT7 EV	DH5α	Kan	Y2H
13	pGADT7-PSR2	DH5α	Amp	Y2H
14	pGADT7-AtAGO4	DH5α	Amp	Y2H
15	pGADT7-AtAGO9	DH5α	Amp	Y2H
16	pGADT7-AtAGO10	DH5α	Amp	Y2H
17	pGBKT7-RCN1	Top10	Kan	Y2H
18	pEG100-3×Flag-PSR2	DH5α	Kan	Protein expression in *N. b.*
19	pEG103 EV	DB3.1	Kan	Protein expression in *N. b.*
20	pEG104 EV	DB3.1	Kan	Protein expression in *N. b.*
21	pVYCE-RCN1	DH5α	Kan	BiFC
22	pVYCE(R)-RCN1	DH5α	Kan	BiFC
23	pGADT7 EV	DH5α	Amp	Y2H
24	pGADT7-PSR2	DH5α	Amp	Y2H
25	pGBKT7-PDF1	JM109	Kan	Y2H
27	pGBKT7-PiPSR2	DH5α	Kan	Y2H
29	pVYNE-AtAGO1	DH5α	Kan	BiFC
37	pGBKT7-PP2AC1	DH5α	Kan	Y2H
38	pGBKT7-PP2AC2	DH5α	Kan	Y2H
39	pGBKT7-PP2AC3	DH5α	Kan	Y2H
40	pGBKT7-PP2AC4	DH5α	Kan	Y2H
41	pGBKT7-PP2AC5	DH5α	Kan	Y2H
42	pGBKT7-PSR2	DH5α	Kan	Y2H

EV: empty vector, Kan: kanamycin, Amp: ampicillin.

Table 2.1 (Continued)

No.	Plasmid name	Strain	Antibiotics	Purpose/Description
43	pGADT7-PiPSR2	DH5α	Amp	Y2H
43	pGADT7-PP2AC1	DH5α	Amp	Y2H
44	pGADT7-PP2AC2	DH5α	Amp	Y2H
45	pGADT7-PP2AC3	DH5α	Amp	Y2H
46	pGADT7-PP2AC4	DH5α	Amp	Y2H
47	pGADT7-PP2AC5	DH5α	Amp	Y2H
48	pGADT7-WNK4	DH5α	Amp	Y2H
49	pTsk108 (no Flag) EV	DH5α	Kan	Protein expression in *N. b.*
50	pENTR1a EV	DH5α	Kan	Protein expression in *N. b.*
51	pTsk108-3×Flag	DH5α	Kan	Protein expression in *N. b.*
52	pTsk108-3×Flag-RCN1	DH5α	Kan	Protein expression in *N. b.*
53	pTsk108-3×Flag-PDF2	DH5α	Kan	Protein expression in *N. b.*
54	pEG100 EV	DB3.1	Kan	Protein expression in *N. b.*
55	pEG101 EV	DB3.1	Kan	Protein expression in *N. b.*
56	DH5α competent cell	DH5α	—	Competent cell preparation
57	pBluescript-SK(+) AtU6-26	DH5α	Amp	CRISPR genome editing
58	pCAMBIA1300-221 pYao-Cas9	DH5α	Kan	CRISPR genome editing
59	pEG100-3×Flag-RCN1	NEB10*β*	Kan	Protein expression in *N. b.*
60	pEG100-3×Flag-PDF2	NEB10*β*	Kan	Protein expression in *N. b.*
61	pAtU6-26-PDF1-target1	DH5α	Amp	CRISPR genome editing
62	pAtU6-26-PDF1-target2	DH5α	Amp	CRISPR genome editing
63	pCAMBIA1300-pYaoCas9- PDF1-target1	DH5α	Kan	CRISPR genome editing
64	pCAMBIA1300-pYaoCas9- PDF1-target1	DH5α	Kan	CRISPR genome editing
65	pGBKT7-AtAGO1-N100	unknown	Kan	Y2H
66	pGBKT7-AtAGO1-PAZ	unknown	Kan	Y2H
67	pGBKT7-AtAGO1-MID	unknown	Kan	Y2H
68	pGBKT7-AtAGO1-PIWI	unknown	Kan	Y2H
69	pENTR1a EV	DH5α	Kan	Protein expression in *N. b.*
70	pRSFDuet EV (with SUMO)	DH5α	Kan	In vitro pull-down
71	pGEX-4T-2 EV	DH5α	Amp	In vitro pull-down
72	pRSF-His-SUMO-PSR2	BL21-RIL	Kan, Cam	In vitro pull-down
73	pGEX-GST-RCN1	BL21-RIL	Amp, Cam	In vitro pull-down
74	pVYCE-PP2AC2	DH5α	Kan	BiFC

EV: empty vector, Kan: kanamycin, Amp: ampicillin, Cam: chloramphinicol

Table 2.1 (Continued)

No.	Plasmid name	Strain	Antibiotics	Purpose/Description
75	pVYCE-PP2AC3	DH5α	Kan	BiFC
76	pVYCE-PP2AC4	DH5α	Kan	BiFC
77	pVYCE-PP2AC5	DH5α	Kan	BiFC
78	pVYCE-PDF1	DH5α	Kan	BiFC
79	pVYCE-PDF2	DH5α	Kan	BiFC
80	pVYNE-PSR2NLS	DH5α	Kan	BiFC
81	pGEX-4T-2 EV	BL21-RIL	Amp, Cam	In vitro pull-down
82	pRSFDuet EV (with SUMO)	BL21-RIL	Kan, Cam	In vitro pull-down
84	pENTR1a-PDF1	DH5α	Kan	Protein expression in *N. b.*
85	pGEX-GST-PDF1	DH5α	Amp	In vitro pull-down
86	pRSF-His-SUMO-B′α	DH5α	Kan	In vitro pull-down
87	pRSF-His-SUMO-B′γ	DH5α	Kan	In vitro pull-down
88	pRSF-His-SUMO-Bβ	DH5α	Kan	In vitro pull-down
89	pGEX-GST-PDF1	BL21-RIL	Amp, Cam	In vitro pull-down
90	pRSF-His-SUMO-B′α	BL21-RIL	Kan, Cam	In vitro pull-down
91	pRSF-His-SUMO-B′γ	BL21-RIL	Kan, Cam	In vitro pull-down
92	pRSF-His-SUMO-Bβ	BL21-RIL	Kan, Cam	In vitro pull-down
93	pEG101-PDF1-YFP	DH5α	Kan	Protein expression in *N. b.*
94	pGEX-GST-PDF1	RosettaII	Amp, Cam	In vitro pull-down
95	pRSF-His-SUMO-B′α	RosettaII	Kan, Cam	In vitro pull-down
96	pRSF-His-SUMO-B′γ	RosettaII	Kan, Cam	In vitro pull-down
97	pRSF-His-SUMO-Bβ	RosettaII	Kan, Cam	In vitro pull-down
98	pTsk-3×Flag-PSR2$^{\Delta N}$	DH5α	Kan	Protein expression in *N. b.*
99	pTsk-3×Flag-PSR2$^{\Delta WY1}$	DH5α	Kan	Protein expression in *N. b.*
100	pTsk-3×Flag-PSR2$^{\Delta LWY2}$	DH5α	Kan	Protein expression in *N. b.*
101	pTsk-3×Flag-PSR2$^{\Delta LWY3}$	DH5α	Kan	Protein expression in *N. b.*
102	pTsk-3×Flag-PSR2$^{\Delta LWY4}$	DH5α	Kan	Protein expression in *N. b.*
103	pTsk-3×Flag-PSR2$^{\Delta LWY5}$	DH5α	Kan	Protein expression in *N. b.*
104	pTsk-3×Flag-PSR2$^{\Delta LWY6}$	DH5α	Kan	Protein expression in *N. b.*
105	pTsk-3×Flag-PSR2$^{\Delta LWY7}$	DH5α	Kan	Protein expression in *N. b.*
106	pTsk-3×Flag-PSR2$^{\Delta LWY3+4}$	DH5α	Kan	Protein expression in *N. b.*
107	pTsk-3×Flag-PSR2$^{399-414}$	DH5α	Kan	Protein expression in *N. b.*
108	pTsk-3×Flag-PSR2$^{400-415}$	DH5α	Kan	Protein expression in *N. b.*

EV: empty vector, Kan: kanamycin, Amp: ampicillin, Cam: chloramphinicol

Table 2.1 (Continued)

No.	Plasmid name	Strain	Antibiotics	Purpose/Description
109	pGBKT7-PSR2$^{\Delta N}$	DH5α	Kan	Y2H
110	pGBKT7-PSR2$^{\Delta WY1}$	DH5α	Kan	Y2H
111	pGBKT7-PSR2$^{\Delta LWY2}$	DH5α	Kan	Y2H
112	pGBKT7-PSR2$^{\Delta LWY3}$	DH5α	Kan	Y2H
113	pGBKT7-PSR2$^{\Delta LWY4}$	DH5α	Kan	Y2H
114	pGBKT7-PSR2$^{\Delta LWY5}$	DH5α	Kan	Y2H
115	pGBKT7-PSR2$^{\Delta LWY6}$	DH5α	Kan	Y2H
116	pGBKT7-PSR2$^{\Delta LWY7}$	DH5α	Kan	Y2H
117	pGBKT7-PSR2$^{\Delta LWY3+4}$	DH5α	Kan	Y2H
118	pGBKT7-PSR2$^{399-414}$	DH5α	Kan	Y2H
119	pGBKT7-PSR2$^{400-415}$	DH5α	Kan	Y2H
120	pGADT7-RCN1$^{396-588}$	DH5α	Amp	Y2H
121	pGADT7-RCN1$^{1-397}$	DH5α	Amp	Y2H
122	pENTR1a-RCN1$^{396-588}$	DH5α	Kan	Protein expression in *N. b.*
123	pENTR1a-RCN1$^{1-397}$	DH5α	Kan	Protein expression in *N. b.*
124	pRSF-His-SUMO-JAZ6	BL21-RIL	Kan, Cam	In vitro pull-down
125	pRSF-His-SUMO-GFP	RosettaII	Kan, Cam	In vitro pull-down
126	pGEX-AALP	BL21-RIL	Amp, Cam	In vitro pull-down.
128	pENTR1a-RCN1	DH5α	Kan	Protein expression in *N. b.*
129	pGWB512-Flag-RCN1	DH5α	Spec	*A. t.* plant transformation
130	pGWB514-RCN1-3×HA	DH5α	Spec	*A. t.* plant transformation
131	pGWB512-Flag-RCN1$^{396-588}$	DH5α	Spec	*A. t.* plant transformation
132	pGWB515-3×HA-RCN1$^{396-588}$	DH5α	Spec	*A. t.* plant transformation

EV: empty vector, Kan: kanamycin, Amp: ampicillin, Cam: chloramphenicol, Spec: spectinomycin

Table 2.2 *Agrobacterium tumefaciens* strains and plasmids used in this thesis research.

No.	Plasmid name	Strain	Antibiotics	Purpose/Description
3	pEG100 EV	GV3101	RKG	IP-LC/MS
6	pEG100-3×Flag-PSR2	GV3101	RKG	IP-LC/MS, co-IP
9	pEG100-3×Flag- HopZ1a^{C216A}	GV3101	RKG	IP-LC/MS, co-IP
10	35S::GFP	Agrobacterium	RK	RNAi induction in 16C
16	35S::2b	Agrobacterium	RK	RNAi suppressor
21	pEG101 EV	GV3101	RKG	Co-IP
22	pEG104 EV	GV3101	RKG	Co-IP
23, 24	pEG101-RCN1	GV3101	RKG	Co-IP, subcellular localization
31	pVYNE-PSR2	GV3101	RKG	BiFC
32	pVYCE-RCN1	GV3101	RKG	BiFC, co-IP
33	pVYCE(R)-RCN1	GV3101	RKG	BiFC
34	pVYNE EV	GV3101	RKG	BiFC
35	pVYCE(R) EV	GV3101	RKG	BiFC
39	pVYNE-AGO1	GV3101	RKG	BiFC, co-IP
41	pVYNE-PSR2NES	GV3101	RKG	BiFC
53	pEG100-3×Flag-RCN1	GV3101	RKG	Co-IP, *A.t.* transformation
54	pEG100-3×Flag-PDF2	GV3101	RKG	Co-IP
55	pEG102-PSR2-CFP	GV3101	RKG	Subcellular localization
57	pEG100-3×Flag	GV3101	RKG	IP-LC/MS
58	GV3101 competent cell stock	GV3101	RG	Competent cell preparation
59	pCAMBIA1300-Yao-PDF1-target1	GV3101	RKG	*pdf1* CRISPR mutant
60	pCAMBIA1300-Yao-PDF1-target2	GV3101	RKG	*pdf1* CRISPR mutant
62	pVYCE-C2	GV3101	RKG	BiFC, co-IP
63	pVYCE-C3	GV3101	RKG	BiFC, co-IP
64	pVYCE-C4	GV3101	RKG	BiFC, co-IP
65	pVYCE-C5	GV3101	RKG	BiFC, co-IP
66	pVYCE-PDF1	GV3101	RKG	BiFC, co-IP
67	pVYCE-PDF2	GV3101	RKG	BiFC, co-IP
68	pVYNE-PSR2NLS	GV3101	RKG	Subcellular localization
69	pEG101-PDF1-YFP clone 1	GV3101	RKG	Co-IP, subcellular localization
70	pEG101-PDF1-YFP clone 4	GV3101	RKG	Co-IP, subcellular localization
71	pEG100-3×Flag-PSR2$^{\Delta N}$	GV3101	RKG	Co-IP
72	pEG100-3×Flag-PSR2$^{\Delta WY1}$	GV3101	RKG	Co-IP

EV: empty vector, R: rifampicin, K: kanamycin, G: gentamycin

Table 2.2 (Continued)

No.	Plasmid name	Strain	Antibiotics	Purpose/Description
73	pEG100-3×Flag-PSR2$^{\Delta LWY2}$	GV3101	RKG	Co-IP, *A.t.* transformation
74	pEG100-3×Flag-PSR2$^{\Delta LWY3}$	GV3101	RKG	Co-IP, *A.t.* transformation
75	pEG100-3×Flag-PSR2$^{\Delta LWY4}$	GV3101	RKG	Co-IP, *A.t.* transformation
76	pEG100-3×Flag-PSR2$^{\Delta LWY5}$	GV3101	RKG	Co-IP, *A.t.* transformation
77	pEG100-3×Flag-PSR2$^{\Delta LWY6}$	GV3101	RKG	Co-IP, *A.t.* transformation
78	pEG100-3×Flag-PSR2$^{\Delta LWY7}$	GV3101	RKG	Co-IP
79	pEG100-3×Flag-PSR2$^{\Delta LWY3+4}$	GV3101	RKG	Co-IP
80	pEG100-3×Flag-PSR2$^{\Delta 399-414}$	GV3101	RKG	Co-IP
81	pEG100-3×Flag-PSR2$^{55-214}$	GV3101	RKG	Co-IP
82	pGWB512-Flag-RCN1	GV3101	RGSpec	Complement PSR2-5^{OE}*rcn1-6*
83	pGWB514-RCN1-3×HA	GV3101	RGSpec	Complement PSR2-5^{OE}*rcn1-6*
87	pGWB512-Flag-RCN1$^{396-588}$	GV3101	RGSpec	Complement PSR2-5^{OE}*rcn1-6*
88	pGWB515-3×HA-RCN1$^{396-588}$	GV3101	RGSpec	Complement PSR2-5^{OE}*rcn1-6*

R: rifampicin, K: kanamycin, G: gentamycin, Spec: spectinomycin, pGWB: improved Gateway Binary vector system

Table 2.3 *Saccharomyces cerevisiae* strain and plasmids used in this thesis research.

No.	Plasmid name	Strain	Medium	Purpose
1	AH109 empty	AH109	YPAD	Y2H
6	pGADT7 EV	AH109	SD^{Leu-}	Y2H
7	pGADT7-RCN1	AH109	SD^{Leu-}	Y2H
8	pGADT7-PDF1	AH109	SD^{Leu-}	Y2H
9	pGADT7-PDF2 (At1g13320.2)	AH109	SD^{Leu-}	Y2H
11	pGBKT7 EV	AH109	SD^{Trp-}	Y2H
12	pGBKT7-PSR2	AH109	SD^{Trp-}	Y2H

SD: synthetic dropout medium, YPAD: yeast extract-peptone-adenine-dextrose mediu

Table 2.4 *Arabidopsis thaliana* and *Nicotiana benthamiana* lines used in this study.

Plant name	Background	Gene/Locus	Selection	Source
A. t. WT	*A .t.* Col-0	—	Basta	In this study
PSR2-5^{OE}	*A .t.* Col-0	*P. sojae* Avh146	Basta	In this study
PSR2$^{\Delta LWY2\text{-}OE}$ (line 13)	*A .t.* Col-0	—	Basta	In this study
PSR2$^{\Delta LWY3\text{-}OE}$ (line 8-5)	*A .t.* Col-0	—	Basta	In this study
PSR2$^{\Delta LWY4\text{-}OE}$ (line s)	*A .t.* Col-0	—	Basta	In this study
PSR2$^{\Delta LWY6\text{-}OE}$ (line 30)	*A .t.* Col-0	—	Basta	Qiao et al. (2013)
RCN1-10-18^{OE}	*A .t.* Col-0	At1g25490	Basta	In this study
RCN1-10-14^{OE}	*A .t.* Col-0	At1g25490	Basta	In this study
RCN1-9-7^{OE}	*A .t.* Col-0	At1g25490	—	In this study
rcn1-6 (SALK_059903)	*A .t.* Col-0	At1g25490	—	In this study
pdf1-1 (CRISPR)	*A .t.* Col-0	At3g25800	Hyg	In this study
pp2ac1 (SALK_102599)	*A .t.* Col-0	At1g59830	—	Segonzac et al. (2014)
pp2ac2 (Ws insertion backcrossed into Col-0)	*A .t.* Col-0	At1g10430	—	Segonzac et al. (2014)
pp2ac3 (SAIL_182_A02)	*A .t.* Col-0	At2g42500	—	Segonzac et al. (2014)
pp2ac4 (SALK_035009)	*A .t.* Col-0	At3g58500	—	Segonzac et al. (2014)
pp2ac5 (SALK_013178)	*A .t.* Col-0	At1g69960	—	Segonzac et al. (2014)
PSR2-5^{OE}*rcn1-6*	*A .t.* Col-0	—	Basta	In this study
PSR2-5^{OE}*pdf1-1* (line 23)	*A .t.* Col-0	—	Hyg	In this study
PSR2-5^{OE}*pdf1-1* (line 26)	*A .t.* Col-0	—	Hyg	In this study
PSR2-5^{OE}*rcn1-6*RCN1	*A .t.* Col-0	—	Hyg	In this study
PSR2-5^{OE}*rcn1-6*RCN1$^{396\text{-}588}$	*A .t.* Col-0	—	Hyg	In this study
N. b. WT	*N. b.*	—	—	In this study
N. b. line 16C	*N. b.*	35S*::*GFP	—	Qiao et al. (2013)

WT: wild type, Hyg: hygromycin.

Table 2.5 Molecular cloning primers, sequencing primers, genotyping primers, RT-PCR primers, and probes used for this thesis research.

No.	Primer/probe name	Primer/probe sequence (5' -> 3')	Purpose
7	AD-PDF1_*Sma*I_F	TCCCCCGGGTATGTCTATGATCGA	Y2H cloning
8	AD-PDF1_*Xho*I_R	CCGCTCGAGTTAGCTAGACATCATCA	Y2H cloning
10	AD-PDF2_*Cla*I_R	CCATCGATTGTCTATGGTTGATGAGCC	Y2H cloning
11	AD-PDF2_*Cla*I_R	CCGCTCGAGTCATTTTGGCCACG	Y2H cloning
12	AD-RCN1_*Bam*HI_F	CGGGATCCTGGCTATGGTAGATGAAC	Y2H cloning
13	AD-RCN1_*Xho*I_R	CCGCTCGAGTCAGGATTGTGCTG	Y2H cloning
—	AtUBQ5_qPCR_F	TCTCCGTGGTGGTGGTAAG	(RT-)PCR
—	AtUBQ5_qPCR_R	GAACCTTTCCAGATCCATCG	(RT-)PCR
—	T7_F	TAATACGACTCACTATAGGGC	BD sequencing
20	AD-AGO1_*Cla*I_F	CCATCGATATGGTGAGAAAGAGAAGAACGG	Y2H cloning
21	AD-AGO1_*Xho*I_R	CCGCTCGAGTCAGCAGTAGAACAT	Y2H cloning
22	PDF2_mid2352_F	ATGAGGGAGAGTGACTTGGTTGATC	Sequencing
24	AGO1_mid2491_F	AGCTCCCAGTCAGGCAATCC	Sequencing
25	AGO1_mid3016_F	TATATTCCGGTGGGCCGGTC	Sequencing
26	AGO1_mid3685_F	ACTTCTCTGGCTTCTGTTGAGG	Sequencing
27	AGO1_mid4209_F	GGTTGGAGGAAGAAACACAGTGC	Sequencing
31	RCN1-RTPCR-F	CCGACGCCTGGATCGTGATTTGATTCGA	RT-PCR
32	RCN1-RTPCR-R	CAATTCAGGATTGTGCTGCTGTGGAACCA	RT-PCR
33	pEG101-YFP5'-R	GAACTTGTGGCCGTTTACGTCG	pEG101 seq.
34	BD-RCN1_*Eco*RI_F	CCGACGCCTGGATCGTGATTTGATTCGA	Y2H cloning
35	BD-RCN1_*Bam*HI_R	CAATTCAGGATTGTGCTGCTGTGGAACCA	Y2H cloning
36	3' AD seq_R	AGATGGTGCACGATGCACAG	AD sequencing
37	Salk_059903C LP_F	GGCCAGCCAGTTAGGTATAGG	Genotyping
38	Salk_059903C RP_R	AAACATAGCCACACGCATTTC	Genotyping
29	Salk_123484C LP_F	TCAATCCCTCAGCCAGATATG	Genotyping
40	Salk_123484C RP_R	CACTCGAGTGTTATCTTCGGC	Genotyping
—	CaMV 35S_F	CTCCTCGGATTCCATTGCC	Sequencing
41	LBb1.3	ATTTTGCCGATTTCGGAAC	Genotyping
42	Salk_132063 LP_F	CACAGACCGAAAGAGAAATCG	Genotyping
43	Salk_132063 RP_R	ACAACGGCTCATCGATCATAG	Genotyping
46	VYCE-RCN1_*Bam*HI_F	CGCGGATCCATGGCTATGGTAGAT	BiFC cloning
47	VYCE-RCN1_*Kpn*I_R	CGGGGTACCGGATTGTGCTGC	BiFC cloning
48	VYCE-PDF1_*Sal*I_F	ACGCGTCGACATGTCTATGATCGATG	BiFC cloning
49	VYCE-PDF1_*Kpn*I_R	CGGGGTACCGCTAGACATCATCAC	BiFC cloning
50	BD-PDF1_*Nco*I_F	CATGCCATGGTGTCTATGATCGATGAGC	Y2H cloning

Table 2.5 (Continued)

No.	Primer/probe name	Primer/probe sequence (5' -> 3')	Purpose
51	BD-PDF1_*Sma*I_R	TCCCCCGGGTTAGCTAGACATCATC	Y2H cloning
—	*Bam* PSR2-F	CGCGGATCCATGACACATGCT	BiFC cloning
54	VYNE-PSR2NLS_R	AACCTTACGCTTCTTTTTAGGCCCCCACCT	BiFC cloning
55	VYNE-PSR2nls_R	AACCTTACGCTTGTTTTTAGGCCCCCACCT	BiFC cloning
56	VYNE-AGO1_*Cla*I_F	CCATCGATATGGTGAGAAAGAGAAGAACGG	BiFC cloning
—	PSR2 Δ1-F	CCCAAAGCCCAAACGACTTTGA	Sequencing
59	BD-C1_*Eco*RI_F	CGGAATTCCCGTTAAACGGAGATCTCG	Y2H cloning
60	BD-C2_*Eco*RI_F	CGGAATTCCCGTCGAACGGAGATC	Y2H cloning
61	BD-C1C2_*Bam*HI_R	GCGGATCCTCACAAAAAATAATCAGGGG	Y2H cloning
62	BD-C3_*Nco*I_F	CATGCCATGGTGGGCGCGAATTCTATT	Y2H cloning
63	BD-C3_*Bam*HI_R	GCGGATCCTCACAGGAAATAGTCTGGAG	Y2H cloning
64	BD-C4_*Nco*I_F	CATGCCATGGTGGGCGCGAATTC	Y2H cloning
65	BD-C4_*Bam*HI_R	GCGGATCCTCAAAGGAAATAGTCAGGTGTC	Y2H cloning
66	BD-C5_*Nco*I_F	CATGCCATGGTGCCGCCGGC	Y2H cloning
67	BD-C5_*Bam*HI_R	GCGGATCCTTACAAAAAATAATCTGGAGTCTTGCGAGTGG	Y2H cloning
68	TskRCN1_*Eco*RI_F	CCGGAATTCGCTATGGTAGATGAACC	Tsk cloning
69	TskRCN1_*Spe*I_R	GGACTAGTTCAGGATTGTGCTGCTG	Tsk cloning
70	TskPDF1_*Sma*I_F	TCCCCCGGGATGTCTATGATCGATGA	Tsk cloning
71	TskPDF2_*Eco*RI_F	CCGGAATTCTCTATGGTTGATGAGCC	Tsk cloning
72	TskPDF1/2_*Spe*I_R	GGACTAGTTTAGCTAGACATCATCACATTGTC	Tsk cloning
73	AD-PiPSR2_*Eco*RI_F	CGGAATTCAACGATTCGCAGATTGTCGC	Y2H cloning
74	AD-PiPSR2_*Cla*I_R	CCATCGATTCACTGCCCGTATCTTTCCATATACTTG	Y2H cloning
75	BD-WNK4_*Eco*RI_F	CGGAATTCATGAATATGAATCAAGTTGCAGAGTATGT	Y2H cloning
76	BD-WNK4_*Bam*HI_R	CGGGATCCCTAGCGCCTTGAGCT	Y2H cloning
77	AD-C3_*Cla*I_F	CCATCGATTGGGCGCGAATTCTATTCC	Y2H cloning
78	AD-C4_*Cla*I_F	CCATCGATTGGGCGCGAATTCGCT	Y2H cloning
79	AD-C5_*Bam*HI_F	CGGGATCCTGCCGCCGGCGA	Y2H cloning
80	AD-C5_*Xho*I_R	CCGCTCGAGTTACAAAAAATAATCTGGAGTCTTGCG	Y2H cloning
81	BDΔ34Δ6_*Nco*I_fwd	CATGCCATGGCACATGCTCCTCCTAACG	Y2H cloning
82	ADΔ34Δ6_*Bam*HI_rev	CGGGATCCTTACCCCCACCTGACTTTG	Y2H cloning
83	WNK4_mid_F	TTGCCTCCGATGAGTCCTGG	Sequencing
84	1a-atgPDF1_*Kpn*I_F	GGGGTACCGAATGTCTATGATCGATGAGCCGT	ENTR1a cloning
85	1a-PDF1/2nostop_*Xho*I_R	CCGCTCGAGGCTAGACATCATCACATTGTCAATAG	ENTR1a cloning
86	PDF1-target 1_F	ATTGAGTACGGCGATTGGGTACAA	CRISPR
87	PDF1-target 1_R	AAACTTGTACCCAATCGCCGTACT	CRISPR
88	PDF1-target 2_F	ATTGTTAGTTAAGCGACTTGCCGC	CRISPR

Table 2.5 (Continued)

No.	Primer/probe name	Primer/probe sequence (5' -> 3')	Purpose
89	PDF1-target 2_R	AAACGCGGCAAGTCGCTTAACTAA	CRISPR
—	OCS-R	GGTTTGACCGGTTCTGCCG	pEG100 seq
—	SK-gRNA_F	CTCACTATAGGGCGAATTGG	CRISPR seq
90	RCN1-mid506_R	GTAGCCCGTAACTCAGTCTT	Sequencing
91	RCN1-mid1298_R	CCTATACCTAACTGGCTGGC	Sequencing
92	PDF2-mid201_F	GGCTATGGCGGAAGAGTTGG	Sequencing
93	PDF2-mid933_F	AAACCCTGAACTCGCTATCC	Sequencing
94	BD-PSR2_*Eco*RI_F	GGAATTCATGACACATGCTCCTC	Y2H cloning
95	BD-PSR2_*Bam*HI_R	CGGGATCCTTACCCCCACCTGA	Y2H cloning
96	VYCER-C2_*Spe*I_F	GGACTAGTATGCCGTCGAACGGAGATCTGG	BiFC cloning
97	VYCER-C2_*Kpn*I_R	GGGGTACCCAAAAAATAATCAGGGGTCTTCCG	BiFC cloning
98	VYCER-C3_*Spe*I_F	GGACTAGTATGGGCGCGAATTCTATTCCGACG	BiFC cloning
99	VYCER-C3_*Kpn*I_R	GGGGTACCCAGGAAATAGTCTGGAGTCCT	BiFC cloning
100	VYCER-C4_*Spe*I_F	GGACTAGTATGGGCGCGAATTCGCTTCCAA	BiFC cloning
101	VYCER-C4_*Kpn*I_R	GGGGTACCAAGGAAATAGTCAGGTGTCCTTCG	BiFC cloning
102	VYCER-C5_*Spe*I_F	GGACTAGTATGCCGCCGGCGACCG	BiFC cloning
103	VYCER-C5_*Kpn*I_R	GGGGTACCCAAAAAATAATCTGGAGTCTTGCGAGT	BiFC cloning
104	VYCER-PDF1_*Spe*I_F	GGACTAGTATGTCTATGATCGATGAGCCGTTGTACCC	BiFC cloning
105	VYCER-PDF1_*Kpn*I_R	GGGTACCGCTAGACATCATCACATTGTCAATAGATTGTAGA	BiFC cloning
106	VYCER-PDF2_*Spe*I_F	GGACTAGTATGTCTATGGTTGATGAGCCTTTATACCCG	BiFC cloning
107	VYCER-PDF2_*Kpn*I_R	GGGTACCGCTAGACATCATCACATTGTCAATAGATTGGAG	BiFC cloning
108	1a_RCN1_F_*Eco*RI	AGCGAATTCGCATGGCTATGGTA	ENTR1a cloning
109	1a_RCN1_R_*Xho*I	TATCTCGAGTGGGATTGTGCTGC	ENTR1a cloning
111	1a-atgC2_*Bam*HI_F	CGGGATCCGGATGCCGTCGAACGG	ENTR1a cloning
112	1a-C2nonstop_*Xho*I_R	CCGCTCGAGCAAAAAATAATCAGGGGTCTTCC	ENTR1a cloning
113	1a-atgC3_*Bam*HI_F	CGGGATCCGGATGGGCGCGAATTCT	ENTR1a cloning
114	1a-C3nonstop_*Xho*I_R	CCGCTCGAGCAGGAAATAGTCTGGAGTCCT	ENTR1a cloning
115	1a-atgC4_*Bam*HI_F	CGGGATCCGGATGGGCGCGAATTCG	ENTR1a cloning
116	1a-C4nonstop_*Xho*I_R	CCGCTCGAGAAGGAAATAGTCAGGTGTCCTTCG	ENTR1a cloning
117	1a-atgC5_*Bam*HI_F	CGGGATCCGGATGCCGCCGGC	ENTR1a cloning
118	1a-C5nonstop_*Xho*I_R	CCGCTCGAGCAAAAAATAATCTGGAGTCTTGCGA	ENTR1a cloning
119	1a-atgPDF2_*Kpn*I_F	GGGGTACCGAATGTCTATGGTTGATGAGCCTTTAT	ENTR1a cloning
120	PDF1_mid529_F	CCGATGGTAAGGAGAGCTGC	Sequencing
121	PDF2_mid2083_R	CAATCCCAATAACCTGGTTCAC	Sequencing
122	BiFC_35Sseq_F	TCCAACCACGTCTTCAAAGC	Sequencing
123	BiFC-CE_cVenus_R	GTGTTCTGCTGGTAGTGGTCG	Sequencing

Table 2.5 (Continued)

No.	Primer/probe name	Primer/probe sequence (5' -> 3')	Purpose
124	BiFC-NER/CER_seq_R	CATCGCAAGACCGGCAACAG	Sequencing
125	RSF/GEX- B´α_*Eco*RI_F	CGGAATTCATGTTTAAGAAGATCATGAAAGGGGCAAATCG	Pull-down cloning
126	RSF/GEX- B´α_*Xho*I_R	CCGCTCGAGCTAAGAAGTGATCATAGGATCTTCT	Pull-down cloning
127	RSF/GEX- B´γ_*Bam*HI_F	CGGGATCCATGATCAAACAGATATTTGGGAAATTGC	Pull-down cloning
128	RSF/GEX- B´γ_*Xho*I_R	CCGCTCGAGTCAACTACCCGAAGTTTTACC	Pull-down cloning
129	RSF/GEX- Bβ_ *Eco*RI _F	CGGAATTCATGAACGGTGGTGACGATGC	Pull-down cloning
130	RSF/GEX- Bβ_ *Xho*I _R	CCGCTCGAGTCATGCATAGTACATGTACAAGC	Pull-down cloning
131	GEX-atgPDF1_*Sma*I_F	TCCCCCGGGATGTCTATGATCGATGAGC	Pull-down cloning
132	GEX-PDF1stop_*Xho*I_R	CCGCTCGAGTTAGCTAGACATCATCACATTGTCAATAGATTGT	Pull-down cloning
—	ΔA_F	TCGGAAGCTTCCGCCGTTATG	Sequencing
—	Δ1_F	CCCAAAGCCCAAACGACTTTGA	Sequencing
—	Δ2_F	CCCGACGAGAAGACGACGGT	Sequencing
—	Δ5_R	GTTCGCCGTGTTGTACTTCTC	Sequencing
—	ΔB_R	GACGGGGGCTTTGTCGTTGAA	Sequencing
—	pENTR1a-F_321	CCTGTTAGTTAGTTACTTAAGC	1a sequencing
—	pENTR1a-R	GTAACATCAGAGATTTTGAGACA	Sequencing
—	pGEX-4T-2-F	ACGTATTGAAGCTATCCCAC	Sequencing
—	pGEX-4T-2-R	CCGGGAGCTGCATGTGTCAG	Sequencing
—	pRSFsumo-F	CAAGCTGATCAGACCCCTGAAG	Sequencing
—	pRSFsumo-R2	AGTGCGTAGTAGACGAGTCCAT	Sequencing
135	PDF1_mid_700R	GTTGGACACAATCCTGAGGCTC	Sequencing
136	PDF1_mid_1236R	CTCCAGTGTCTATCTTCAGCAAGT	Sequencing
137	B'α_mid_555F	GTTGCTGCTGAGATACATTGTTCC	Sequencing
138	B'γ_mid_368F	GAGACAGACTTTGCTTGAGCTTG	Sequencing
139	B' γ_mid_1295R	CTCTCCATAGCCGGGAACACAAT	Sequencing
140	Bβ_mid_362F	TCAGCCAGCTAATGGTGCATTG	Sequencing
141	Bβ_mid_1318R	GTGTCTGGATTTGCCTCCTCATC	Sequencing
142	PDF1_mid_1101F	GAAAGATGAGTTCCCGGATGTACG	Sequencing
143	CrisprPDF1_5'UTR_F	GTTGAGGTAAGACCCAATTTCC	CRISPR
144	CrisprPDF1_1stExon_R	CCTCAAACATGGACATAACGTC	CRISPR
149	CisprPDF1-lose56nt_F	TGAGCCGTTGTACCCAATCG	CRISPR
—	TskN3F-PDF1_XbaI_F	GCTCTAGAATGTCTATGATCGATGAGCCGTTGTACCCA	Tsk cloning
—	TskN3F-PDF1_NotI_R	ATAGTTTAGCGGCCGCTTAGCTAGACATCATCACATTGTCA ATAGATTGTA	Tsk cloning
145	RCN1 RT_F (665)	CTGTTGAAGGGTGTGCAGCTC	RT-PCR
146	RCN1 RT_CZ-R (1403)	CCAAACTCCTCTGCGAGGCGC	RT-PCR
147	PSR2 RT-PCR_F (633)	GCTGTCGAACAAGGAGAACC	RT-PCR

Table 2.5 (Continued)

No.	Primer/probe name	Primer/probe sequence (5' -> 3')	Purpose
148	PSR2 RT-PCR_R (1497)	CATCGTTTGTTCCTTGCCGGG	RT-PCR
150	Oligo(dT) 15+18	TTTTTTTTTTTTTTT(TTT)	RT
151	PSR2-RT-F	ACGAGGTTCTGTCGGGTATG	RT-PCR
152	PSR2-RT-R	GTCAAGCGATAGCAACGTGA	RT-PCR
—	BD-PSR2-*Eco*RI-F	GGAATTCATGACACATGCTCCTCCTAACGTT	Y2H cloning
—	BD-PSR2-*Bam*HI-R	CGGGATCCTTACCCCCACCTGACTTTGAA	Y2H cloning
153	BD-PSR2$^{\Delta N}$_*Eco*RI_F	CGGAATTCATGAAGCTTTTGAAGTGGGCGGATG	Y2H cloning
154	BD-ΔLWY7_*Bam*HI_R	CGGGATCCTTAGGCTTTGTCGTTGAACGC	Y2H cloning
155	1aRCN1$^{396-588}$_*Xho*I_R	CCGCTCGAGTCAGGATTGAGATAGTAGATCA	pENTR1a cloning
156	1aRCN1$^{1-397}$_*Bam*HI_F	CGGGATCCAATCCTTGTTACCGGCC	pENTR1a cloning
157	*rcn1-6* null RT_3'_F	GCCAAACTTCTGCAATCCCTCATC	RT-PCR
158	*rcn1-6* null CZ-qRT_F	AGCTCGGAGCCCTTTGCATGC	RT-PCR
159	*rcn1-6* null RT_5'_F	GCGCATGTTCTTCTTCCTCCTTTG	RT-PCR
160	*rcn1-6* null RT_5'_R	CTGCAAACCATTCACCACCCG	RT-PCR
161	*pdf1* null RT_5'UTR_F	GACATTTCGCCATTAGATCCTC	RT-PCR
162	*pdf1* null RT_5'_R	CACACCCAATTCTTCAGCCATT	RT-PCR
163	*pdf1* null CZ-qRT_3'F	TGCGTGCGGTGTCTCTTCTTG	RT-PCR
164	*pdf1* null CZ-qRT_3'R	AGCTCCACAAGCCCAGGACG	RT-PCR
165	ATG-Flag_F	ATGGACTACAAAGACGATGACGACAAAGAC	Genotyping
176	PSR2-A-Rev	CGCCTGCAGTTAGTCGGTCTGCGCGACCGA	Genotyping
166	*c1*_Salk102599C_LP	ACAGGTTTTCTGTTTGCATGG	Genotyping
167	*c1*_Salk102599C_RP	TCGATGCCTTATAACAACGAAG	Genotyping
168	*c3*_Sail182A02_CZ_LP	TTTCCATCGTTGAGATCTTGG	Genotyping
169	*c3*_Sail182A02_CZ_RP	CCATAACCAACTGGTGAGCTC	Genotyping
170	*c3*_Salk069250_LP	TAATTGGTATCAGGGCACTGC	Genotyping
171	*c3*_Salk069250_RP	TGTTTCCTGATCTGTTTTCCG	Genotyping
172	*c4*_Salk035009C_LP	GCTTGAAAGAACAGCATTTCG	Genotyping
173	*c4*_Salk035009C_RP	GTGGATTATCACCATCCATCG	Genotyping
174	*c5*_Salk013178C_LP	CTCTCGAACATATGTGCATGG	Genotyping
175	*c5*_Salk013178C_RP	CCATAAGCTGCTCGATCTGAC	Genotyping
177	LB3	TAGCATCTGAATTTCATAACCAATCTCGATACAC	Genotyping
—	QAt-UBIQ10 -F	AAATCTCGTCTCTGTTATGCTTAAGAAG	(RT)-PCR
—	QAt-UBIQ10 -R	AAAGAGATAACAGGAACGGAAACATAGT	(RT)-PCR
178	C2 (CZ)_qRT-PCR_F	TACCGGTGTGGAAACATGGCTGC	RT-PCR
179	C2 (CZ)_qRT-PCR_R	CGAGGAGCTGGATCGAACTGGA	RT-PCR
180	C5 (CZ)_qRT-PCR_F	CGTTGTGGCAACATGGCTGCG	RT-PCR

Table 2.5 (Continued)

No.	Primer/probe name	Primer/probe sequence (5' -> 3')	Purpose
181	C5 (CZ)_qRT-PCR_R	TGCGAGTGGTTTCGGGTTCGAC	RT-PCR
184	C1 (CZ)_qRT-PCR_F	ACAGATGTGGAAACATGGCCGCA	RT-PCR
185	C1 (CZ)_qRT-PCR_R	TGCGCGTGGTATCGGGTTCG	RT-PCR
186	C3 (CZ)_qRT-PCR_F	AAGTGCCCCATGAAGGGCCG	RT-PCR
187	C3 (CZ)_qRT-PCR_R	CCGGCACCCCGAGGAGAGAT	RT-PCR
188	C4 (CZ)_qRT-PCR_F	GCACCGAGGAGAGGAGAGCCA	RT-PCR
189	C4 (CZ)_qRT-PCR_R	CCGGAAGCTGCAGGAGGAGC	RT-PCR
192	PP2A-2_mid_F	GGAGGGCTTTCACCTTCTCTGGA	Sequencing
193	PP2A-3_mid_F	GGGAGACTATGTGGACCGTGGTT	Sequencing
194	PP2A-5_mid_F	GCTAATGTATGGAAGCACTTCACTGATC	Sequencing
197	GEX-RCN1_F_*Bam*HI	CGTGGATCCATGGCTATGGTAG	Pull-down cloning
198	GEX-RCN1_R_*Xho*HI	CGCTCGAGTTCAGGATTGTGCT	Pull-down cloning
201	*TAS1*-tasi255	TACGCTATGTTGGACTTAGAA	Northern probe
202	*TAS2*-tasi1511	AAGTATCATCATTCGCTTGGA	Northern probe
203	*TAS3*-5D8	AAAGGCCTTACAAGGTCAAGA	Northern probe
204	miR173	GTGATTTCTCTCTGTAAGCGA	Northern probe
205	miR393	GATCAATGCGATCCCTTTGGA	Northern probe
206	U6	AGGGGCCATGCTAATCTTCTC	Northern probe

Table 2.6 Western blotting antibodies used in this thesis research.

Antibody	Host	Company
Anti-DYKDDDDK (FLAG) Antibody	Mouse	Cat. # CL635691, Clontech
Monoclonal ANTI-FLAG M2-HRP antibody	Mouse	Cat. #A8592, Sigma
OctA-Probe Antibody (H-5)	Mouse	Cat. #sc-166355, Santa Cruz
Anti-HA High Affinity	Rat	Cat. # 11867423001, Roche
GST (Z-5)	Rabbit	Cat. #sc-459, Santa Cruz
His Tag HRP-conjugated Antibody	Mouse	Cat. #MAB050H, R&D Systems
Living Colors EGFP Monoclonal Antibody	Mouse	Cat. # 632569, Clontech
GFP Antibody (B-2)	Rabbit	Cat. # sc-9996, SantaCurz
c-Myc Monoclonal Antibody	Mouse	Cat. #631206, Clontech
AtAGO1 antibody	Rabbit	Cat. #AS09-527, Agrisera
PSR2-specific antiserum	Rabbit	—

2.4 Mass spectrometry-based proteomic analysis

Total protein was extracted from 1 g of agroinfiltrated *N. benthamiana* leaves using 1 mL extraction buffer {GTEN (10% [v/v] glycerol, 25 mM Tris-HCl pH 7.5, 1 mM EDTA, 150 mM NaCl) + 10 mM DTT + 0.1% Tween20 + 1×protease inhibitor cocktail (Sigma-Aldrich, Cat. #9599)]. The total protein extracts were incubated with the anti-Flag M2 affinity gel (Sigma-Aldrich, Cat. #A2220) overnight at 4°C with gentle rocking. The unbound proteins were washed out by washing with cold GTEN washing buffer (10% [v/v] glycerol, 25 mM Tris-HCl pH 7.5, 1 mM EDTA, 150 mM NaCl) for 5 times. Proteins bound with the anti-Flag affinity gel was eluted using elution buffer (0.1M glycine-HCl, pH 3.5). The IP products were then concentrated by StrataClean resin (Agilent Technologies, Cat. #400714) and analyzed by SDS-PAGE followed by colloidal coomassie gel staining (GelCode Blue Stain Reagent, Thermo Scientific, Cat. #24590) and silver staining (Pierce Silver Stain Kit, Thermo Scientific, Cat. #24612). IP products with good quality were then submitted to IIGB Proteomics Core at UC Riverside for mass spectrometry analysis. Briefly, the submitted IP products were digested using trypsin protease at 37°C overnight and then analyzed by LC-MS/MS. Both UPLC/Q-TOF-MS (Ultraperformance Liquid Chromatography coupled with Quadrupole Time of Flight Mass Spectrometry) and the next generation LTQ-Orbitrap Fusion LC/MS (ThermoFisher Scientific, Waltham, MA) were used in this research thesis. Protein identities were determined using the Mascot search engine against the *N. benthamiana* proteomic database (Boyce Thompson Institute for Plant Research, http://bti.cornell.edu/nicotiana-benthamiana/).

2.5 Phylogenetic analysis

PP2A amino acid sequences of *N. benthamiana* and *A. thaliana* Col-0 were obtained from BTI website (http://bti.cornell.edu/ nicotiana-benthamiana/) and TAIR website (https://www.arabidopsis.org/), respectively. The sequence alignments were then used for phylogenetic reconstruction for each of the PP2A gene families by the Maximum Likelihood method using MEGA6 software (Tamura et al., 2013). While generating phylogenetic trees in MEGA6, the Jones-Taylor-Thornton substitution model was selected for calculating probabilities of change along branches. The reliability of branches was inferred from a bootstrap analysis of 100 replicates in a partial deletion mode. The rest of the parameters used in MEGA6 were set to default.

2.6 Yeast-two-hybrid (Y2H)

The Y2H assay was performed using *Saccharomyces cerevisiae* strains AH109. The yeast media preparation, growth, transformation and selection of transformants were performed as described in the manufacturer's instruction (Matchmaker GAL4 Two-Hybrid System 3, Clontech, #PT3247-1). AH109 was co-transformed with pGBKT7 and pGADT7 constructs expressing the protein pairs of interest. Six colonies obtained on each transformant-selecting plate lacking tryptophan and leucine ($SD^{Trp-Leu-}$) were re-suspended in water and plated on 1) a new $SD^{Trp-Leu-}$ medium, 2) the $SD^{Trp-Leu-His-}$ medium lacking tryptophan, leucine, and histidine, and 3) the $SD^{Trp-Leu-His-Ade-}$ medium lacking tryptophan, leucine, histidine, and adenine. Note that the $SD^{Trp-Leu-His-}$ medium was supplemented with 1–10 mM of 3-AT for suppressing leaky *HIS3* (the histidine

biosynthesis gene) expression. Cell growth was recorded after incubation for 2–3 days at 30 °C.

2.7 Co-immunoprecipitation (Co-IP)

Co-IP constructs were made using pTsk108-N3F and pENTR1a entry vectors, followed by pEarleyGate and pVYNE/pVYCE destination vectors. Agrobacteria harboring each of the bait and prey plasmids at OD_{600} 0.8 were co-infiltrated into *N. benthamiana* leaves. Total protein was extracted from 2 g of agroinfiltrated leaves using 1 mL extraction buffer {GTEN (10% [v/v] glycerol, 25 mM Tris-HCl pH 7.5, 1 mM EDTA, 150 mM NaCl) + 10 mM DTT + 2% [w/v] PVPP + 0.1% Tween20 + 1×protease inhibitor cocktail (Sigma-Aldrich, Cat. #9599)}. Both anti-Flag M2 affinity gel (Sigma-Aldrich, Cat. #A2220) and Pierce anti-HA agarose (Thermo Scientific, Cat. #26181) were used for IP. After an overnight incubation at 4°C with gentle rocking, the beads were washed 3–5 times with cold GTEN washing buffer. The proteins were eluted using 2×SDS loading buffer [0.125M Tris-HCl (pH6.8), 10% (v/v) β-meracptoethanol, 4% (w/v) SDS, 20% (v/v) glycerol, 0.04% (w/v) bromophenol blue] and boiled for 5 min. The presence of specific proteins in the immunocomplex was detected by western blotting where different antibodies were used accordingly. The antibody information of this thesis research can be found in **Table 2.6**.

2.8 Pull-down-based competition assay

GST pull-down method was applied for the PSR2-ATB′α competition assay. The procedures were followed according to the manufacturer's instructions (Thermo Scientific, Cat. #21516). Briefly, pull-down constructs were made using the pGEX-4T-2 (GST tag) and the pRSFDuet-1 (His-SUMO tag) vectors. Fusion proteins of pGEX-4T-2 and pRSFDuet-1 constructs were produced in *E.coli* BL21-RIL cells upon IPTG chemical induction, and the supernatant of cell lysate was obtained by sonication for the following pull-down assay. TKET buffer with 200 mM NaCl was used throughout the pull-down experiment as extraction, incubation, and washing buffer. After a 2-hour incubation at 4°C with gentle rocking followed by a 2 washes, GST-fusion protein (RCN1-GST) was purified by Pierce Glutathione Agarose (Thermo Scientific, Cat. #16100). The His-SUMO-fusion proteins (His-SUMO-ATB′α) were than incubated with the beads with or without the presence of His-SUMO-PSR2 (the competitor). After an overnight incubation at 4°C with gentle rocking, the beads were washed 3–5 times and the proteins were eluted using 2×SDS loading buffer [0.125M Tris-HCl (pH6.8), 10% (v/v) β-meracptoethanol, 4% (w/v) SDS, 20% (v/v) glycerol, 0.04% (w/v) bromophenol blue] and boiled for 5 min. Anti-GST and anti-His antibodies were used in western blotting for protein detection.

2.9 Bimolecular fluorescence complementation (BiFC)

For BiFC assay, I used the BiFC vectors described previously (Waadt et al., 2008). Briefly, the coding sequences of PSR2 and AGO1 were sub-cloned into the pVYNE vector to generated PSR2-nVenus and AGO1-nVenus, respectively. The coding

sequences of PP2A A subunits and PP2A C subunits were amplified by PCR and cloned into the pVYCE or pVYCE(R) vectors to generate the cVenus C′ and N′ fusion proteins. These constructs were transformed into *A. tumefaciens* GV3101 and the bacterial culture at OD_{600} 0.1 was used to infiltrate *N. benthamiana* leaf epidermal cells. After co-infiltration of desired combinations of Venus fusion proteins for 2 days, the fluorescent images of infiltrated leaves were acquired using a Leica SP5 confocal microscope with 400 Hz scan speed in 512×512 or 1024×1024 pixel formats. Image stacks were acquired at 1-μm optical sections. For imaging BiFC fluorescence, an excitation wavelength of 514 nm was used, and 526–600 nm emissions were collected. Unless otherwise noted, all images were presented as maximum projections of the z stack generated using Leica LAS AF software.

2.10 Subcellular localization analysis

The subcellular localization of PP2A A subunit (RCN1) and PSR2 were examined by infiltrating *A. tumefaciens* GV3101 carrying either pEG101-RCN1-YFP or pEG102-PSR2-CFP into *N. benthamiana* leaf epidermal cells. For co-expression, equal volumes of two construct-bearing strains were mixed together and then infiltrated into *N. benthamiana* leaf epidermal cells. All bacterial cultures at OD_{600} 0.1 were used for infiltration. The protein expression was visualized by a Leica SP5 confocal microscope with 400 Hz scan speed in 512×512 or 1024×1024 pixel formats. Image stacks were acquired at 1-μm optical sections. An excitation wavelength of 514 nm was used for RCN1-YFP imaging, and 526–616 nm emissions were collected. For visualization of

PSR2-CFP, an excitation wavelength of 458 nm was used, and emissions were collected between 442–526 nm. To avoid crosstalk between the fluorescence channels, sequential scanning was used for co-expression of RCN1-YFP and PSR2-CFP. Unless otherwise noted, all images were presented as maximum projections of the z stack generated using Leica LAS AF software.

2.11 Arabidopsis T-DNA insertion mutant genotyping

Genotyping of Arabidopsis T-DNA insertion SALK lines were followed according to the online website "T-DNA Primer Design" (http://signal.salk.edu/tdnaprimers.2.html) provided by Salk Institute Genomic Analysis Laboratory. Briefly, LP (left genomic primer) and RP (right genomic primer) specific to individual SALK line, and the LBb1.3 (left border primer of the T-DNA insertion, 5′-ATTTTGCCGATTTCGGAAC-3′) were used for genotyping PCR. Wild-type plants with no insertion were expected to have PCR amplicons about 900−1100 bps (from LP to RP). Homozygous mutants with insertions in both chromosomes were expected to have amplicons size of 410+N bps (from RP to insertion site 300+N bases, plus 110 bases from LBb1.3 to the left border of the vector). Heterozygous mutants with insertion into only one chromosome were expected to have both PCR bands. Not that the *pp2ac3* mutant used in this study was a SAIL line that the LB3 (5′-TAGCATCTGAATTTCATAACCAATCTCGATACAC-3′) instead of LBb1.3 was used as the left border primer of the T-DNA insertion for genotyping. Two ubiquitin genes, UBQ5 and UBQ10, were used as internal controls for genomic DNA PCR.

2.12 Agrobacterium-mediated plant transformation

Agrobacterium-mediated plant transformation technique was used to in this thesis research for making transgenic Arabidopsis overexpressing exogenous genes. *A. tumefaciens* carrying the desired construct was grown overnight at 28°C in 250 mL of LB supplement with antibiotics. The fresh culture was pelleted and re-suspended in 60 mL of transformation solution [Murashige and Skoog (MS) medium, pH 5.7, 5% (w/v) sucrose, 0.4% (w/v) Silwet L-77]. Next, the floral dip method was used for Arabidopsis transformation (Clough & Bent, 1998). Plants with numerous immature floral buds and few siliques were inoculated by immersing the immature floral buds into the *A. tumefaciens* solution for 10 mins. Inoculated plants were kept at dark for 36 hours and moved to the growth room with 12h light/12h dark at 23−25°C. Seeds of the inoculated plants were harvested about 3 weeks after transformation, and the potential transformants were screened by selecting the survival seedlings on MS phytagel plates [4.41g/L MS (MP Biomedicals, Cat. #0926231) pH5.7, 3% (w/v) sucrose, 0.4% (w/v) phytagel] supplemented with Bayer's Basta (phosphinothricin glufosinate) or hygromycin (30 mg/L).

2.13 Generation of pdf1 CRISPR mutant

YAO promoter-driven CRISPR/Cas9 system (Yan et al., 2015) was used in this study to generate the *pdf1* CRISPR mutants in Arabidopsis. The guide RNA targeting to the first exon of *PDF1* gene was designed using "Optimized CRISPR Design−MIT" website (http://crispr.mit.edu/). DNA of the guide RNA sequence (5'-

AGTACGGCGATTGGGTACAA-3') was cloned into AtU6-26-sgRNA-SK entry vector (the guide RNA cassette), and then was sub-cloned into pCAMBIA1300-pYAO:Cas9 destination vector (the plant transformation cassette) through recombination. The final construct carrying both guide RNA and *Cas9* gene was delivered into *A. tumefaciens* for Arabidopsis plant transformation. Plant transformants expressing guide RNA and Cas9 were selected using MS phytagel plates supplement with hygromycin (30 mg/L). The genomic edited sites were confirmed by sequencing analysis. Plant transformants with 56-nt deletion of *PDF1* genes (*pdf1-1*) were maintained several generations until the homozygous mutant lines were obtained.

2.14 Small RNA Northern blotting

Probes used in this thesis research are listed in **Table 2.5**. Small RNA Northern blotting was carried out as described previously (Pall & Hamilton, 2008, Li & Zamore, 2018). Briefly, total RNAs of Arabidopsis with different genotypes were extracted from 0.1 g leaves using the TRIzol reagent (Invitrogen). For Northern blotting assay, each lane of the denaturing urea-PAGE was loaded with 4 μg of total RNAs. Small RNA probes were labeled with [^{32}P]-dCTP using T4 polynucleotide kinase kit (Thermo Scientific). The hybridization results were visualized using the Typhoon 9410 PhosphorImager, and the radioactive signals were quantified using the ImageQuant TL software package (version 7.0, GE Healthcare Life Sciences). Relative expression levels of small RNA species were obtained by normalizing the scanned densities of each band to the U6 internal control.

2.15 Phytophthora strain and zoospore preparation

Phytophthora capsici isolate LT263 was used for the infection assay in this thesis research. Zoospores of *P. capsici* were induced as described previously (Wang et al., 2013, Xiong et al., 2014). Briefly, a piece of mycelial plug (5 mm) from pure culture of LT263 was inoculated onto V8 agar [10% (v/v) clear V8 juice (Campbell Soup Co., Camden, NJ, U.S.A.), 0.02% CaCO3, and 2% agar], and incubated in darkness at room temperature (RT) for 4 days. The mycelial plugs from the margin of the fresh 4-day-old growing colony were further isolated in a new petri-dish with 10% V8 broth and incubated in darkness at RT for 2 days. Next, the LT263 culture was starved by replacing 10% V8 broth with sterile tap water (refreshed once every 30 min up to four times), and incubate in darkness at RT for 1.5 days. To induce the sporangium development, the LT263 culture was transferred to a constant light condition at RT for 1 day. To release the zoospores, a cold shock treatment was used by incubating the LT263 culture in 4 °C fridge for 30-60 mins. Finally, the zoospores were filtered through one layer of Miracloth (pore size: 20–25 μm, EMD Millipore, Cat. #475855-1R), and the desired concentrations of zoospores was adjusted for infection assays.

2.16 Phytophthora capsici-Arabidopsis infection assay

A detached leaf infection assay was used in this study to determine the disease susceptibility of Arabidopsis with different genotypes. Arabidopsis were grown under the conditions described previously with a single seedling growing in a pot, and the 4-week-old plants with good health condition were used for infection. Each plant contributes 3

detached leaves (usually the 4^{th}, 5^{th}, and 6^{th} leaf from the top) for examining susceptibility. Note that the age of leaf matters resistance a lot that old leaves are more susceptible, while young leaves are more resistant.

In each experiment, 12−30 adult leaves from 4−10 plants of each genotype were placed up-side-down on the 0.8% water agar plate, and each leaf was inoculated with 10 μL of zoospore suspension (approximate 10^5 zoospores/mL) as a droplet on the abaxial side. The plates were wrapped with Parafilm and incubated in darkness at RT for 2−4 days, and the disease severity could be evaluated any time during incubation (usually 2 dpi, 3 dpi, and 4 dpi). Note that the disease progression dynamics and the recording timing may not be the same in different sets of experiments.

Using disease severity index (DSI) with the scale from 0 to 3, the infection area of leaf was measured visually based on the following criteria: Leaves with no visible disease symptoms or only small necrotic flecks restricted to the inoculation area were scored as DSI 0. A DSI score of 1 has the water soaking-like lesion spreading from the inoculation spot but only covering less than 50% of the leaf. A DSI score of 2 has the water soaking-like lesion covers 50% to 75% of the leaf. A DSI score of 3 has a completely wilted and fully infected leaf. The total DSI of total infected leaves were show in the stacked bar graph in all the results. To compare DSI from different groups of plants with statistical analysis, the mean DSI of each plant was calculated according to a modified version of equation described previously (Wang et al. 2013).

$$\text{Mean DSI of each plant} = \frac{\{\sum_{\text{index no.}} [(\text{index no.}+1)\times(\text{amount of leaves in each index})]\}}{\text{Total amount of leaves } (3\ \textit{leaves each plant})}$$

2.17 Statistical analysis

All *Phytophthora* infection data are presented as mean ± S.E.M. Statistical tests were conducted using Prism 7. All the experiments were performed in parallel with both control and experimental genotypes. Differences between means of two groups were evaluated for statistical significance with unpaired t test and for different groups with parametric one-way ANOVA followed by *post-hoc* Tukey's test.

Chapter III

RESULTS

3.1 Systematic proteomics analysis of PSR2-associated complexes in plants

To elucidate the molecular mechanism by which PSR2 suppresses RNA silencing and promotes infection, I aim to identify its target cellular machineries in plants. A previous study shows that synthetic small RNA oligos that are 21 nt in length cannot be bound to PSR2 *in vitro* (Qiao et al., 2013), suggesting that PSR2 may target to proteins that function in regulating plant RNA silencing and defense responses. To identify the PSR2-associated proteins, I performed a systemic proteomic analysis using immunoprecipitation (IP) followed by mass spectrometry.

To study the PSR2 interactome *in planta*, the very first step is to exogenously express *Phytophthora* PSR2 in plants for isolating interacting proteins (**Figure 3.1**), I used *Nicotiana benthamiana* for this analysis given its well-established Agrobacterium-mediated transient gene expression method. The transient expression of target gene(s) can be achieved using Agroinfiltration, by which the engineered plant bacterial pathogen *Agrobacterium tumefaciens* utilizes its T-DNA transfer machinery to insert target gene(s) into plant genome for protein expression. Using this system, 3×Flag-PSR2 (pEG100-3×Flag-PSR2 was cloned by Dr. Qin Xiong) was transiently expressed in *N. benthamiana* leaves and the PSR2-associated protein complexes were then immunoprecipitated (Xiong et al., 2014).

1. Clone target genes into the protein expression vectors and transform them into *Agrobacterium*.

2. Agro-infiltration

3. Protein expression in *Nicotiana benthatmiana*

4. Total protein extraction from the agro-infiltrated leaves

5. Immunoprecipitation (IP)

6. IP product analyses

7. PSR2 potential target identification

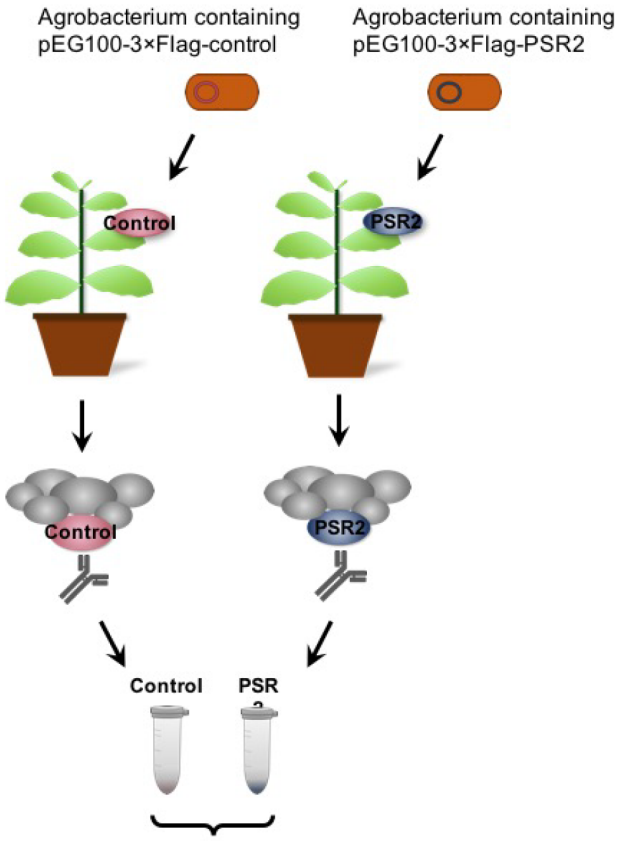

A. SDS-PAGE analysis

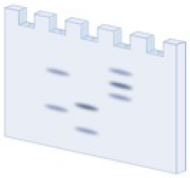

B. LC/MS analysis and protein identification against *N. benthamiana* proteomics database

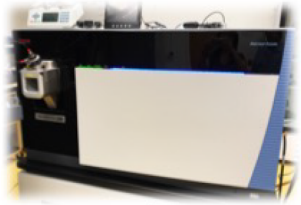

Blast the protein hits to Arabidopsis proteomic database

Figure 3.1. A flow chart of proteomics analysis of PSR2-associating protein complexes in plants. 3×Flag-PSR2 and controls (empty vector and 3×Flag-HopZ1a^{C216A}) are transiently expressed in *N. benthamiana* by Agroinfiltration. Total proteins are immunoprecipitated using anti-Flag resin followed by either SDS-PAGE analysis or LC/MS analysis.

IP products were firstly visually inspected by SDS/PAGE followed by both colloidal coomassie G-250 gel staining and silver staining (**Figure 3.2A**). One extra band with the size between 55~70 kDa was observed exclusively in the PSR2 sample, but not in the empty vector (EV) control and the HopZ1a^{C216A} control, a non-related bacterial effector mutant (**Figure 3.2A and B**). Western blot was also performed to evaluate the IP quality by showing the bait proteins, 3×Flag-PSR2 and 3×Flag- HopZ1a^{C216A}, had been successfully immunoprecipitated (**Figure 3.2C**). These results indicated the existence of potential PSR2-associated protein(s) with the size between 55~70 kDa in plants.

To reveal the identity of the PSR2-associated protein(s), IP products were further analyzed by mass spectrometry conducted by Dr. Songqin Pan at the IIGB Proteomics Core at UC Riverside. Specifically, Ultraperformance Liquid Chromatography coupled with Quadrupole Time of Flight Mass Spectrometry (UPLC/Q-TOF-MS) was used, and protein identities of top candidates were determined by the Mascot search engine against the *N. benthamiana* proteomic database (Boyce Thompson Institute for Plant Research, http://bti.cornell.edu/nicotiana-benthamiana/) (**Figure 3.1**). Whole set of mass spectrometry-based IP proteomic screening was repeated twice. Around 47~120 protein hits were found in each sample, and around 35~40 protein hits were found specifically in PSR2-expressing samples but not in the controls.

3.2 PP2As are the most enriched hits in the PSR2-associated protein complexes

Mascot search engine uses scoring algorithm for protein identification and provide a ranking for the protein hits. The mass spectrometry data indicated potential PSR2-

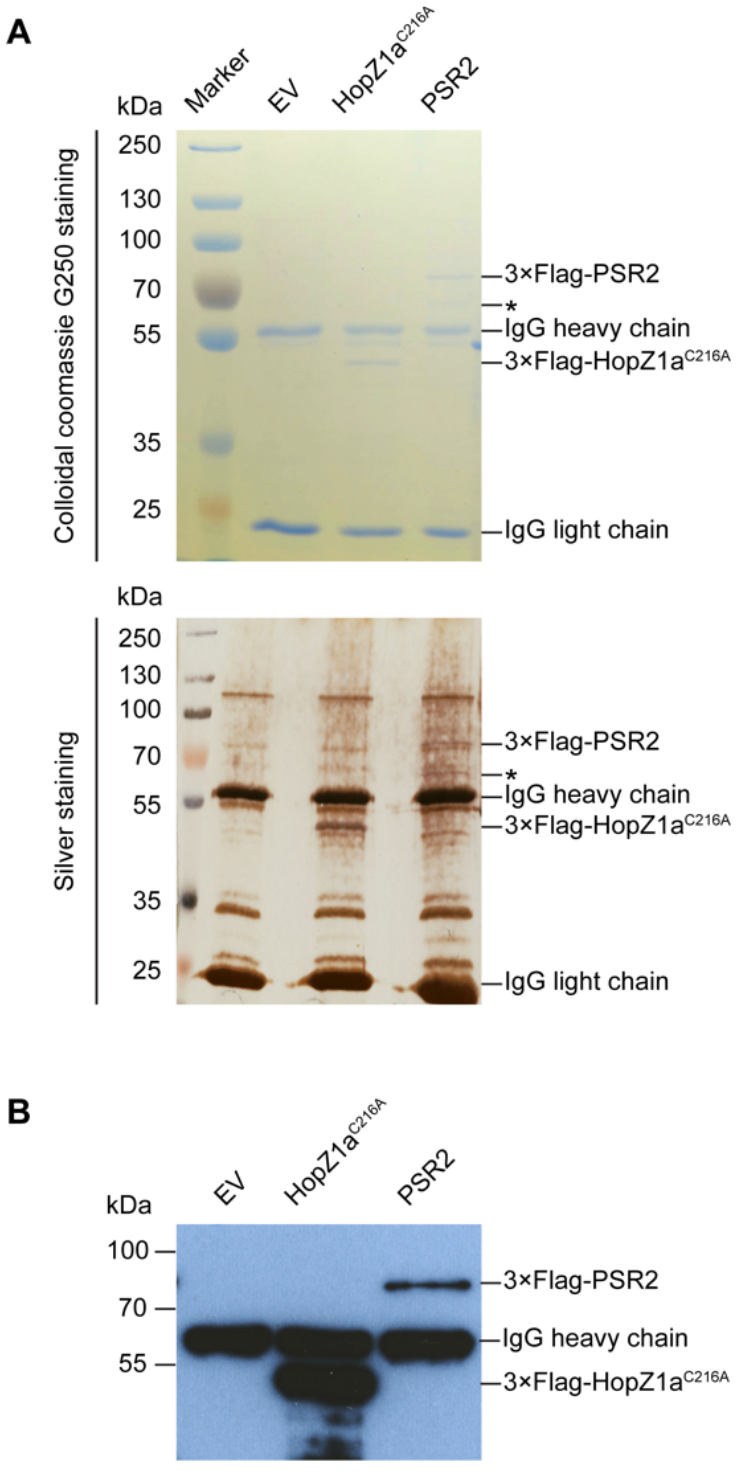
A
Marker
EV
HopZ1a^C216A
PSR2
kDa
250
130
100
70
55
35
25
Colloidal coomassie G250 staining
3×Flag-PSR2
*
IgG heavy chain
3×Flag-HopZ1a^C216A
IgG light chain
kDa
250
130
100
70
55
35
25
Silver staining
3×Flag-PSR2
*
IgG heavy chain
3×Flag-HopZ1a^C216A
IgG light chain
B
EV
HopZ1a^C216A
PSR2
kDa
100
70
55
3×Flag-PSR2
IgG heavy chain
3×Flag-HopZ1a^C216A

Figure 3.2. Candidate protein(s) with the size between 55~70 kDa were observed in the immunocomplexes of PSR2. (A-B) Analysis of IP products from *N. benthamiana* leaves transiently expressing indicated proteins using SDS-PAGE followed by either colloidal coomassie G-250 gel staining (A) or silver staining (B) showed candidate PSR2-associating protein(s) with molecular mass of 55~70 kDa (indicated by *) were present in the immunocomplexes of PSR2, but not empty vector or HopZ1a^{C216A} controls. **(C)** Western blot analysis confirmed the presence of the baits proteins (3×Flag-PSR2 and 3×Flag- HopZ1a^{C216A}) with their expected sizes in corresponding IP products.

associated proteins included serine/threonine protein phosphatase 2As (PP2As), serine/threonine mitogen-activated protein kinase (MAPK), glycolate oxidase, helicase, methyltransferases, aminotransferases, auxin-induced proteins, pentatricopeptide repeat protein, calmodulin-binding transcription activator, and heat shock protein 70s. (**Table 3.1**). Among all the possible candidates, PP2As are the most enriched in the PSR2-associated protein complexes in both replicates (**Table 3.1** and **3.2**).

The top three PSR2-interacting protein hits (NbS00006732g0010.1, NbS00023637g0006.1, and NbS00031201g0004.1) were found to be the A subunits of PP2A, also known as the PP2A scaffolding subunits and the PP2A 65kDa regulatory subunits, consistent with the potential protein candidates with the size range of 55~70 kDa observed in the PSR2 IP products (**Figure 3.2** and **Table 3.2**). These hits also showed high Mascot score 1672~394 and high sequence coverage 52%~17%. In addition, four PP2A catalytic subunits (NbS00009650g0005.1, NbS00043074g0007.1, NbS00007440g0018.1, and NbS00010634g0008.1) were also present in PSR2-containing protein complex with 143~62 of Mascot score and 16%~9% of sequence coverage (**Table 3.2**). To sum up, a total of seven PSR2-specific protein hits were identified as PP2A components.

Protein composition of PSR2-immunoprecipitated complexes was further analyzed using the next generation LTQ-Orbitrap Fusion mass spectrometer (ThermoFisher Scientific, Waltham, MA). With a better resolution and accuracy in detecting protein sequences and abundancy, LTQ-Orbitrap Fusion identified 213 hits in PSR2-associated protein complexes, around three times more than the original dataset. In addition to the

previously-identified PP2A hits, five more PP2A catalytic subunits (NbS00020903g0004.1, NbS00024071g0014.1, NbS00040706g0007.1, NbS00013026g0010.1, and NbS00051180g0008.1) were found to associate with PSR2 (**Table 3.1** and **Figure 3.3**).

In these mass spectrometry-based IP proteomic analyses, PP2As were identified as the most enriched proteins in the PSR2-associated complexes. Interestingly, there was no B subunit detected in the PSR2-containg complexes, and all the PP2A hits were annotated as PP2A A or C subunits that themselves can form the PP2A core enzymes.

Table 3.1 List of potential PSR2-associated proteins identified by UPLC/Q-TOF-MS in *N. benthamiana*.

Nb accession number	Best match in *At*	Description
Serine/Threonine protein phosphatase 2A		
NbS00006732g0010.1	At3g25800	Protein phosphatase 2A subunit A2, PP2AA2, PDF1, PR 65
NbS00023637g0006.1	At1g13320	Protein phosphatase 2A subunit A3, PP2AA3, PDF2, PR 65
NbS00031201g0004.1	At3g25800	Protein phosphatase 2A subunit A2, PP2AA2, PDF1, PR 65
NbS00010634g0008.1	At2g42500	Protein phosphatase 2A catalytic subunit, protein phosphatase 2A-3, PP2A-3
NbS00009650g0005.1	At3g58500	Protein phosphatase 2A catalytic subunit, protein phosphatase 2A-4, PP2A-4
NbS00043074g0007.1	At3g58500	Protein phosphatase 2A catalytic subunit, protein phosphatase 2A-4, PP2A-4
NbS00020903g0004.1	At3g58500	Protein phosphatase 2A catalytic subunit, protein phosphatase 2A-4, PP2A-4
NbS00007440g0018.1	At1g10430	Protein phosphatase 2A catalytic subunit, protein phosphatase 2A-2, PP2A-2
NbS00040706g0007.1	At1g10430	Protein phosphatase 2A catalytic subunit, protein phosphatase 2A-2, PP2A-2
NbS00013026g0010.1	At1g10430	Protein phosphatase 2A catalytic subunit, protein phosphatase 2A-2, PP2A-2
NbS00051180g0008.1	At1g10430	Protein phosphatase 2A catalytic subunit, protein phosphatase 2A-2, PP2A-2
Serine/Threonine protein kinase		
NbS00024829g0011.1	At5g58350	Serine/threonine-protein kinase WNK4, NN mitogen-activated protein kinase
Others		
NbS00024535g0016.1	At3g14420	Glycolate oxidase, GOX1
NbS00008446g0012.1	At2g46020	ATP-dependent helicase BRM-like, ATBRM
NbS00004699g0014.1	At1g60710	ATB2, auxin-induced protein PCNT115-like isoform 1
NbS00009622g0021.1	At1g60710	ATB2, auxin-induced protein PCNT115-like isoform 1
NbS00044823g0005.1	At5g49910	Heat shock protein 70-7, HSC70-7; chloroplast heat shock protein 70-2, CPHSC70-2
NbS00005376g0008.1	At5g09590	Heat shock protein 70-5, HSC70-5; mitochondrial heat shock protein 70-2, MTHSC70-2
NbS00029684g0026.1	At4g24280	Chloroplast heat shock protein 70-1, CPHSC70-1
NbS00019758g0008.1	At2g13360	Alanine/Glyoxylate aminotransferase 1, AGT1, Hop-interacting protein THI032
NbS00027670g0006.1	At4g37930	Serine hydroxymethyltransferase 1, SHMT1
NbS00003479g0020.1	At5g54160	catechol O-methyltransferase, caffeate O-methyltransferase 1, ATCOMT1
NbS00005326g0011.1	At1g70580	Alanine aminotransferase, AOAT2
NbS00006727g0004.1	At4g24580	Rho GTPase activation protein, RhoGAP; ROP1 enhancer 1, REN1
NbS00013248g0016.1	At5g02830	Pentatricopeptide repeat-containing protein, tetratricopeptide repeat-like superfamily protein
NbS00036257g0003.1	At1g67310	Calmodulin-binding transcription activator
NbS00010795g0010.1	At2g18880	Vernalization insensitive 3-like protien, VIN3-like 3, VIL3

Table 3.2 Mass spectrometry table of PSR2-associated PP2As identified in *N. benthamiana*.

Nb accession number	Nominal mass (Mr)	UPLC/Q-TOF-MS replicates	Mascot ranking	Mascot score	Matches	Seq.	EmPAI	Seq. coverage	Full length amino acid sequence and the matched peptides (in bold)
NbS00006732g0010.1	53625	1st	1 (out of 60)	1188	35(27)	17(15)	3.71	48%	M**AMVDEPLYPIAVLIDELKNDDIQLR**LNSIR**RLSTIAR**ALGEERTRKELI PFLSENNDDDDEVLLAMAEELGVFIPYVGGVEHAHVLLPPLETLCTVEET CR**LAAGEWFTAR**VSACGLFHIAYSSAPEMLKAELRSIYNQLCQDDMPMVR RSAATNLGK**FAATVESTYLKSDIMSIFDDLTQDDQDSVR**LLAVEGCAALG KLLEPQDCVAHILPVIVNFSQELSSDSSQHVR**SALASVIMGMAPVLGKDA TIEHLLPIFLSLLKDEFPDVR**LNIISK**LDQVNQVIGIDLLSQSLLPAIVE LAEDRHWR**VRLAIIEYIPLLASQLGIGFFDDKLGALCMQWLQDKVYSIRD AAANNLKR**LAEEFGPEWAMQHIIPQVLDMTTSPHYLYR**MTILRAISLLAP VMGSEITCSK**LLPVVITATK**DRVPNIKFNVAK**VLQSLIPIVDHSVVEKTV RPSLVELAEDPDVDVRFYANQALQSIDNVMMSG**
		2nd	1 (out of 86)	1672	46(36)	18(15)	4.63	52%	M**AMVDEPLYPIAVLIDELKNDDIQLR**LNSIR**RLSTIAR**ALGEERTRKELI PFLSENNDDDDEVLLAMAEELGVFIPYVGGVEHAHVLLPPLETLCTVEET CR**LAAGEWFTAR**VSACGLFHIAYSSAPEMLKAELRSIYNQLCQDDMPMVR **RSAATNLGKFAATVESTYLKSDIMSIFDDLTQDDQDSVR**LLAVEGCAALG KLLEPQDCVAHILPVIVNFSQELSSDSSQHVR**SALASVIMGMAPVLGKDA TIEHLLPIFLSLLKDEFPDVRLNIISKLDQVNQVIGIDLLSQSLLPAIVE LAEDR**HWRVRLAIIEYIPLLASQLGIGFFDDKLGALCMQWLQDKVYSIRD AAANNLKR**LAEEFGPEWAMQHIIPQVLDMTTSPHYLYR**MTILRAISLLAP VMGSEITCSK**LLPVVITATKDRVPNIK**FNVAK**VLQSLIPIVDHSVVEKTV RPSLVELAEDPDVDVRFYANQALQSIDNVMMSG**
NbS00023637g0006.1	66386	1st	2 (out of 60)	618	18(14)	10(6)	0.47	17%	TTDQSSDQTSATLIPLIASPVRISLSHTHTQRIPFRCLAFDILVSRTFFP YFLYLEVQVFSRFVFYKLHHIITYNMLTSGISTLQEAMSVVDEPLYPIAV LIDELKNEDIQLRLNSIR**RLSTIAR**ALGEERTRKELIPFLSENNDDDDEV LLAMAEELGVFIPYVGGVEHASVLLPPLEGLCSVEETCVREKAVESLCRI GSQMRESDLVESFIPLVKR**LAAGEWFTAR**VSSCGLFHIAYPSAPEPLKNE LRTIYSQLCQDDMPMVRRAAATNLGKFAATIEQPHLK**TDIMSMFETLTQD DQDSVR**LLAVEDCAALGKLLEPKDCVAQILPVIVNFAQELSSDSSQHVRS ALASVIMGMAPILGK**DATIEQLLPIFLSLLKDEFPDVR**LNIISK**LDQVNQ VVGIDLLSQSLLPAIVELAEDRHWR**VRLAIIEYIPLLASQLGVGFFDDKL GALCMQWLKDKVYSIRDAAANNVKRLAEEFGPTWAMEHIIPQVLDMINDP HYLYRMTILHAISLLAPVMGSEITCSKLLPVVITASKDRVPNIKFNVAKV LQSLIPIVEQSVVETTIRPCLVELSEDPDVDVR**FFANQALQATK**
		2nd	2 (out of 86)	621	21(14)	9(6)	0.54	23%	TTDQSSDQTSATLIPLIASPVRISLSHTHTQRIPFRCLAFDILVSRTFFP YFLYLEVQVFSRFVFYKLHHIITYNMLTSGISTLQEAMSVVDEPLYPIAV LIDELKNEDIQLRLNSIR**RLSTIAR**ALGEERTRKELIPFLSENNDDDDEV LLAMAEELGVFIPYVGGVEHASVLLPPLEGLCSVEETCVREKAVESLCRI GSQMRESDLVESFIPLVKR**LAAGEWFTAR**VSSCGLFHIAYPSAPEPLKNE LRTIYSQLCQDDMPMVRRAAATNLGK**FAATIEQPHLKTDIMSMFETLTQD DQDSVR**LLAVEDCAALGKLLEPKDCVAQILPVIVNFAQELSSDSSQHVR**S ALASVIMGMAPILGK**DATIEQLLPIFLSLLKDEFPDVRLNIISK**LDQVNQ VVGIDLLSQSLLPAIVELAEDR**HWRVRLAIIEYIPLLASQLGVGFFDDKL GALCMQWLKDKVYSIRDAAANNVKR**LAEEFGPTWAMEHIIPQVLDMINDP HYLYR**MTILHAISLLAPVMGSEITCSKLLPVVITASK**DRVPNIK**FNVAKV LQSLIPIVEQSVVETTIRPCLVELSEDPDVDVR**FFANQALQATK**

Table 3.2 (Continued)

Nb accession number	Nominal mass (Mr)	UPLC/Q-TOF-MS replicates	Mascot ranking	Mascot score	Matches	Seq.	EmPAI	Seq. coverage	Full length amino acid sequence and the matched peptides (in bold)
NbS00031201g0004.1	63099	1st	3 (out of 60)	418	15(10)	10(5)	0.36	22%	MKNIKRGNNNFIKSTGISRSFPSSPTTDQSSDQTSATLIRLIASPTSISTLQKTMSMVDEPLYPIAVLIDELKNEDIQLRLNSI**RRLSTI**ARALGEERTRKELIPFLSENNDDDDEVLLAMAEELGVFIPYVGGVEHASVLLPPLEGLCSVEETCVREKAVESLCRIGSQMRESDLVESFIPLVKRLAAG**EWFTARV**SSCGLFHIAYPSAPEPLKNELRTIYSQLCQDDMPMVRRAAATKLGKFAATIEQPHLKTDIMSMFETLTQDGMVFSFCAHQDSVRLLAVEDCAALGKLLEPKDCVAQILPVIVNFAQELSSDSSQHVRSALASVIMGMAPILG**KDATIEQLLPIFLSLLKDEFPDVRL**NIIS**KLDQVNQVVGIDLLSQSLLPAIVELAEDRHWRV**RLAIIEYIPLLASQLGVGFFDDKLGALCMQWLKDKVYSIRDAAANNVK**RLAEEFGPTWAMEHIIPQVLDMINDPHYLYRM**TILHAISLLAPVMGSEITCSKLLPVIITASKDRVPNIKFNVAKVLQSLIPIVEQSVVETTIRPCLVELSEDPDVDV**RFFANQALQATK**
		2nd	3 (out of 86)	394	19(10)	9(5)	0.36	22%	MKNIKRGNNNFIKSTGISRSFPSSPTTDQSSDQTSATLIRLIASPTSISTLQKTMSMVDEPLYPIAVLIDELKNEDIQLRLNSI**RRLSTIAR**ALGEERTRKELIPFLSENNDDDDEVLLAMAEELGVFIPYVGGVEHASVLLPPLEGLCSVEETCVREKAVESLCRIGSQMRESDLVESFIPLVKR**LAAGEWFTAR**VSSCGLFHIAYPSAPEPLKNELRTIYSQLCQDDMPMVRRAAATKLGK**FAATIEQPHLK**TDIMSMFETLTQDGMVFSFCAHQDSVRLLAVEDCAALGKLLEPKDCVAQILPVIVNFAQELSSDSSQHVR**SALASVIMGMAPILGK**DATIEQLLPIFLSLLKDEFPDVRLNIISK**LDQVNQVVGIDLLSQSLLPAIVELAEDR**HWRVRLAIIEYIPLLASQLGVGFFDDKLGALCMQWLKDKVYSIRDAAANNVKR**LAEEFGPTWAMEHIIPQVLDMINDPHYLYR**MTILHAISLLAPVMGSEITCSK**LLPVIITASKDRVPNIK**FNVAKVLQSLIPIVEQSVVETTIRPCLVELSEDPDVDVR**FFANQALQATK**
NbS00007440g0018.1	29081	1st	13 (out of 60)	143	2(1)	2(1)	0.24	12%	MPSNADVDRQIEQLMECKPLAEAEVKILCDQARAILVEEWNVQPVKCPVTVCGDIHGQFYDLIELFRIGGNAPDTNYLFMGDYVDRGYYSVETVTLLVALKVRYRDRITILRGNHESRQITQVYGFYDECLRK**YGNANVWK**YFTDLFDYLPLTALIESQIFCLHGGLSPSLDTLDNIRSLDRIQEVPHEGPMCDLLWSDPDDRCGWGISPR**GAGYTFGQDIASQFNHTNGLTLISR**AHQLVMEGFNWCQDKNVVT
		2nd	Not detected						
NbS00010634g0008.1	35748	1st	28 (out of 60)	71	2(1)	2(1)	0.19	9%	MSSSDLVAASTQGNLDEQISQLMQCKPLSEPDVRTLCEKAKEILMEESNVQPVKSPVTICGDIHGQFHDLAELFRIGGQCPDTNYLFMGDYVDRGYYSVETVTLLVALKVRYPQRLTILRGNHESRQITQVYGFYDECLRK**YGNANVWK**TFTDLFDYFPLTALVESEIFCLHGGLSPSIETLDNVRSFDRVQEVPHEGAMCDLLWSDPDDRCGWGMSPR**GAGYTFGQDISEQFHQTNNLK**LIARAHQLVMEGYNWSHEQKVVTIFSAPNYCYRCGNMASILEVDDCRGHTFIQFDPAPRRGEPDVTRRTPDYFL
		2nd	Not detected						

Table 3.2 (Continued)

Nb accession number	Nominal mass (Mr)	UPLC/Q-TOF-MS replicates	Mascot ranking	Mascot score	Matches	Seq.	EmPAI	Seq. coverage	Full length amino acid sequence and the matched peptides (in bold)
NbS00009650g0005.1	35947	1st	36 (out of 60)	62	4(1)	3(1)	0.3	10%	MDPVPSSASHGNLDEQIAQLMQCKPLSEQEVRGLCEKAKEILMEESNVQP VKSPVTICGDIHGQFHDLAELFRIGGKCPDTNYLFMGDYVDRGYYSVETV TLLVALKVRYPQRITILRGNHESRQITQVYGFYDECLRK**YGNANVWK**TFT DLFDYFPLTALVESEIFCLHGGLSPSIETLDNIRNFDRVQEVPHEGAMCD LLWSDPDDRCGWANEAFCYLVNELQQDISEQFNHTNNLKLIAR**AHQLVME GFNWAHDQK**VVTIFSAPNYCYRCGNMASILEVDDSRER**TFIQFEPAPR**RG EPDVTRRTPDYFL
		2nd	16 (out of 86)	130	7(3)	5(3)	0.42	16%	MDPVPSSASHGNLDEQIAQLMQCKPLSEQEVRGLCEKAK**EILMEESNVQP VK**SPVTICGDIHGQFHDLAELFRIGGKCPDTNYLFMGDYVDRGYYSVETV TLLVALK**VRYPQR**ITILRGNHESRQITQVYGFYDECLRKYGNANVWKTFT DLFDYFPLTALVESEIFCLHGGLSPSIETLDNIRNFDRVQEVPHEGAMCD LLWSDPDDRCGWANEAFCYLVNELQQDISEQFNHTNNLKLIAR**AHQLVME GFNWAHDQK**VVTIFSAPNYCYRCGNMASILEVDDSRER**TFIQFEPAPRRG EPDVTR**RTPDYFL
NbS00043074g0007.1	35447	1st	Not detected						
		2nd	43 (out of 86)	69	5(1)	4(1)	0.31	13%	MSLDPVVSSQGNLDEQIAQLMQCKPLSEQEVRGLCGKAK**EILMNESNVQP VK**SPVTICGDIHGQFHDLAELFRIGGKCPDTNYLFMGDYVDRGYYSVETV TLLVALK**VRYPQR**ITILRGNHESRQITQVYGFYDECLRKYGNANVWKTFT DLFDYFPLTALVESEIFCLHGGLSPSIETLDNIRNFDRVQEVPHEGAMCD LLWSDPDDRCGWGISPRGAGYTFGQDISEQFNHTNNLKLIAR**AHQLVMEG FNWAHDQK**VVTIFSAPNYCYRCGNMASILEVDDCNGHTFIQFEPAPR**RGE PDVTR**RTPDYFL

3.3 PP2A in N. benthamiana and Arabidopsis

After identifying the potential plant targets of PSR2, I shifted the research system from *N. benthamiana* to Arabidopsis given that *Arabidopsis thaliana* ecotype Col-0 is the most wildly used plant research model with lots of tools and information for the following mechanistic study. In Arabidopsis, PP2A A subunits are encoded by three genes (RCN1, PDF1, and PDF2), B subunits are encoded by 17 genes, and C subunits are encoded by five genes (PP2AC1, PP2AC2, PP2AC3, PP2AC4, and PP2AC5). The gene information and the isoform structure of Arabidopsis PP2A A and C subunits are shown in **Table 3.3** and **Figure 3.3,** respectively.

The Arabidopsis homologs of the PSR2-associated PP2A hits were identified using NCBI BLAST protein browser (Basic Local Alignment Search Tool, https://blast.ncbi.nlm.nih.gov/Blast.cgi). All the BLAST results were listed in **Table 3.1**. The top three protein hits of A subunits were blasted to Arabidopsis PDF1 (also known as PP2AA2) and PDF2 (also known as PP2AA3). Other catalytic subunits hits were blasted to three of the five Arabidopsis PP2A C subunits: PP2A-3 (also known as PP2AC3), PP2A-4 (also known as PP2AC4), and PP2A-2 (also known as PP2AC2).

Table 3.3 Gene information of *Arabidopsis thaliana* PP2A A and C subunits.

Gene name	Locus number	Protein size (a.a.)	cDNA size (bp)	Database
PP2AA1 (RCN1)	AT1G25490	588	1767	TAIR
PP2AA2 (PDF1)	AT3G25800	587	1764	TAIR
PP2AA3 (PDF2)	AT1G13320	587	1764	TAIR
PP2AC1 (PP2A-1)	AT1G59830	306	921	TAIR
PP2AC2 (PP2A-2)	AT1G10430	306	921	TAIR
PP2AC3 (PP2A-3)	AT2G42500	313	942	TAIR
PP2AC4 (PP2A-4)	AT3G58500	313	942	TAIR
PP2AC5 (PP2A-5)	AT1g69960	307	924	TAIR

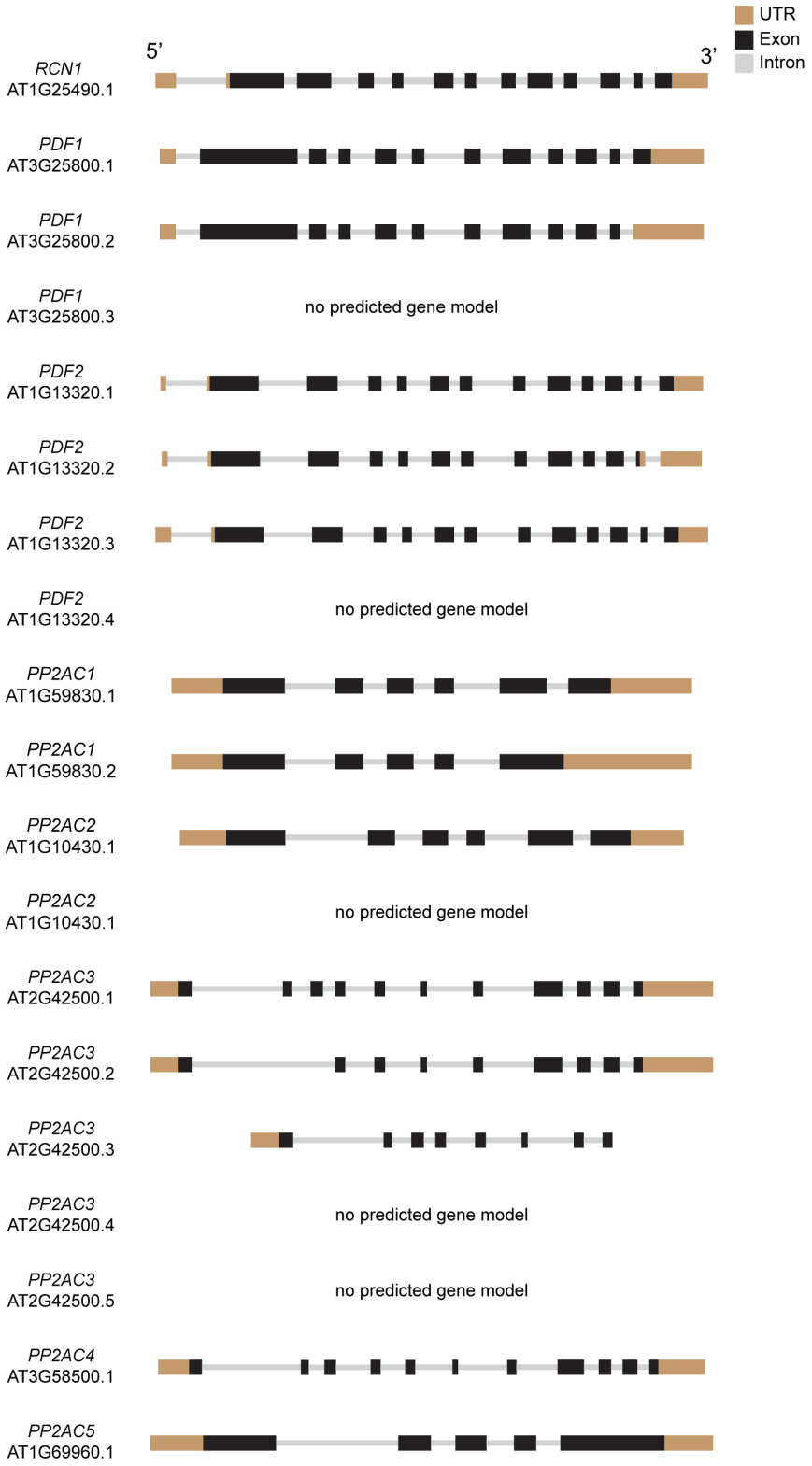
UTR
Exon
Intron
5’
3’
RCN1
AT1G25490.1
PDF1
AT3G25800.1
PDF1
AT3G25800.2
PDF1
AT3G25800.3
no predicted gene model
PDF2
AT1G13320.1
PDF2
AT1G13320.2
PDF2
AT1G13320.3
PDF2
AT1G13320.4
no predicted gene model
PP2AC1
AT1G59830.1
PP2AC1
AT1G59830.2
PP2AC2
AT1G10430.1
PP2AC2
AT1G10430.1
no predicted gene model
PP2AC3
AT2G42500.1
PP2AC3
AT2G42500.2
PP2AC3
AT2G42500.3
PP2AC3
AT2G42500.4
no predicted gene model
PP2AC3
AT2G42500.5
no predicted gene model
PP2AC4
AT3G58500.1
PP2AC5
AT1G69960.1

Figure 3.3. Gene structures and isoforms for Arabidopsis PP2A A and C subunits. Schematics of all the gene structures and isoforms for PP2A A and C subunits. Brown boxes represent untranslated regions (UTR). Black boxes represent exons and gray boxes represent introns. The gene name and the locus number of each subunit are also provided, where RCN1, PDF1, and PDF2 belong to A subunits, while PP2AC1, PP2AC2, PP2AC3, PP2AC4, and PP2AC5 belong to C subunits.

To better understand the molecular evolution relationship between the Arabidopsis PP2As and the PP2A hits from the mass spectrometry data, a phylogenetic analysis was performed using MEGA6 phylogenetic software (**Figure 3.4**) (Tamura et al., 2013). PP2A amino acid sequences of *N. benthamiana* and Arabidopsis used for establishing the phylogenetic tree were obtained from the BTI proteomics database and TAIR (The Arabidopsis Information Resource, https://www.arabidopsis.org/), respectively. PP2A subunits are encoded by gene families, a group of genes generally share similar biochemical functions. Three PP2A A subunits (RCN1, PDF1, and PDF2) had been identified in Arabidopsis (Farkas et al., 2007, Uhrig et al., 2013). BLAST results showed the top three protein hits of A subunits (NbS00006732g0010.1, NbS00023637g0006.1, and NbS00031201g0004.1) were the homologs of Arabidopsis PDF1 and PDF2 (**Table 3.1**). Phylogenetic analysis also suggested these protein hits are evolutionary similar to PP2A A subunits (**Figure 3.4**).

Five different PP2A catalytic subunits (PP2AC1/C2/C3/C4/C5) have been identified in Arabidopsis, where they were divided into two clades (Farkas et al., 2007, Uhrig et al., 2013). One is the PP2AC3/C4 clade. Catalytic subunit hits identified from the original UPLC/Q-TOF-MS analyses (NbS00010634g0008.1, NbS00043074g0007.1, and NbS00009650g0005.1) and one additional hit identified by the LTQ-Orbitrap Fusion (NbS00020903g0004.1) were in this clade. The other clade includes PP2AC1, PP2AC2, and PP2AC5. One catalytic subunit hit (NbS00007440g0018.1) of the original data and four additional hits (NbS00024071g0014.1, NbS00040706g0007.1,

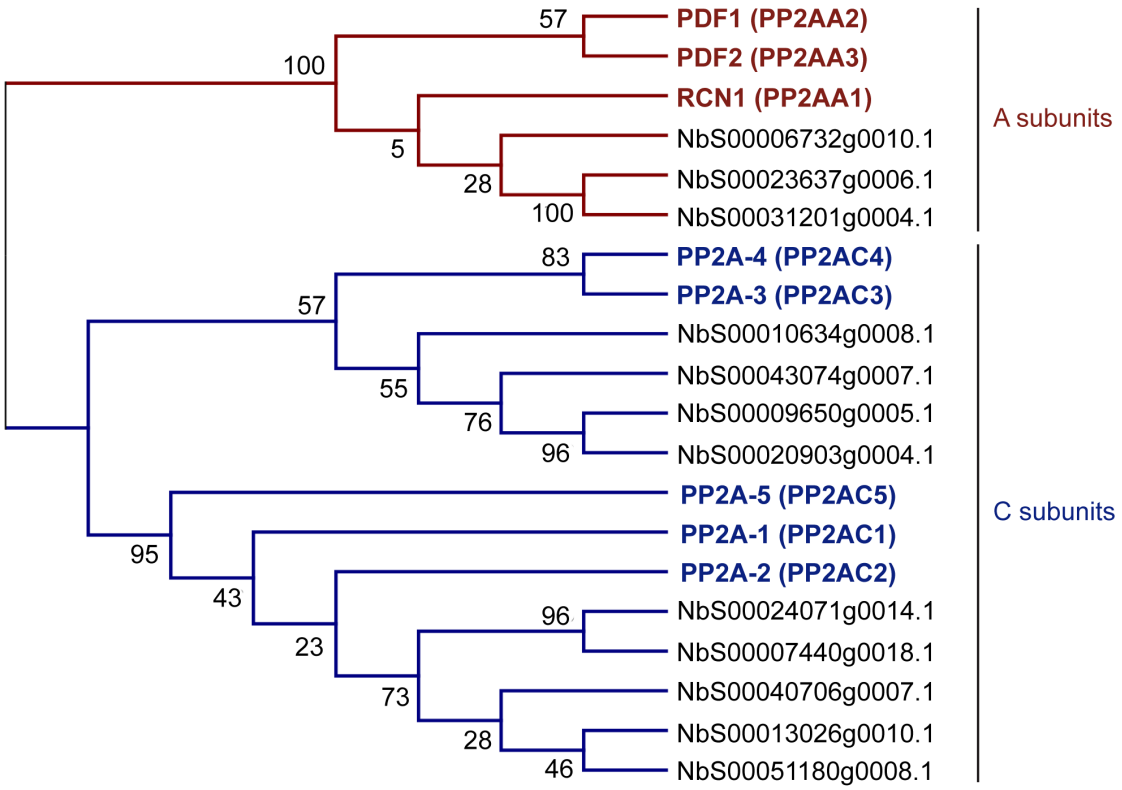

Figure 3.4. Phylogenetic analysis of PP2A A and C subunits. The phylogenetic tree of PP2A amino acid sequences of *N. benthamiana* mass spectrometry hits (*Nb* accession numbers) and all Arabidopsis PP2A As and Cs (in bold) was constructed in the MEGA6 software using Maximum Likelihood methods. The numbers shown at the branches of the phylogenetic tree were bootstrap numbers. Three Arabidopsis PP2A A subunits (RCN1, PDF1, and PDF2) are shown in red and five PP2A C subunits (including PP2AC1-C5) are shown in blue.

NbS00013026g0010.1, and NbS00051180g0008.1) of the LTQ-Orbitrap Fusion data belonged to this clade, where they cluster with Arabidopsis PP2AC2.

Altogether, this phylogenetic analysis provides a candidate list of PP2A A and C subunits in Arabidopsis that are evolutionary close to the PP2A hits found in PSR2-containing protein complexes in *N. benthamiana*. To study how different PP2A subunits are involved in PSR2-mediated regulations, the Arabidopsis PP2A homologs were used afterwards to confirm protein-protein interactions with PSR2 and the functional assays. In this following sections, protein-protein interactions between the A subunits of Arabidopsis PP2As and PSR2 were confirmed using yeast-two-hybrid (Y2H), co-immunoprecipitation (co-IP), and bimolecular fluorescence complementation (BiFC).

3.4 PSR2 interacts with A subunits, RCN1 and PDF1, in yeast

Y2H is a robust and popular tool for identifying protein-protein interactions; thus, this *in vivo* yeast-based system was firstly performed to test PSR2 interactions with the three PP2A A subunits. RCN1, PDF1, and PDF2 were cloned into AD vector (pGADT7) to express the PP2A fusions of GAL4 activating domain; while PSR2 was cloned into BD vector (pGBKT7) to express the PSR2 fusion of GAL4 binding domain (pGBKT7-PSR2 was cloned by Dr. Yongli Qiao) (**Figure 3.5A**). Both AD and BD plasmids were co-transformed into yeast strain AH109 and the protein interactions were determined by the growth of transformed yeast on Synthetic Dropout (SD) media.

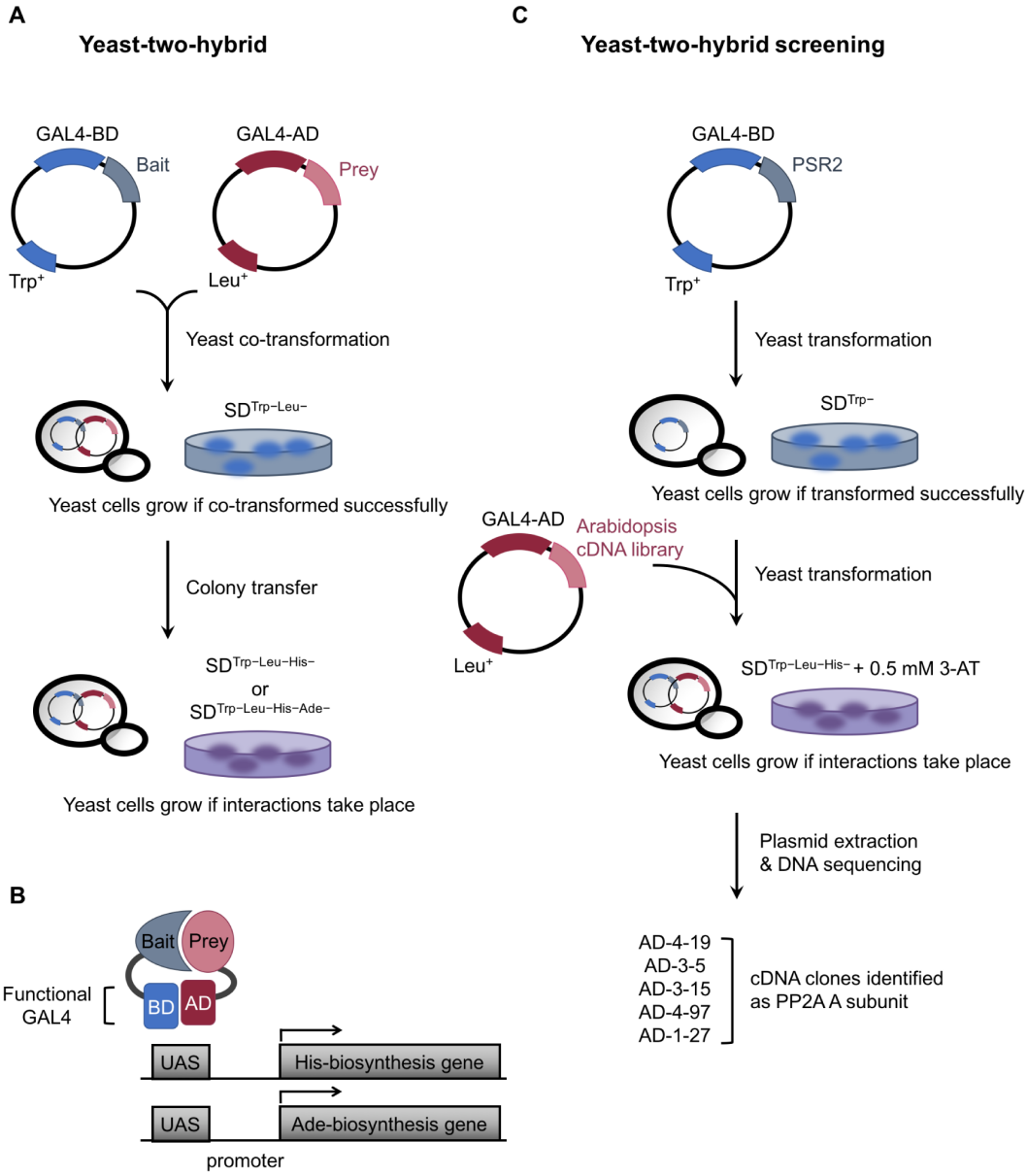
A
Yeast-two-hybrid
GAL4-BD
Bait
Trp+
GAL4-AD
Prey
Leu+
Yeast co-transformation
SDTrp−Leu−
Yeast cells grow if co-transformed successfully
Colony transfer
SDTrp−Leu−His−
or
SDTrp−Leu−His−Ade−
Yeast cells grow if interactions take place
B
Bait
Prey
Functional
GAL4
BD
AD
UAS
His-biosynthesis gene
UAS
Ade-biosynthesis gene
promoter
C
Yeast-two-hybrid screening
GAL4-BD
PSR2
Trp+
Yeast transformation
SDTrp−
Yeast cells grow if transformed successfully
GAL4-AD
Arabidopsis
cDNA library
Leu+
Yeast transformation
SDTrp−Leu−His− + 0.5 mM 3-AT
Yeast cells grow if interactions take place
Plasmid extraction
& DNA sequencing
AD-4-19
AD-3-5
AD-3-15
AD-4-97
AD-1-27
cDNA clones identified
as PP2A A subunit

Figure 3.5. Schematic diagrams showing the yeast-two-hybrid (Y2H) based protein-protein interaction assay, as well as genome-wide screening assay. (A, C) cDNA of targeted proteins (A) or genome-wide Arabidopsis cDNA library (C) were cloned into the GAL4-AD vector as preys; whereas PSR2 was cloned into the GAL4-BD vector as a bait. Both bait and prey plasmids were introduced by transformation into yeast reporter strain AH109 either simultaneously (A) or sequentially (C). Successful yeast co-transformants were selected by $SD^{Trp-Leu-}$ medium and the protein-protein interactions were examined by $SD^{Trp-Leu-His-}$ and $SD^{Trp-Leu-His-Ade-}$ selective media. **(B)** A schematic diagram showing the interaction between bait and prey proteins allows the formation of functional GAL4 transcription factor, as well as the expressions of His- and Ade-biosynthesis genes.

The nutrient-deficient $SD^{Trp-Leu-}$ medium selected yeast tranformants carrying both the AD and BD plasmids, since they carry marker genes producing tryptophan and leucine, respectively (**Figure 3.5A**). The selective media, $SD^{Trp-Leu-His-}$ and $SD^{Trp-Leu-His-Ade-}$, selected positive protein-protein interactions. When interaction takes place, binding between two proteins brings their GAL4 fusion domains, AD and BD, close enough to form a functional GAL4 transcription factor (**Figure 3.5B**). Such functional GAL4 activates reporter gene expression (the histidine and adenine-biosynthesis genes) in yeast, allowing the yeast cell to produce histidine and adenine and survive from the selection.

The Y2H results showed that PSR2 interacted with two of the Arabidopsis PP2A A subunits, RCN1 and PDF1. Yeast cells of PSR2/RCN1 and PSR2/PDF1 samples successfully grew on both $SD^{Trp-Leu-His-}$ and $SD^{Trp-Leu-His-Ade-}$ plates (**Figure 3.6A**). No cell from the negative controls grew on the selective media, except the BD-EV/AD-RCN1 sample (**Figure 3.6A bottom**). I noted that there was a mild self-activation activity in yeasts carrying AD-RCN1 and BD empty vector on $SD^{Trp-Leu-His-}$ medium in the presence of 1 mM of 3-Amino-1,2,4-triazole (3-AT), which suppresses leaky *HIS3* (the histidine biosynthesis gene) expression had been added. However, the results using $SD^{Trp-Leu-His-Ade-}$ medium still suggested that RCN1 and PSR2 interact in yeast.
In contrast to RCN1 and PDF1, PDF2 showed no interaction with PSR2 in this assay (**Figure 3.6A**). The AD-PDF2 showed positive interaction with other proteins in other Y2H experiments done in our lab (data not shown, data of Dr. Xiaoren Chen), suggesting that the AD-PDF2 has protein expression in yeast. Thus, the negative interaction between

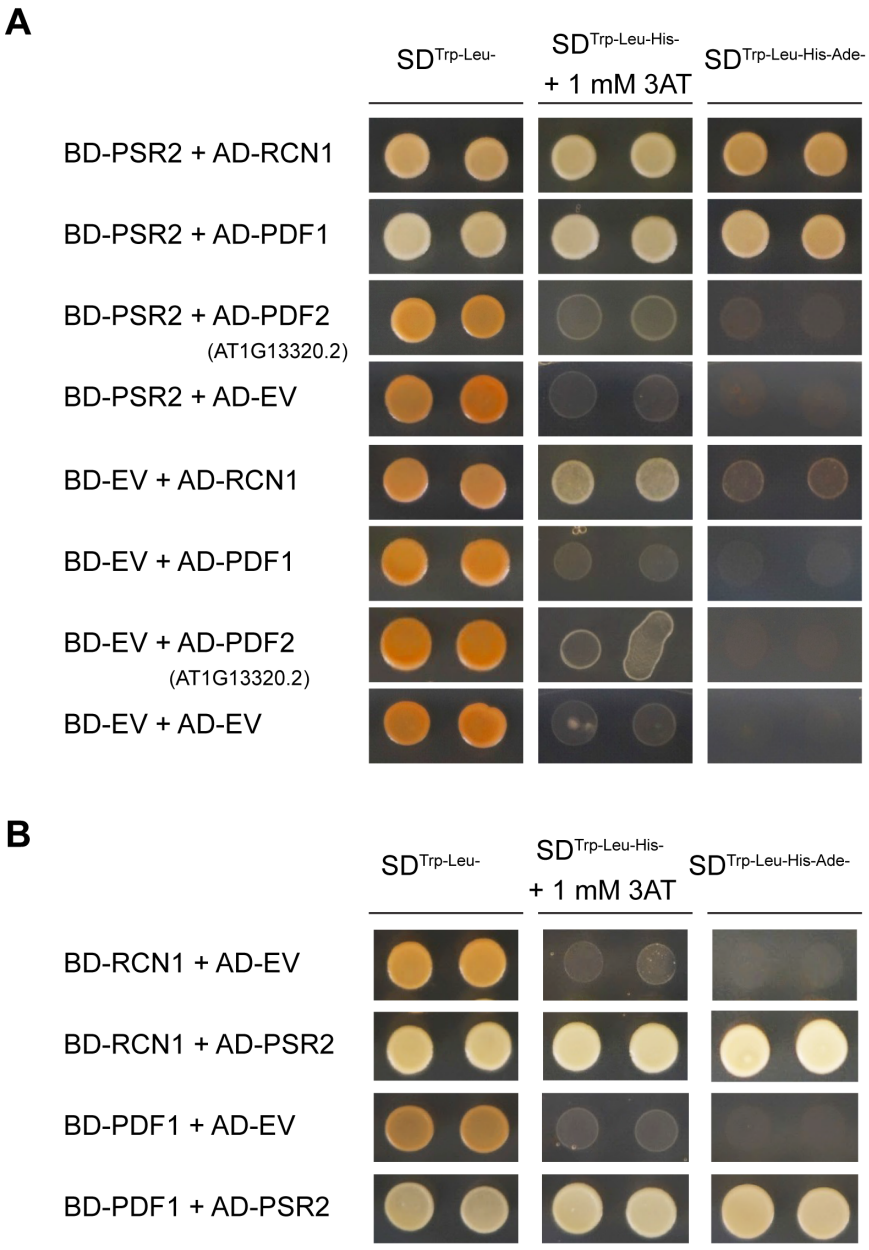
A
SD Trp-Leu-
SD Trp-Leu-His- + 1 mM 3AT
SD Trp-Leu-His-Ade-
BD-PSR2 + AD-RCN1
BD-PSR2 + AD-PDF1
BD-PSR2 + AD-PDF2 (AT1G13320.2)
BD-PSR2 + AD-EV
BD-EV + AD-RCN1
BD-EV + AD-PDF1
BD-EV + AD-PDF2 (AT1G13320.2)
BD-EV + AD-EV
B
SD Trp-Leu-
SD Trp-Leu-His- + 1 mM 3AT
SD Trp-Leu-His-Ade-
BD-RCN1 + AD-EV
BD-RCN1 + AD-PSR2
BD-PDF1 + AD-EV
BD-PDF1 + AD-PSR2

Figure 3.6. PSR2 interacted with two PP2A A subunits in Y2H assay.

(A-B) PSR2 interacted with two Arabidopsis PP2A A subunit proteins, RCN1 and PDF1. Interaction of Y2H was selected on Synthetic Dropout (SD) media lacking tryptophan, leucine, and histidine ($SD^{Trp-Leu-His-}$) and media lacking tryptophan, leucine, histidine, and adenine ($SD^{Trp-Leu-His-Ade-}$). EV: empty vector control. **(C)** Interactions between PSR2 and RCN1 and PDF1 were also observed in the reciprocal orientations of the yeast-two-hybrid vectors. Note that AD-PDF2 cloning used the isoform 2 of PDF2 (AT1G13320.2) as the template, instead of isoform 1 (AT1G13320.1).

PSR2 and PDF2 might not be due to the lack of protein expression of AD-PDF2. A reciprocal Y2H was also performed by switching the BD and AD vectors (**Figure 3.6B**). Unlike the AD-RCN1 plasmid, BD-RCN1 did not have the self-activation effect. Both BD-RCN1 and BD-PDF1 interact with AD-PSR2.

3.5 Genome-wide Y2H screening supported PSR2-PDF1 interaction

A genome-wide Y2H screening using PSR2 as a bait and *Arabidopsis thaliana* Col-0 cDNA library as preys was conducted in parallel to identify potential PSR2-interacting proteins (screening done by Dr. Yi Zhai) (**Figure 3.5C**). Five Arabidopsis cDNA clones representing PDF1 subunit were identified. Repeated Y2H experiments using these clones (AD-4-19, AD-3-5, AD-3-15, AD-4-97, and AD-1-27) showed that three of them (AD-3-15, AD-4-97, and AD-1-27) still positively interacted with PSR2 (**Figure 3.7**). Notably, only PDF1 but not RCN1 nor PDF2 was revealed from the whole-genome Y2H screening.

3.6 PSR2 interacts with all three PP2A A subunits in planta

Next, I used co-IP assay to further confirm the interactions between PSR2 and PP2A A subunits i*n planta*. 3×Flag-PSR2 was co-expressed with HA-tagged RCN1, PDF1 or PDF2 in *N. benthamiana* and the total protein extracts were used for co-IP. Flag-tagged baits (3×Flag-PSR2 and the negative control 3×Flag-HopZ1a^{C216A}) were immunoprecipatated by anti-Flag resin, and the co-IP products were further examined in western blotting using anti-Flag and anti-HA antibodies. The results showed that both

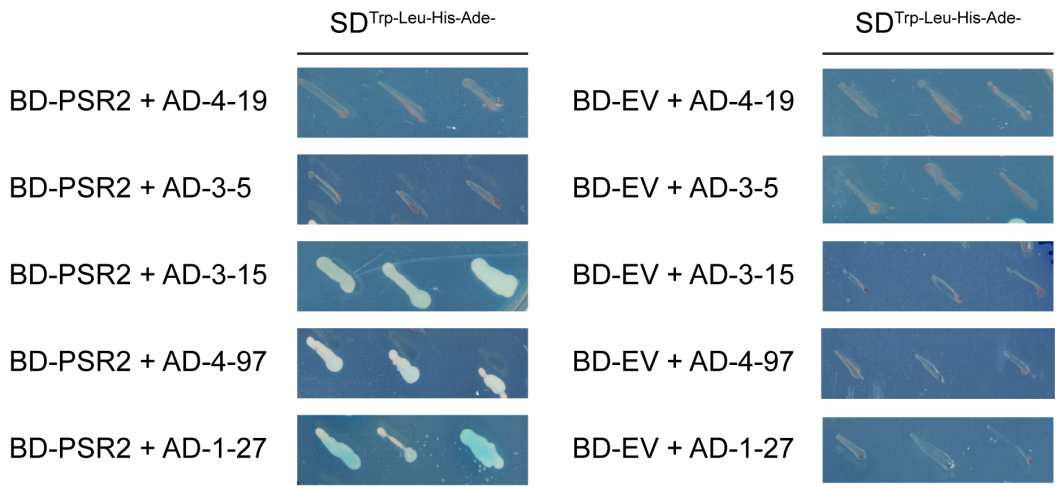

Figure 3.7. Some of the *PDF1*-containing clones identified from genome-wide Y2H screening were confirmed to interact with PSR2 in Y2H assay. A genome-wide Y2H screening (performed by Dr. Yi Zhai) using PSR2 as a bait and *Arabidopsis thaliana* Col-0 cDNA library as preys identified five potential PSR2-interacting proteins. All these positive AD clones encoded PDF1. Repeating Y2H assays confirmed three (AD-3-15, AD-4-97, and AD-1-27) of the five positive AD clones remained positive. $SD^{Trp–Leu–His–Ade–}$ is a selective medium lacking tryptophan, leucine, histidine, and adenine for protein interaction selection. EV: empty vector control.

RCN1-HA and PDF1-HA were detected in the 3×Flag-PSR2 outputs, but not in the control outputs (**Figure 3.8A and B**), indicating their positive interactions with PSR2.

Similarly, PDF2-HA could also be immunoprecipitated by 3×Flag-PSR2 from the protein extract containing 3×Flag-PSR2, PDF2-HA, and AGO1-cMyc (negative control). AGO1-cMyc was not immunoprecipitated by 3×Flag-PSR2 (**Figure 3.8C**). In conclusion, all three Arabidopsis PP2A A subunits presented in the PSR2-containing complexes and interacted with PSR2 *in planta*.

3.7 PSR2 interacts with PP2A A subunits in cytoplasm, occasionally on nuclear membrane

Information about the subcellular location where protein interactions take place could provide clues into the potential cellular pathways that might be involved in or affected by their interaction. To visualize where in the plant cells PP2A and PSR2 interact, I conducted the bimolecular fluorescence complementation (BiFC) assay in *N. benthamiana* leaves. Specifically, BiFC pVYNE/pVYCE vector system, which applied the Venus fluorescence protein as the reporter, (an improved version of YFP) was used (Waadt et al., 2008). Venus protein was split into non-fluorescent N terminal part (nVenus) and C terminal part (cVenus), and each part was fused with PSR2 and PP2A A subunits, respectively (pVYNE-PSR2 was cloned by Dr. Yingnan Hou). A reconstitution of the fluorescence takes place when PSR2 and PP2A A subunits interact *in vivo*.

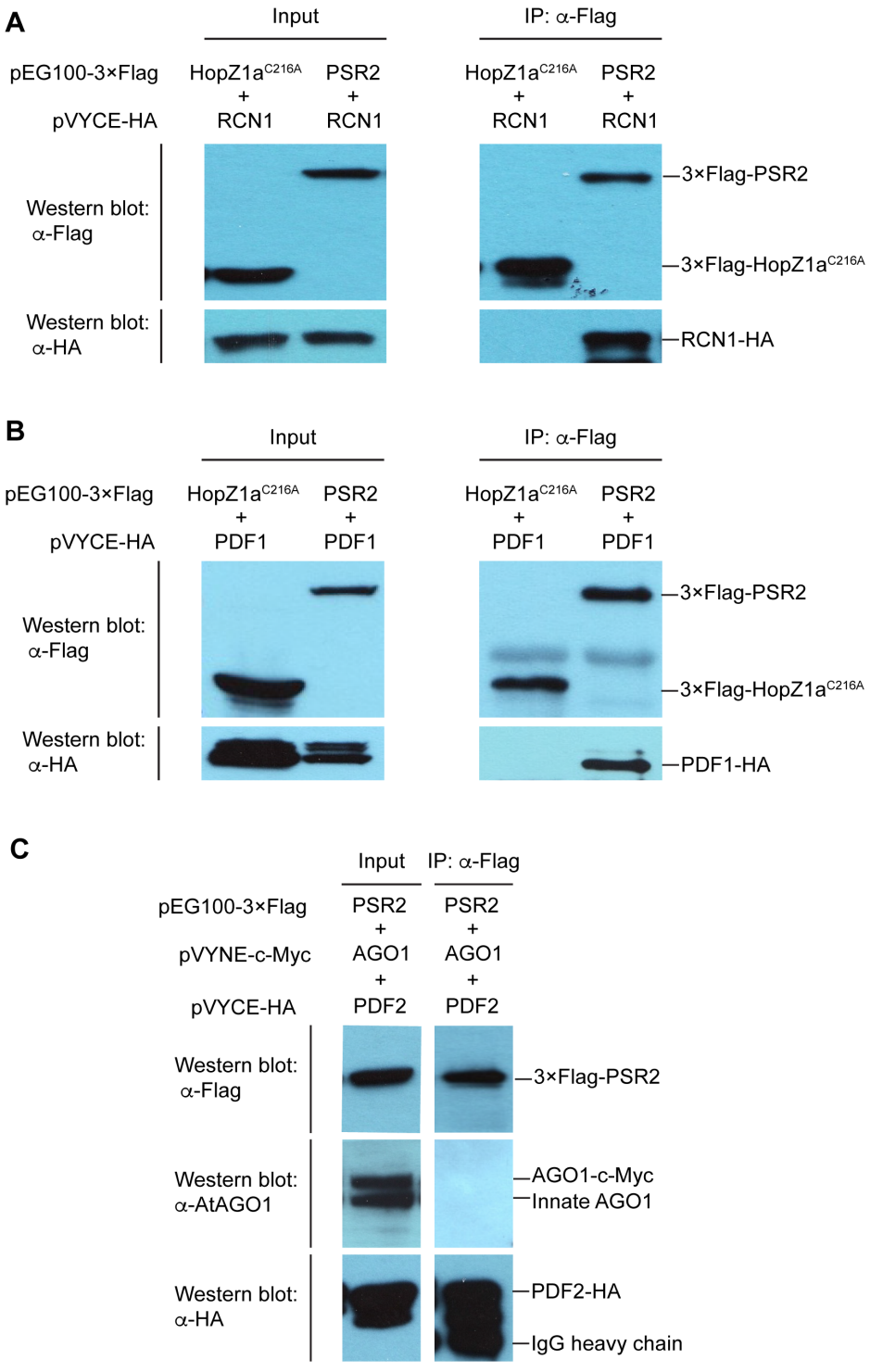
A
Input
IP: α-Flag
pEG100-3×Flag
HopZ1a^C216A + pVYCE-HA RCN1
PSR2 + RCN1
HopZ1a^C216A + RCN1
PSR2 + RCN1
Western blot: α-Flag
Western blot: α-HA
3×Flag-PSR2
3×Flag-HopZ1a^C216A
RCN1-HA
B
Input
IP: α-Flag
pEG100-3×Flag
HopZ1a^C216A + pVYCE-HA PDF1
PSR2 + PDF1
HopZ1a^C216A + PDF1
PSR2 + PDF1
Western blot: α-Flag
Western blot: α-HA
3×Flag-PSR2
3×Flag-HopZ1a^C216A
PDF1-HA
C
Input
IP: α-Flag
pEG100-3×Flag
PSR2
pVYNE-c-Myc
AGO1
pVYCE-HA
PDF2
Western blot: α-Flag
Western blot: α-AtAGO1
Western blot: α-HA
3×Flag-PSR2
AGO1-c-Myc
Innate AGO1
PDF2-HA
IgG heavy chain

Figure 3.8. PSR2 interacted with all three PP2A A subunits *in planta* using co-immunoprecipitation (co-IP) assay. 3×Flag-PSR2 was co-expressed with HA-tagged RCN1 **(A)**, PDF1 **(B)** or PDF2 **(C)** in *N. benthamiana*, and the total protein extracts were subjected to a co-IP assay using anti-Flag resin. Immunoprecipitates were detected using anti-Flag, anti-HA, and anti-c-myc western blotting, respectively. 3×Flag-HopZ1a^{C216A} was used as a negative control.

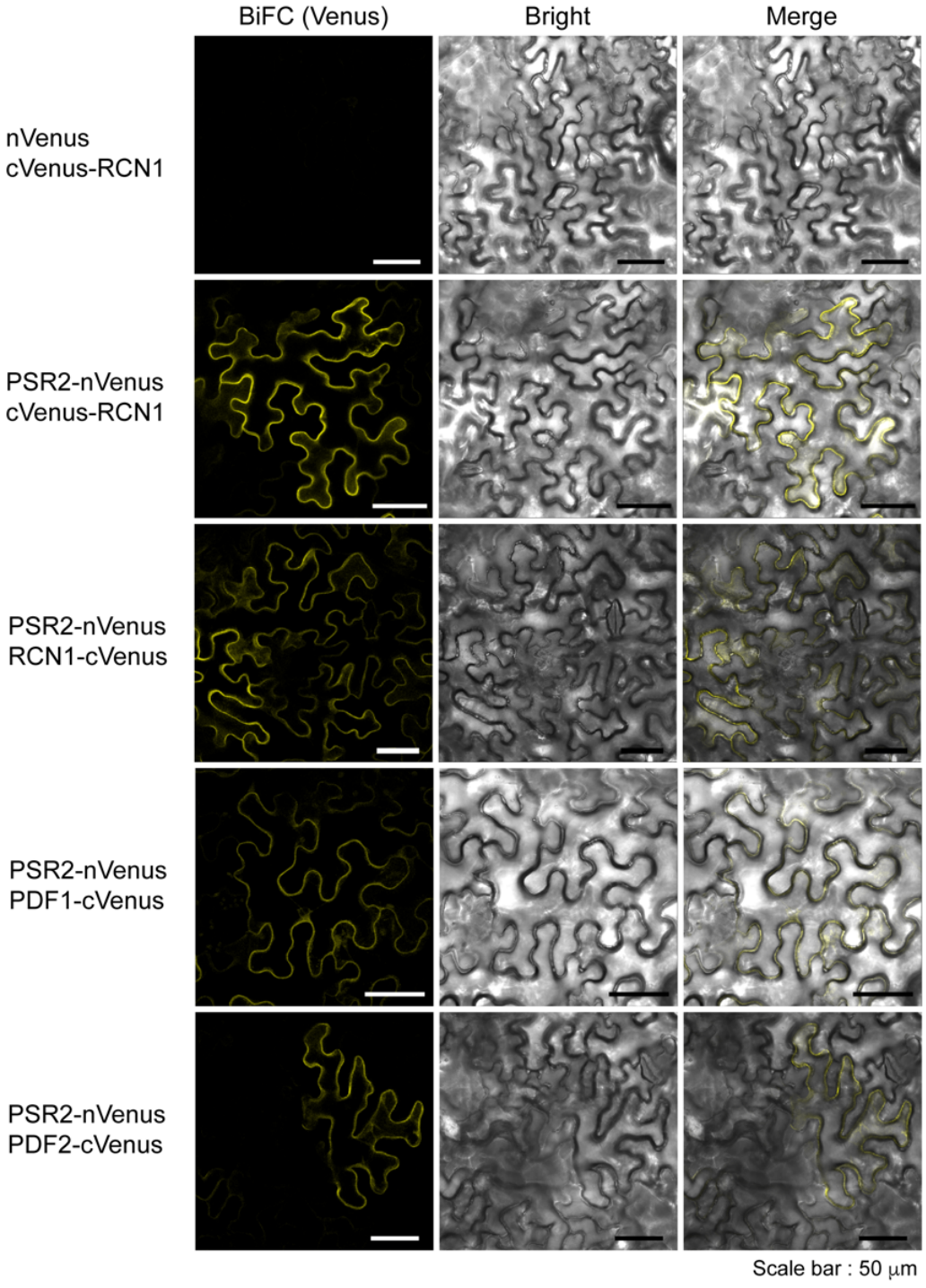
BiFC (Venus)
Bright
Merge
nVenus
cVenus-RCN1
PSR2-nVenus
cVenus-RCN1
PSR2-nVenus
RCN1-cVenus
PSR2-nVenus
PDF1-cVenus
PSR2-nVenus
PDF2-cVenus
Scale bar : 50 μm

Figure 3.9. Bimolecular fluorescence complementation (BiFC) assay of the PSR2-PP2A A subunit interactions in *N. benthamiana* leaves. *N. benthamiana* leaves were infiltrated with Agrobacteria carrying indicated constructs. Fluorescence was detected mostly in cytosol for PSR2-nVenus with either PP2A-cVenus or cVenus-PP2A groups. nVenus protein alone was used as a control of PSR2-nVenus that showed no interaction with PP2A A subunits. Scale bar = 50 μm.

The BiFC assays showed the interactions between PSR2-nVenus and both RCN1-cVenus and cVenus-RCN1 with yellow fluorescence signal evenly-distributed in cytoplasm of leaf epidermal cells (**Figure 3.9A**). Slightly different from the PSR2-RCN1 interactions, PSR2-nVenus/PDF1-cVenus as well as PSR2-nVenus/PDF2-cVenus (**Figure 3.9B**) interacted not only in cytoplasm but also around nuclei.

Consistent with the *in planta* co-IP results, the BiFC assay showed that PSR2 interacted with all three Arabidopsis PP2A A subunits in plant cells. Such interactions occurred in cytoplasm and occasionally on the nuclear membrane, suggesting PSR2 and PP2A may regulate the cellular functions that take place in these places.

To further understand whether PSR2 affects the subcellular localization of plant PP2A and thus manipulate its function, the PP2A localization patterns in the presence or absence of PSR2 were compared. I first overexpressed RCN1-YFP (pEG101-RCN1) and PSR2-CFP (pEG102-PSR2) in *N. benthamiana* cells and examined their subcellular localization individually. I found that RCN1-YFP and PSR2-CFP were localized broadly in both cytoplasm and nucleus (**Figure 3.10A and B**). Subsequently, co-expression of RCN1-YFP and PSR2-CFP showed similar subcellular localization of either protein (**Figure 3.10C**), suggesting that RCN1 did not change its subcellular localization in the presence of PSR2.

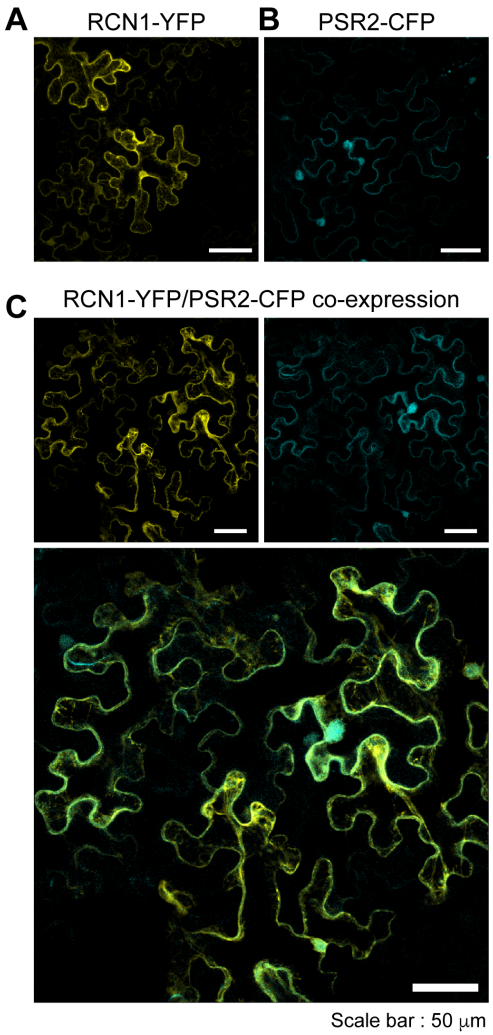

Figure 3.10. Subcellular localization of RCN1-YFP and PSR2-CFP fusion proteins in *N. benthamiana* leaves. Leaves infiltrated with either RCN1-YFP **(A)**, PSR2-CFP **(B)**, or together **(C)** were examined by the confocal microscopy. **(A-B)** Both RCN1-YFP and PSR2-CFP fluorescence dispersed throughout the cell presenting in both cytosol and nucleus, where PSR2-CFP fluorescence seemed stronger in the nucleus than in the cytosol. **(C)** Co-infiltration of both RCN1-YFP and PSR2-CFP did not significantly change the subcellular localization of either protein. Scale bar = 50 μm.

3.8 PSR2 homolog of Phytophthora infestans also interacts with PP2A A subunits

PSR2 was originally identified from *P. sojae* (Qiao et al., 2013). PiPSR2 (PITG_15152), a close homolog of PSR2, was found in *Phytophthora infestans* with 46% of protein sequence identity to PSR2. Like PSR2, PiPSR2 was able to suppress RNA silencing and enhance host disease susceptibility when expressed in plants (Xiong et al., 2014), suggesting that PSR2 and PiPSR2 may share same/similar cellular mechanisms by targeting to same plant proteins. In order to understand whether PiPSR2 also associates with PP2A A subunits, the Y2H system was used. Consistent with the PSR2 results, PiPSR2 interacted with PDF1, but not with PDF2 (**Figures 3.11**). PiPSR2 might also interact with RCN1; however, the self-activation of AD-RCN1 plasmid occurred in this assay, which made result uninterpretable. Interaction between PiPSR2 and RCN1 will need further examination using $SD^{Trp-Leu-His-}$ medium supplemented with higher concentration (10 mM is suggested) of 3-AT to suppress leaking *HIS* expression (**Figure 3.11**). In summary, PP2A might be a conserved target of both PSR2 and PiPSR2.

3.9 Examination of protein-protein interaction between PSR2 and Arabidopsis PP2A catalytic subunits

In addition to PP2A A subunits, the IP-mass spectrometry also identified PP2A catalytic subunits (C subunits) as potential PSR2-associating proteins in plants (**Figure 3.4; Tables 3.1 and 3.2**). To validate protein interactions between PSR2 and the Arabidopsis catalytic subunits, *in planta* co-IP were performed. Co-IP data showed that both HA-tagged PP2AC2 and PP2AC5 catalytic subunits were immunoprecipitated by

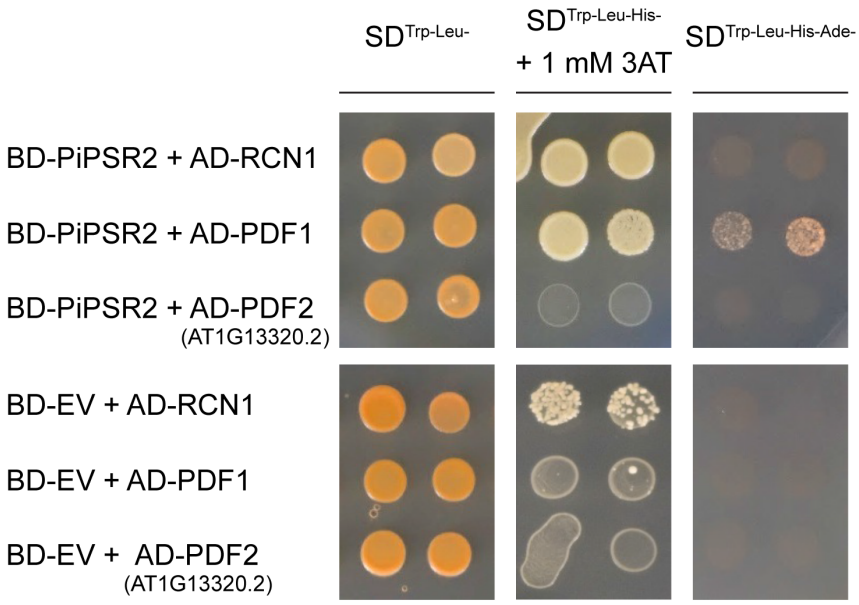

Figure 3.11. PiPSR2 interacted with PP2A A subunit in Y2H assay. PiPSR2 interacted with Arabidopsis PP2A A subunit PDF1, probably also with RCN1. The protein interactions were selected by the nutrient-deficient SD media, including $SD^{Trp-Leu-His-}$ and $SD^{Trp-Leu-His-Ade-}$. EV: empty vector control. Self-activation of AD-RCN1 plasmid occurred in this assay on the $SD^{Trp-Leu-His-}$ medium supplemented with 1 mM 3-AT, therefore the interaction between PiPSR2 and RCN1 need further examination. Note that AD-PDF2 cloning used the isoform 2 of PDF2 (AT1G13320.2) as the template, instead of isoform 1 (AT1G13320.1).

the 3×Flag-PSR2 bait, but not by the negative control bait 3×Flag-HopZ1a^{C216A} (**Figure 3.12A and B**). These results suggested that PSR2 had *in planta* associations with PP2A catalytic subunits, at least with PP2AC2 and PP2AC5. In this thesis research, I only obtained the co-IP interaction results of PSR2/PP2AC2 and PSR2/PP2AC5. The interaction between PSR2 and other C subunits will need further examinations.

BiFC was further conducted to examine subcellular location where PSR2 and PP2A catalytic subunits interact. The PP2AC2, PP2AC3, PP2AC4, and PP2AC5 subunits were assayed using the pVYNE/pVYCE vector system; however; none of the *N. benthamiana* cells expressing catalytic subunits and PSR2 showed fluorescence (**Figure 3.13**), indicating PSR2 did not interact with all these four PP2A catalytic subunits using BiFC systerm. Note that the protein expression of pVYCE-C2, pVYCE-C3, pVYCE-C4, and pVYCE-C5 constructs was confirmed using anti-HA western blotting.

Finally, Y2H was performed to test the protein interactions between PSR2 and all five PP2A catalytic subunits. (**Figure 3.14**) According to the SD$^{Trp-Leu-His-Ade-}$ results, there was no interaction between all PP2A C subunits and PSR2, while there is a mild self-activation in controls on SD$^{Trp-Leu-His}$. There are five catalytic subunits in Arabidopsis and some of them might present in PSR2-associated protein complexes. My results suggested that PSR2 only showed interaction with PP2A catalytic subunits by using co-IP assay, not by BiFC or Y2H assays.

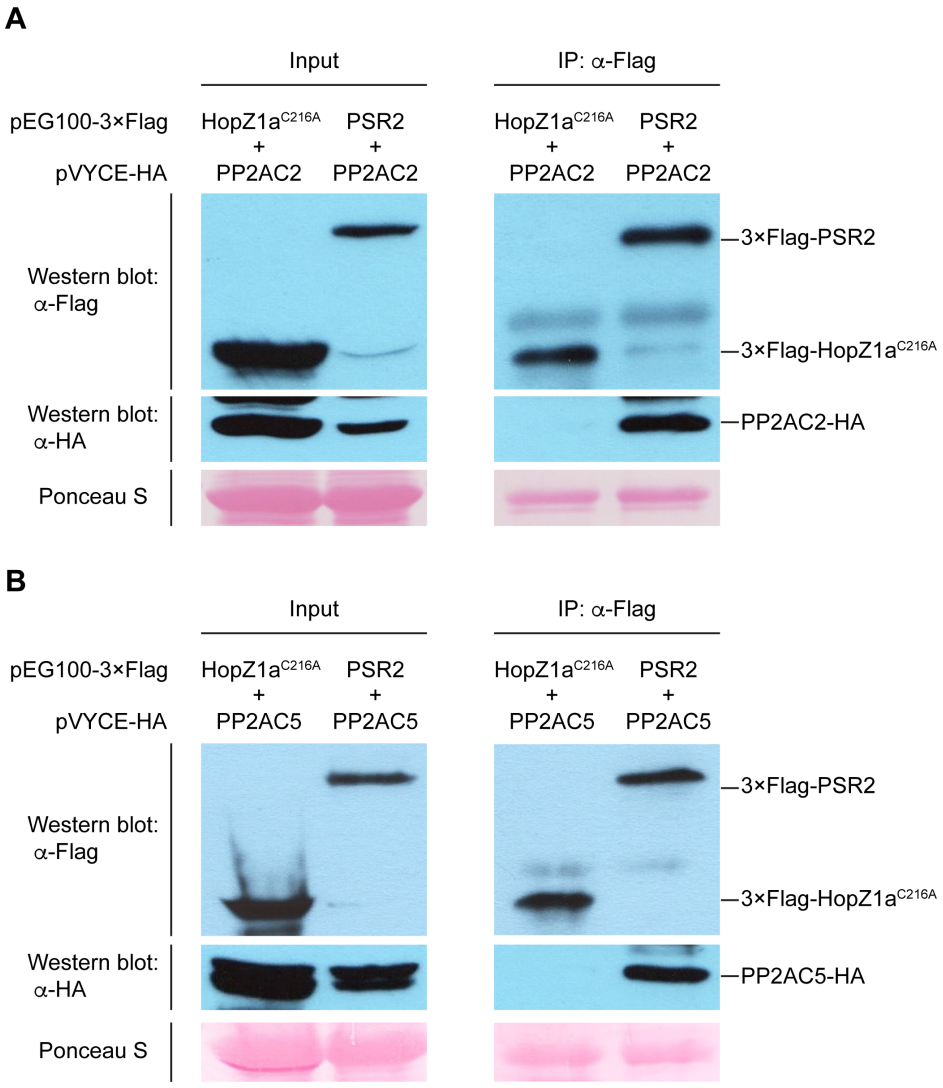

Figure 3.12. PSR2 interacted with PP2AC2 and PP2AC5 in co-IP assay. 3×Flag-PSR2 was co-expressed with HA-tagged PP2AC2 **(A)** or PP2AC5 **(B)** in *N. benthamiana* and the total protein extracts were subjected to a co-IP assay using anti-Flag resin. Immunoprecipitates were analyzed by western blotting using anti-Flag and anti-HA antibodies, respectively. 3×Flag-HopZ1a^{C216A} was used as a negative control. Ponceau S staining was used as a loading control.

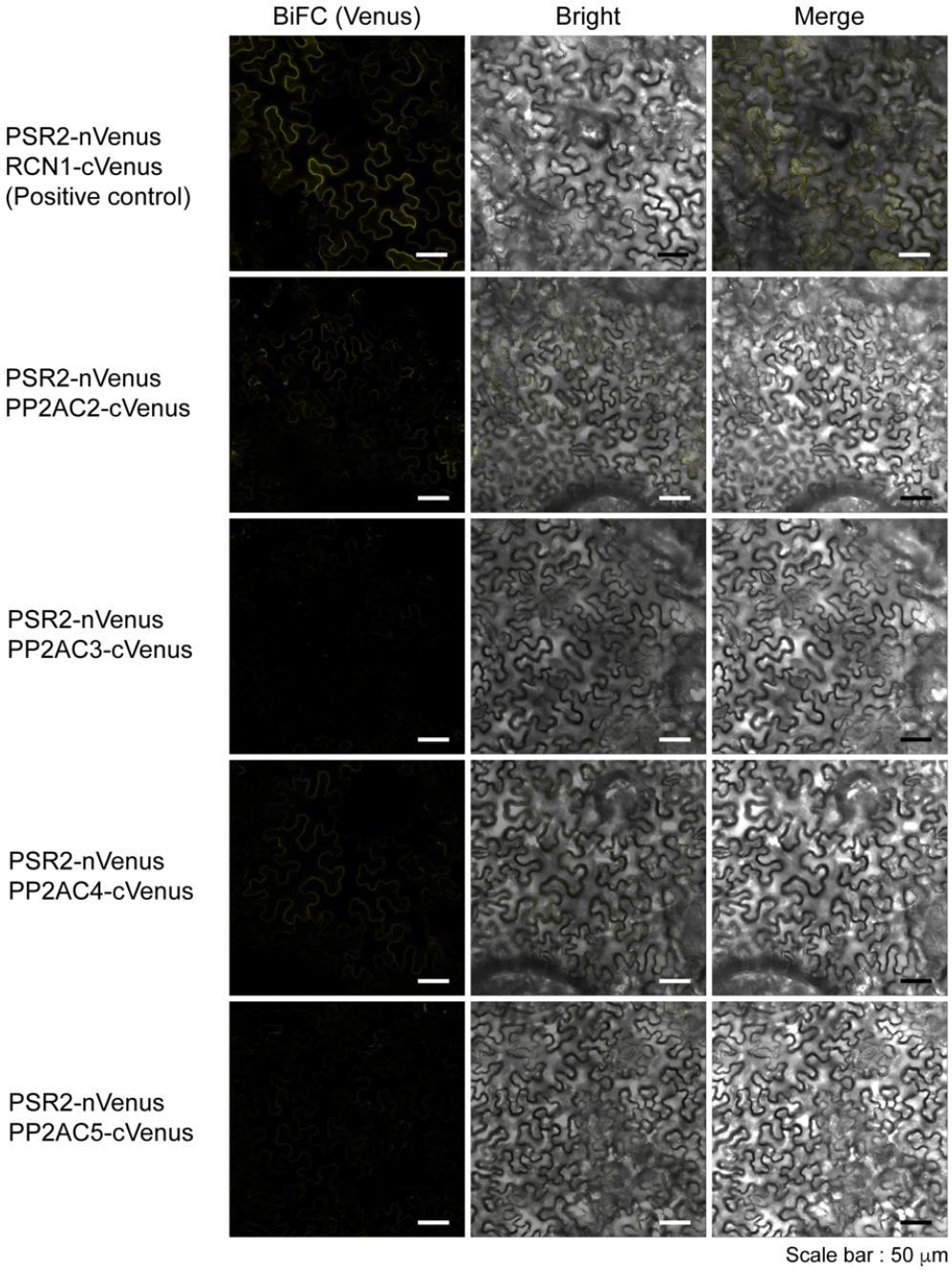
BiFC (Venus)
Bright
Merge
PSR2-nVenus
RCN1-cVenus
(Positive control)
PSR2-nVenus
PP2AC2-cVenus
PSR2-nVenus
PP2AC3-cVenus
PSR2-nVenus
PP2AC4-cVenus
PSR2-nVenus
PP2AC5-cVenus
Scale bar : 50 μm

Figure 3.13. Bimolecular fluorescence complementation (BiFC) assay of protein interaction between PSR2 and PP2AC2-C5 subunits in *N. benthamiana* leaves. *N. Benthamiana* leaves were infiltrated with Agrobacteria bearing indicated constructs. Fluorescences of different PSR2-nVenus/C subunits-cVenus samples were much weaker, compared to the positive control (PSR2-nVenus/RCN1-cVenus). These BiFC results suggested that PSR2 did not have interaction with PP2AC2-C5 subunits. Scale bar = 50 μm.

A

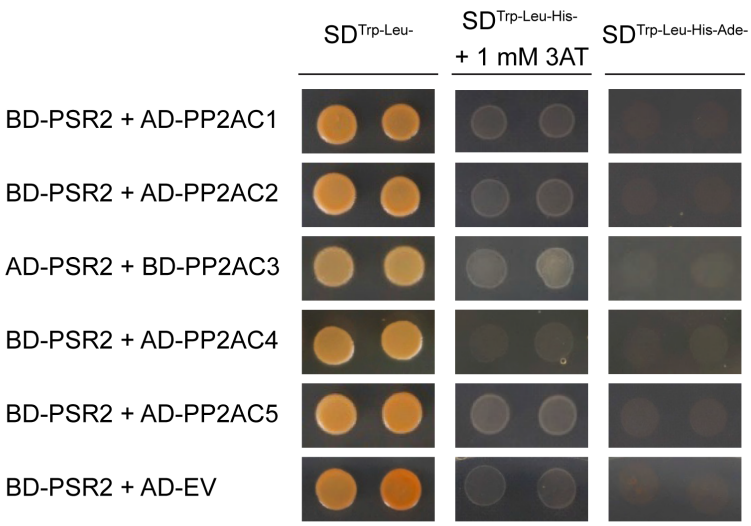
SD Trp-Leu-
SD Trp-Leu-His- + 1 mM 3AT
SD Trp-Leu-His-Ade-
BD-PSR2 + AD-PP2AC1
BD-PSR2 + AD-PP2AC2
AD-PSR2 + BD-PP2AC3
BD-PSR2 + AD-PP2AC4
BD-PSR2 + AD-PP2AC5
BD-PSR2 + AD-EV

B

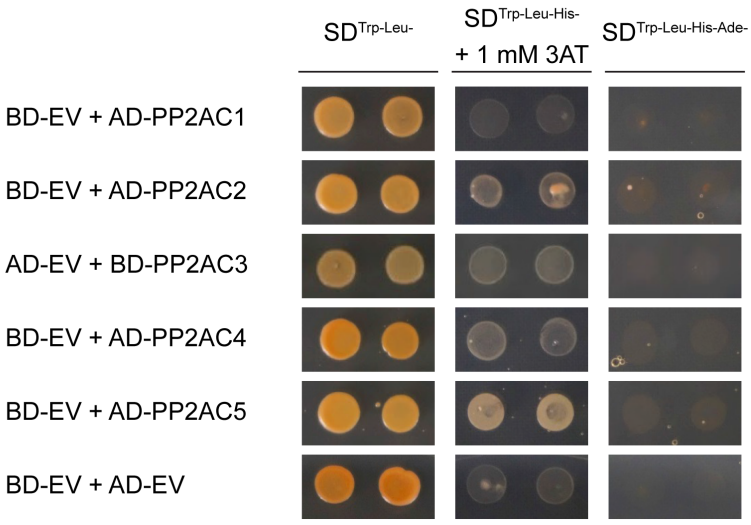
SD Trp-Leu-
SD Trp-Leu-His- + 1 mM 3AT
SD Trp-Leu-His-Ade-
BD-EV + AD-PP2AC1
BD-EV + AD-PP2AC2
AD-EV + BD-PP2AC3
BD-EV + AD-PP2AC4
BD-EV + AD-PP2AC5
BD-EV + AD-EV

Figure 3.14. PSR2 showed no interaction with PP2A C subunit proteins in Y2H assays. Interaction in Y2H assay was selected using nutrient-deficient Synthetic Dropout (SD) media, $SD^{Trp-Leu-His-}$ and $SD^{Trp-Leu-His-Ade-}$. PSR2 could not interact with all five PP2A C subunits in yeast. EV: empty vector control.

3.10 Functional validation of PSR2/PP2A interactions using transgenic Arabidopsis

Phytophthora PSR2 functions as a RNA silencing suppressor in plants and serves as a key virulence determinant of *Phytophthora* species (Qiao et al., 2013, Xiong et al., 2014). Expressing PSR2 in wild-type Arabidopsis suppresses the accumulation of a specific class of small RNAs known as phasiRNAs (phased, secondary, small interfering RNAs) in plants and enhances plant susceptibility to *Phytophthora* infection (Qiao et al., 2013). Given that PSR2 interacts with plant PP2A A and C subunits, especially RCN1 and PDF1, I hypothesized that PP2A A and C subunits may serve as important host factors downstream of PSR2 to regulate RNA silencing and plant immunity. To test this hypothesis, genetic-modified Arabidopsis lines of PSR2 and different subunits of PP2A were generated for the functional assays.

3.11 Generation of Arabidopsis mutants of PP2A A and C subunits

I obtained the Arabidopsis *rcn1-6* (SALK_059903C) mutant from the SALK institute that has T-DNA insertion at the last intron of *RCN1* gene (**Figure 3.15A**). Genotyping PCR with T-DNA specific primers that near the left and right borders of T-DNA insertion was performed to screen the homozygous *rcn1-6* mutant (**Figure 3.15B**). The homozygous *rcn1-6* mutants were further tested using RT-PCR with primers across the T-DNA insertion site and confirmed the interruption of *RCN1* transcript expression in this mutant line (**Figure 3.15C and D**). In addition to the genotyping results, I observed the abnormalities of root development in *rcn1-6* mutant (SALK_059903), whose seedlings developed short and curl roots on the MS medium compared to the wild-type

seedling. This root phenotype was consistent with what has been reported in published literature (Blakeslee et al., 2008). By growing the Arabidopsis seedlings on the MS plates, homozygous *rcn1-6* mutant showed shorter root phenotypes (**Figure 3.15E**). However, no developmental defects were observed in adult *rcn1-6* plants and they were indistinguishable from the wild-type counterparts (**Figure 3.15F**).

To obtain the Arabidopsis homozygous mutant of *pdf1*, I first checked the T-DNA insertion line SALK_132063 from the SALK institute. Unfortunately, I did not successfully obtain the homozygous mutant of SALK_132063C since its LBb1.3/RP primer pair failed to work at various PCR conditions tested. Thus, I used the CRISPR/Cas9 genome-editing technique to generate a *pdf1* mutant allele. Specifically, a guide RNA was designed to target to the first exon of *pdf1* gene using the online Optimized CRISPR Design−MIT website (http://crispr.mit.edu/). Subsequently, this guide RNA was introduced into the YAO Promoter-Driven CRISPR/Cas9 vector system (Yan et al., 2015), and the whole cassette construct was delivered into *Agrobacterium tumefaciens* for Arabidopsis plant transformation. Six individual Arabidopsis transformants were screened by genomic DNA sequencing in the first generations (T1). Among them, I obtained one deletion allele of *pdf1* (line 1) that misses 56 nt within the first exon, including the translation start site ATG (**Figure 3.16A**). Based on its genomic DNA sequence, this deletion allele was predicted to produce a short peptide with only four amino acids using a frame-shifted ATG and is likely to be a null *pdf1* mutant. The second (T2) and the third (T3) generations of this mutant (line 1) were further screened by the genotyping PCR and RT-PCR to recover the homozygous line that named *pdf1-1*

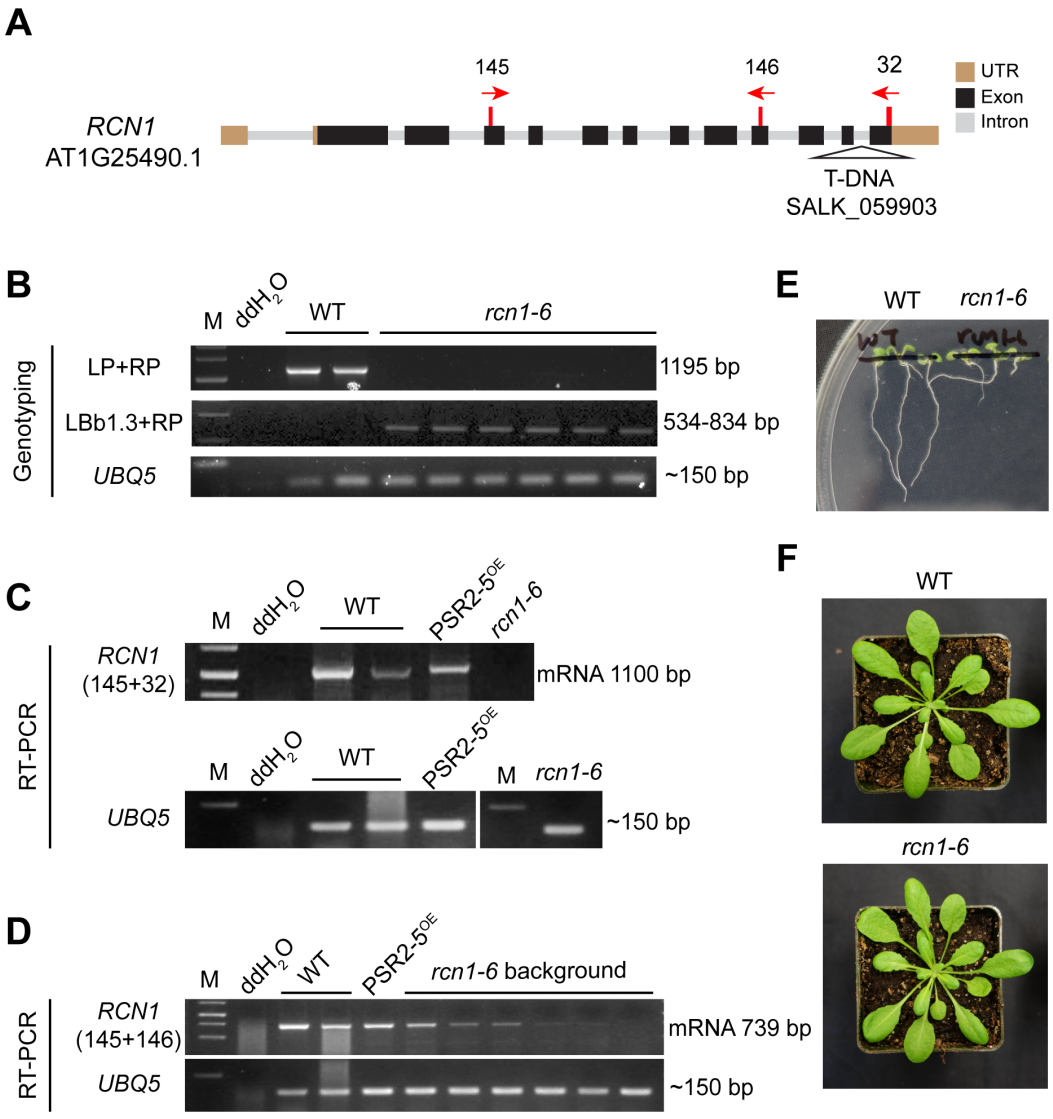
A
145
146
32
UTR
Exon
Intron
RCN1
AT1G25490.1
T-DNA
SALK_059903
B
M
ddH2O
WT
rcn1-6
Genotyping
LP+RP
1195 bp
LBb1.3+RP
534-834 bp
UBQ5
~150 bp
C
RT-PCR
RCN1
(145+32)
PSR2-5OE
mRNA 1100 bp
~150 bp
D
RCN1
(145+146)
rcn1-6 background
mRNA 739 bp
E
F

Figure 3.15. Characterization of Arabidopsis *rcn1-6* mutant. (A) Schematic of Arabidopsis *RCN1* gene structure (isoform 1) and the T-DNA insertion site of *rcn1-6* SALK mutant (SALK_059903). *rcn1-6* has a T-DNA inserted in the last intron of *RCN1* gene. Red arrows indicate the forward (FP) and reverse (RP) primers used in RT-PCR analysis in (C-D). **(B)** PCR-based genotyping of *rcn1-6*. LP and RP refer to SALK_059903-sepcific left and right genomic primers, and LBb1.3 refers to the left border primer of the T-DNA insertion (see materials and methods). Homozygous *rcn1-6* mutants were obtained since all individual plants showed bands of LBb1.3+RP but not LP+RP. **(C-D)** RT-PCR analysis for measuring *RCN1* gene expression in *rcn1-6* mutant. No transcript was detected by primers (145+32) spanning the T-DNA insertion site; however, low level of *RCN1* transcripts could still be detected by primers site (145+146) targeting regions upstream T-DNA insertion site. *rcn1-6* mutant is not a null mutant. **(E-F)** Phenotypes of WT and *rcn1-6* adult plants (E) and seedlings (F). Note that the *rcn1-6* seedlings exhibited characteristic abnormalities of shorter root length. Ubiquitin 5 (UBQ5) was used as an internal control in both PCR and RT-PCR experiments.

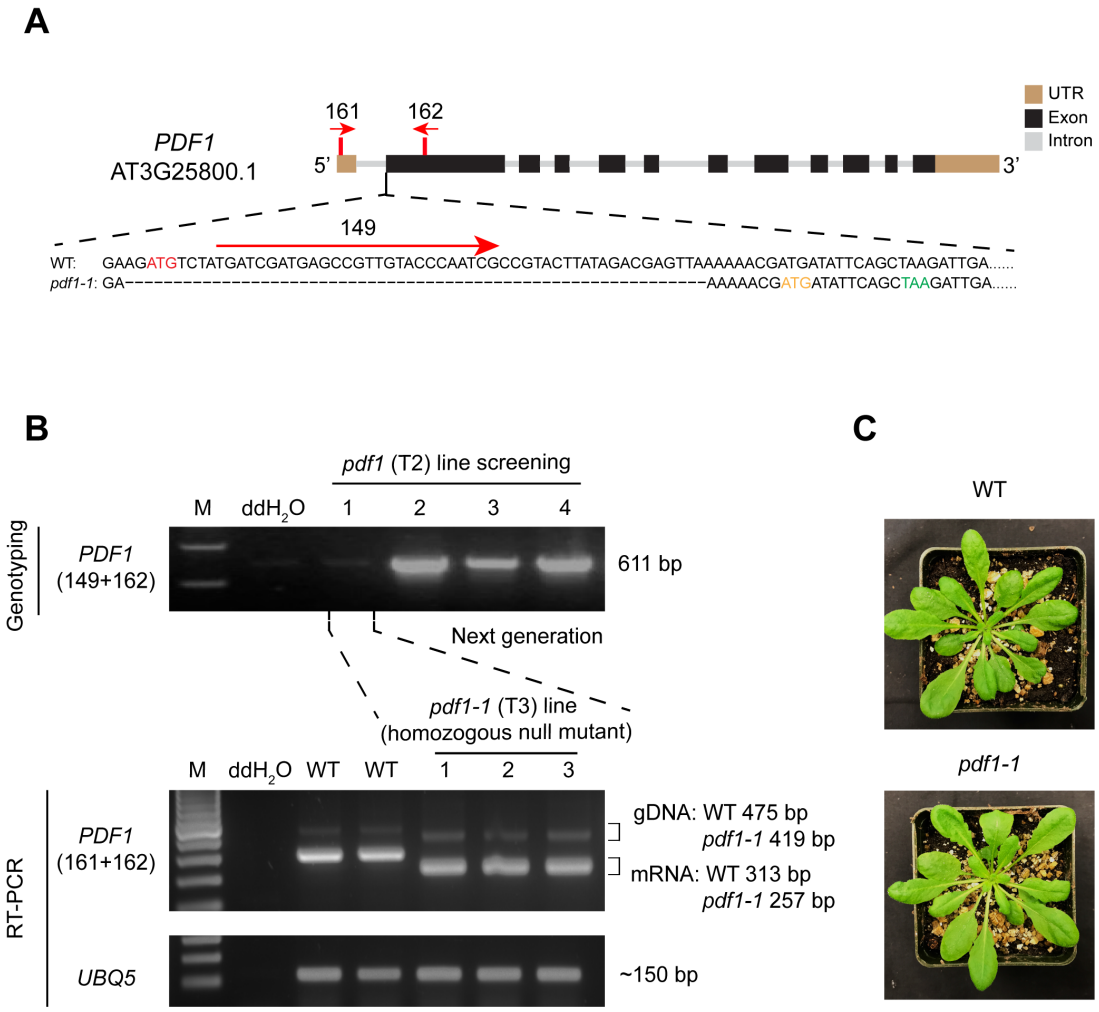
A
PDF1
AT3G25800.1
161
162
5'
3'
UTR
Exon
Intron
149
WT: GAAGATGTCTATGATCGATGAGCCGTTGTACCCAATCGCCGTACTTATAGACGAGTTAAAAAACGATGATATTCAGCTAAGATTGA.....
pdf1-1: GA----------AAAAACGATGATATTCAGCTAAGATTGA.....
B
pdf1 (T2) line screening
M ddH2O 1 2 3 4
Genotyping
PDF1
(149+162)
611 bp
Next generation
pdf1-1 (T3) line
(homozogous null mutant)
M ddH2O WT WT 1 2 3
RT-PCR
PDF1
(161+162)
gDNA: WT 475 bp
pdf1-1 419 bp
mRNA: WT 313 bp
pdf1-1 257 bp
UBQ5
~150 bp
C
WT
pdf1-1

Figure 3.16. Characterization of *pdf1-1* CRISPR mutant. (A) Schematic of Arabidopsis *PDF1* gene structure (isoform 1). Red arrows indicate the forward and reverse primers used in RT-PCR analysis in (B). *pdf1-1* CRISPR mutant allele has 56 nt deletion at the beginning of the CDS, resulting in a new start codon (ATG labeled in yellow) and a premature stop codon (TAA labeled in green). *pdf1-1* may only produce a short peptide with 4-a.a in length. **(B)** PCR-based genotyping of *pdf1-1* T2 generation (top) and RT-PCR analysis (bottom) for *pdf1-1* T3 generation. *pdf1-1* loses 56 nt in genomic DNA sequences, which could not be amplified using primer set 149+162. *pdf1-1* may also produce mRNA transcripts that lose 56 nt by showing smaller size of bands compared to the WT bands using primer set 161+162 of RT-PCR. Supporting by genomic DNA sequencing result, the homozygous *pdf1-1* line was obtained in T2 generation and further confirmed in T3 generation. Ubiquitin 5 (UBQ5) was used as an internal control. **(C)** Phenotypes of WT and *pdf1-1* CRISPR mutant adult plants.

(**Figure 3.16B**). The morphology of adult *pdf1-1* plants was not different from the wild-type counterparts (**Figure 3.16C**).

Lastly, I looked for mutant lines of Arabidopsis PP2A C subunits. I obtained PP2A mutant lines for all five PP2A C subunits from Dr. Cyril Zipfel's Lab at the Sainsbury Laboratory, Norwich, UK (Segonzac et al., 2014). Among all five mutant lines (*pp2ac1*, *pp2ac2*, *pp2ac3*, *pp2ac4*, and *pp2ac5),* the *pp2ac1* (SALK_102599), *pp2ac3* (SAIL_182_A02), *pp2ac4* (SALK_035009), and *pp2ac5* (SALK_013178) mutants were T-DNA insertion lines; whereas the *pp2ac2* mutant was created using Ws insertion backcrossed into Col-0 (Segonzac et al., 2014) (**Figure 3.17A**). I obtained homozygous lines of all these mutants by genotyping PCR. Examination of the morphology of these mutant lines revealed that the *pp2ac2* (small) and *pp2ac4* (slightly small) might have mild developmental phenotypes, while other three mutants grew normally (**Figure 3.17B**).

The mRNA transcript expressions of homozygous PP2A C subunit mutant lines were also examined by RT-PCR. The reverse primers of each C subunit gene in this thesis were the same as the Q-PCR reverse primers reported previously (Segonzac et al., 2014), but the forward primers of each mutant line were re-designed for intron spanning to distinguish PCR products of the mRNA transcript from the genomic DNA contamination (see Method for detail of primer sequences). RT-PCR results indicated that no mRNA transcript was detected in *pp2ac2* and *pp2ac4* (**Figure 3.18B and D**), while transcripts were still detectable in *pp2ac1*, *pp2ac3*, and *pp2ac5* lines (F**igure 3.18A, C and E**). Therefore, I only used *pp2ac2* and *pp2ac4* for further functional studies.

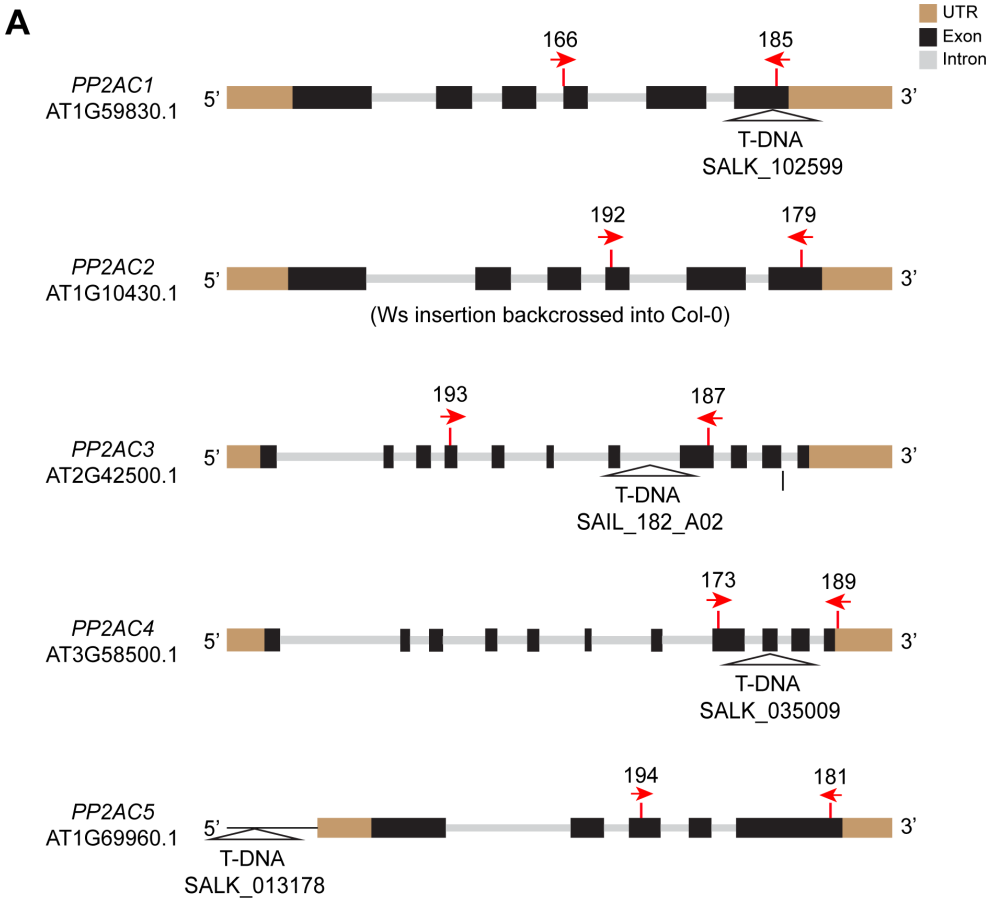
A
UTR
Exon
Intron
PP2AC1
AT1G59830.1
5'
3'
166
185
T-DNA
SALK_102599
PP2AC2
AT1G10430.1
192
179
(Ws insertion backcrossed into Col-0)
PP2AC3
AT2G42500.1
193
187
T-DNA
SAIL_182_A02
PP2AC4
AT3G58500.1
173
189
T-DNA
SALK_035009
PP2AC5
AT1G69960.1
194
181
T-DNA
SALK_013178

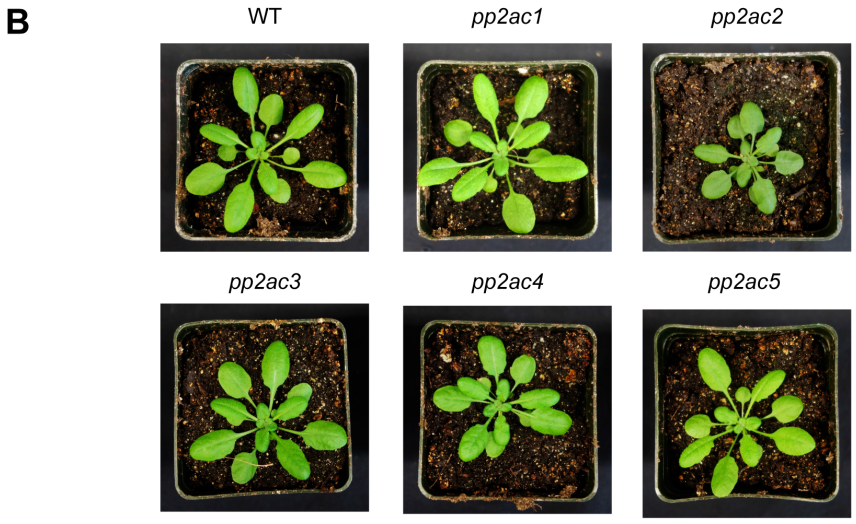
B
WT
pp2ac1
pp2ac2
pp2ac3
pp2ac4
pp2ac5

Figure 3.17. Characterization of PP2A C subunit mutants. C subunit mutants were provided by Dr. Cyril Zipfel Lab at The Sainsbury Laboratory. *pp2ac1*, *pp2ac3*, *pp2ac4*, and *pp2ac5* are T-DNA insertion mutants, while *pp2aa2* has Ws insertion backcrossed to Col-0. **(A)** Schematic of Arabidopsis PP2AC1-C5 gene structures. The SALK or SAIL number of each mutant line as well as the T-DNA insertion site were labeled. Red arrows indicate the forward and reverse primers used for RT-PCR analysis of each mutant line. **(B)** Phenotypes of WT and *pp2ac1-c5* mutant adult plants. *pp2ac2* and *pp2ac4* mutants are smaller in size.

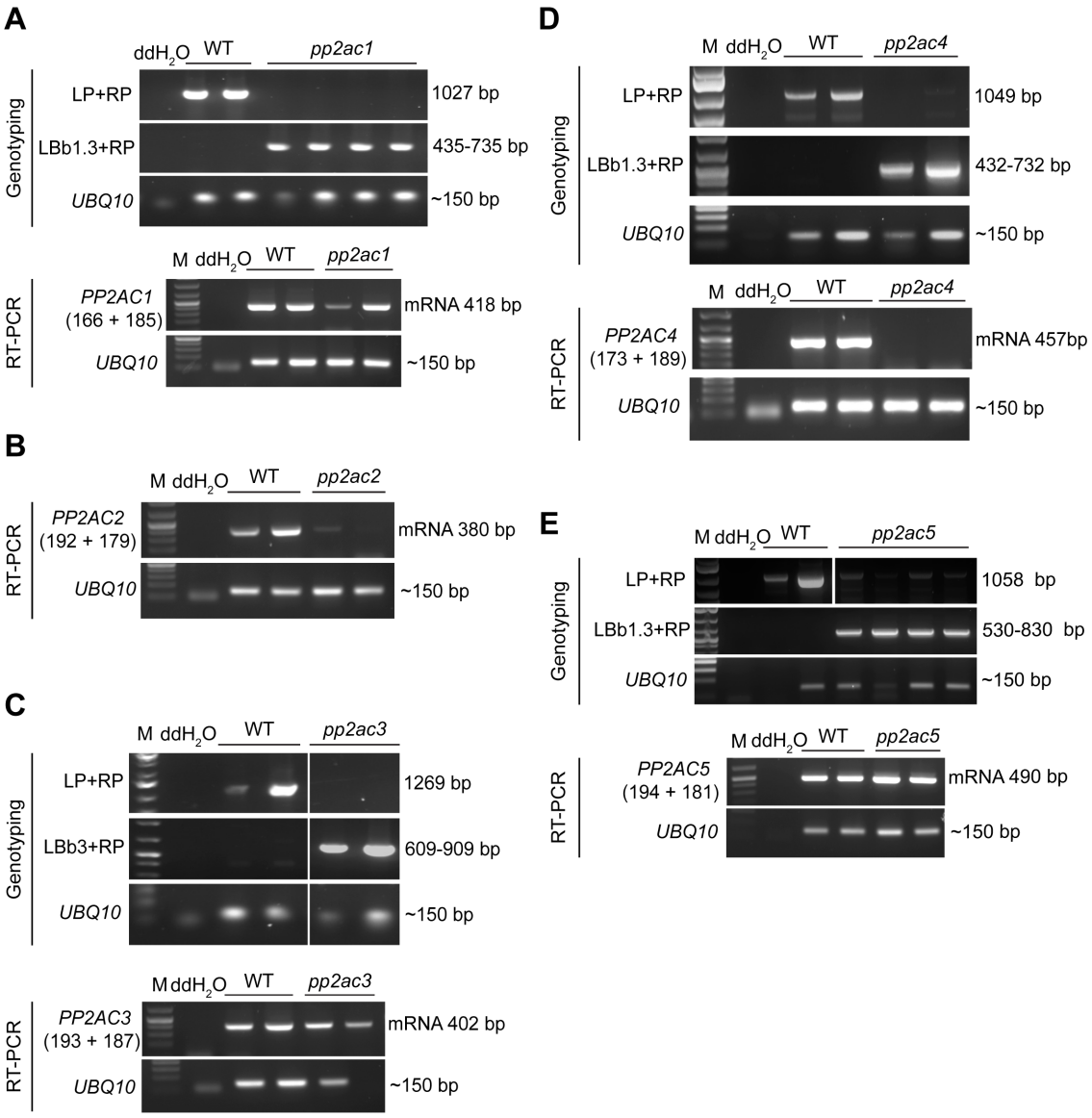
A
ddH2O WT pp2ac1
Genotyping
LP+RP
1027 bp
LBb1.3+RP
435-735 bp
UBQ10
~150 bp
M ddH2O WT pp2ac1
RT-PCR
PP2AC1
(166 + 185)
mRNA 418 bp
UBQ10
~150 bp
B
M ddH2O WT pp2ac2
RT-PCR
PP2AC2
(192 + 179)
mRNA 380 bp
UBQ10
~150 bp
C
M ddH2O WT pp2ac3
Genotyping
LP+RP
1269 bp
LBb3+RP
609-909 bp
UBQ10
~150 bp
M ddH2O WT pp2ac3
RT-PCR
PP2AC3
(193 + 187)
mRNA 402 bp
UBQ10
~150 bp
D
M ddH2O WT pp2ac4
Genotyping
LP+RP
1049 bp
LBb1.3+RP
432-732 bp
UBQ10
~150 bp
M ddH2O WT pp2ac4
RT-PCR
PP2AC4
(173 + 189)
mRNA 457bp
UBQ10
~150 bp
E
M ddH2O WT pp2ac5
Genotyping
LP+RP
1058 bp
LBb1.3+RP
530-830 bp
UBQ10
~150 bp
M ddH2O WT pp2ac5
RT-PCR
PP2AC5
(194 + 181)
mRNA 490 bp
UBQ10
~150 bp

Figure 3.18. Genotyping and RT-PCR analyses of PP2A C subunit mutants. A PCR-based genotyping and RT-PCR of *pp2ac* mutants. **(A, C-E)** *pp2ac1*, *pp2ac3*, *pp2ac4*, and *pp2ac5* are T-DNA insertion mutants, where the LP and RP (left and right genomic primers), together with the LBb1.3 and LB3 (left border primers of the T-DNA insertion) were used for their genotyping (see Materials and Methods). RT-PCR analyses of each mutant were performed using primers indicated in **Figure 3.17**. All these T-DNA insertion mutants, *pp2ac1* (A), *pp2ac3* (C), *pp2ac4* (D), and *pp2ac5* (E), were shown to be homozygous lines. However, only *pp2ac4* had negative RT-PCR results, while others showed RT-PCR positive. **(B)** *PP2AC2* gene expression was examined in the *pp2ac2* mutant, a line with Ws insertion backcrossed to Col-0, and the RT-PCR result was negative (primer targeting sites see **Figure 3.17**). Ubiquitin 10 (UBQ10) was used as an internal control.

3.12 Mutation of PP2A A subunit in Arabidopsis with PSR2-overexpressing genetic background

To study whether the PP2A A subunits (RCN1 and PDF1) participate in regulating PSR2-mediated small RNA and disease phenotypes, I generated Arabidopsis lines expressing PSR2 in either *rcn1* or *pdf1* mutant backgrounds (PSR2-5^{OE}*rcn1-6* and PSR2-5^{OE}*pdf1-1*). Firstly, PSR2-5^{OE}*rcn1-6* mutant was generated by crossing *rcn1-6* mutant (the pistil donor) with PSR2-5^{OE} line (the pollen donor). Genotyping PCR and RT-PCR were used to validate the corresponding genotype and mRNA transcripts of PSR2-5^{OE}*rcn1-6* mutant, respectively (**Figure 3.19A**). I obtained one homozygous line of PSR2-5^{OE}*rcn1-6* (line 17, the F3 generation), which showed the same root development defect as *rcn1-6* mutant (**Figure 3.19B**). In addition, the curl-leaf phenotypes caused by PSR2 expression seen in PSR2-5^{OE} plants was rescued in the *rcn1-6* mutant background (the PSR2-5^{OE}*rcn1-6* mutant) (**Figure 3.19C**).

A similar strategy was used to generate the PSR2-5^{OE}*pdf1-1* mutant line, where *pdf1-1* mutant was the pistil donor and the PSR2-5^{OE} line was the pollen donor. Genotyping PCR combined with the herbicide selection (Basta) were used to screen the genotype of PSR2-5^{OE}*pdf1-1* homozygous mutant (**Figure 3.20**). I recovered two PSR2-5^{OE}*pdf1-1* lines (line 23 and line 26) at the F3 generation as homozygous *pdf1-1* mutation (*pdf1-1*−/−) by genotyping PCR (**Figure 3.20A**). However, these lines were heterozygous for PSR2-5^{OE} transgene (PSR2-5^{OE}+/−) by Basta selection. Instead of screening the homozygous PSR2-5^{OE} transgene with one additional generation, I directly used the F3 generation of PSR2-5^{OE}*pdf1-1* (both line 23 and line 26) for the functional assays by

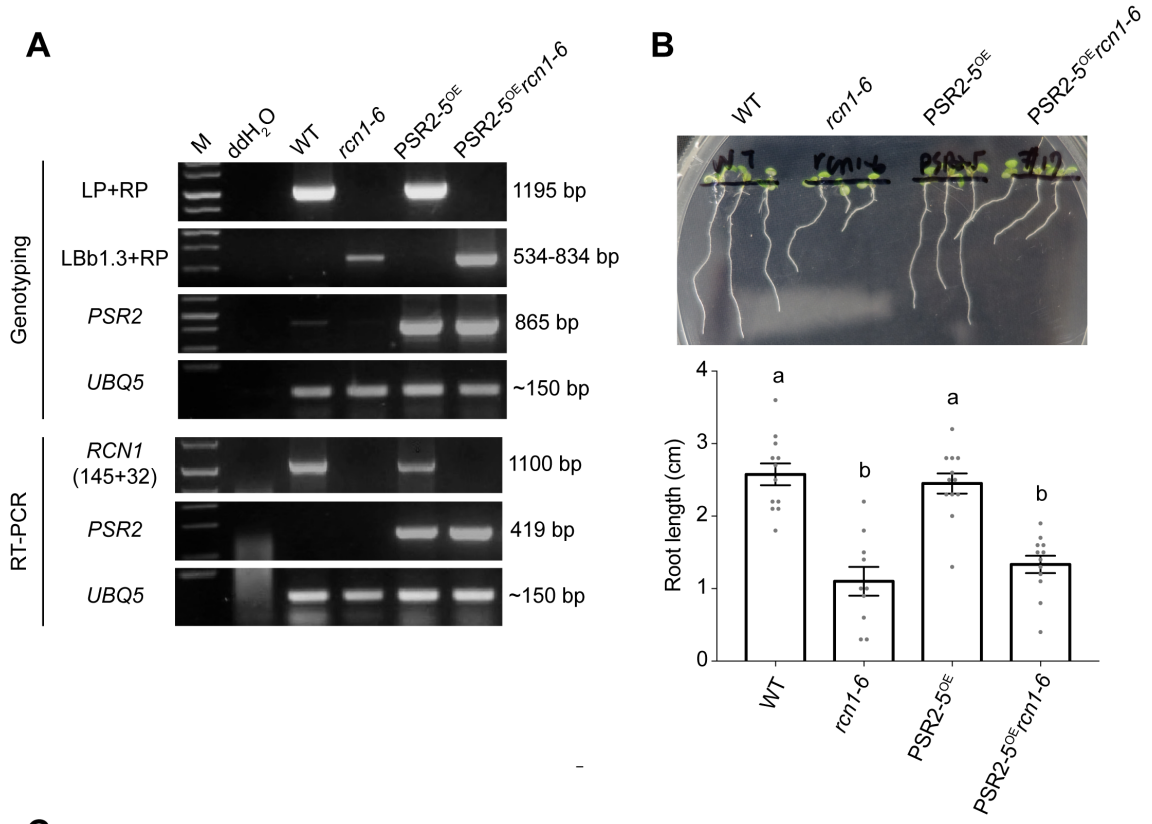
A
M
ddH2O
WT
rcn1-6
PSR2-5OE
PSR2-5OErcn1-6
Genotyping
LP+RP
1195 bp
LBb1.3+RP
534-834 bp
PSR2
865 bp
UBQ5
~150 bp
RT-PCR
RCN1
(145+32)
1100 bp
PSR2
419 bp
UBQ5
~150 bp
B
WT
rcn1-6
PSR2-5OE
PSR2-5OErcn1-6
Root length (cm)
0
1
2
3
4
a
b
a
b
C
WT
rcn1-6
PSR2-5OE
PSR2-5OErcn1-6

Figure 3.19. Characterization of PSR2-5^{OE}*rcn1-6* transgenic line. (A) PCR-based genotyping (top) and RT-PCR analysis (bottom) for PSR2-5^{OE}*rcn1-6* line with WT and its parental lines. LP and RP refer to left and right genomic primers, and LBb1.3 refers to the left border primer of the T-DNA insertion (see Materials and Methods). RT-PCR primers (145+32) were indicated in **Figure 3.15**. Ubiquitin 5 (UBQ5) was used as an internal control. **(B-C)** Phenotypes of WT, PSR2-5^{OE}, *rcn1-6*, and PSR2-5^{OE}*rcn1-6* seedlings (B) and adult plants (C). Note that both *rcn1-6* and PSR2-5^{OE}*rcn1-6* seedlings exhibited characteristic abnormalities of shorter root length.

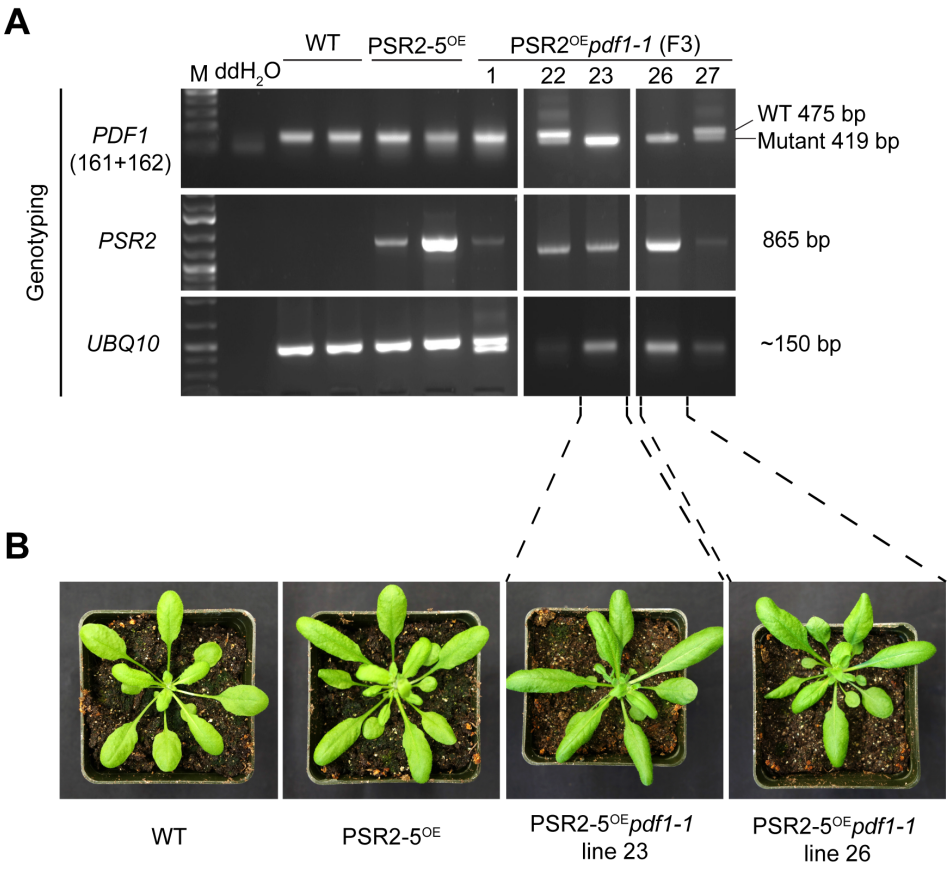

Figure 3.20. Characterization of PSR2-5^{OE}*pdf1-1* transgenic line. (A) PCR-based genotyping for five different PSR2-5^{OE}*pdf1-1* lines at the F3 generation together with WT and PSR2-5^{OE} plants. RT-PCR primers (161+162) were indicated in **Figure 3.16**. PSR2-5^{OE}*pdf1-1* line 23 and line 26 showed mutant *PDF1* size (56 bp shorter in length than wildtype with positive amplification of *PSR2* transgene. Ubiquitin 10 (UBQ10) was used as an internal control. **(B)** Phenotypes of WT, PSR2-5^{OE}, PSR2-5^{OE}*pdf1-1* line 23 and line 26 adult plants. Note that PSR2^{OE}*pdf1-1* lines germinated slower on the MS agar supplemented with Basta compared to the WT, but germinated normally as the WT on MS agar without Basta.

growing them on the MS-Basta medium to ensure the survived seedlings contain the PSR2-5 transgene. Unlike the PSR2-5^{OE}*rcn1-6* line, both lines of PSR2-5^{OE}*pdf1-1* showed delayed germination on the MS-Basta medium and mild curl-leaf phenotype at the adult stage (**Figure 3.20B**).

3.13 Phytophthora infection assay was used to test the disease susceptibility of different Arabidopsis lines

After generating different mutant lines for PP2A A and C subunits, I tested whether PP2A involved in plant immunity against *Phytophthora* infection by using the previously established Arabidopsis-*Phytophthora* pathosystem (Wang et al., 2013). Since *P. sojae* where PSR2 was first discovered from, is not pathogenic to Arabidopsis, an infection compatible species *P. capsici* was used for Arabidopsis infection in this system.

To control the precise amount of zoospore inoculum on leaves, I used the detached, fully expanded leaves for zoospore inoculation (**Figure 3.21A**). In general, three detached leaves (triplicates) collected from each Arabidopsis plant were placed up-side-down on water agar plate for infection (**Figure 3.21A, inset**). Due to the curling of Arabidopsis leaves, the *P. capsici* zoospore suspension could stay on the lower surface of leaf. The infection results were evaluated using Disease Severity Index (DSI) ranging from 0 (healthy) to 3 (the most severe) when visually inspecting the size of water-soaking lesion on each leaf (**Figure 3.21B**). Total number of leaves in each DSI category−0 (light grey), 1 (grey), 2 (dark grey), or 3 (black) were sum up in the stacked-bar graphs for each

genotype. Mean DSI of each genotype was also calculated for statistical analysis (see Materials and Methods for details).

3.14 PP2A single mutants enhanced plant defense against Phytophthora capsici

Previously studies established negative defense regulator roles of PP2A against bacterial pathogen *Pseudomonas syringae* (Segonzac et al., 2014). To understand whether PP2A is also involved in regulating plant immunity against *Phytophthora*, I first examined the *Phytophthora* infection phenotypes of *rcn1-6*, *pdf1-1*, *pp2ac2*, and *pp2ac4* mutants. My results showed that the disease susceptibility of *pdf1-1* and *pp2ac2* single mutants was reduced compared to infected-wild type plants (**Figure 3.22**). However, mutations on either the *RCN1* gene or the *PP2AC4* gene did not significantly change the disease phenotype compared to the wild-type plants. Altogether, these results suggested that Arabidopsis PP2A A (PDF1) and C (PP2AC2) subunits were involved in negatively regulating plant defense against *Phytophthora*.

As previously described (Zhou et al., 2004), *rcn1-6* mutant had the short root phenotype. However, I noticed that the roots among the individuals of *rcn1-6* mutant seedlings were shorter than wild-type seedlings to various degrees. Although my initial results showed no enhanced plant immunity against *Phytophthora* in the *rcn1-6* mutant, preliminary experiments using the *rcn1-6* mutants with the short root phenotype did show enhanced resistance against *Phytophthora* compared to wild-type plants, invoking the possibility of individual variation in the *rcn1-6* mutant population.

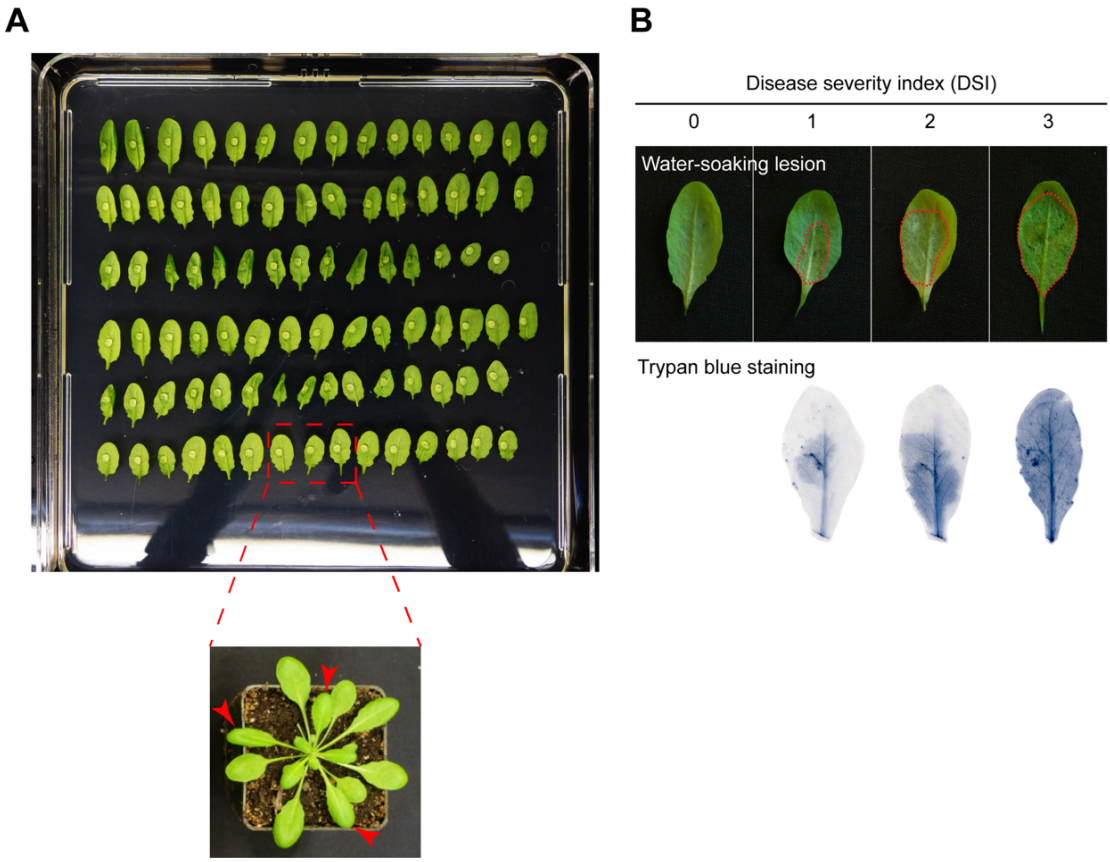

Figure 3.21. *P. capsici*-Arabidopsis infection assay (see Materials and Methods). (A) The representative image showed Arabidopsis detached leaves were placed up-side-down on 0.8% water agar plates with a droplet of zoospore suspension on the abaxial side of each leaf. The inset shows the 4th, 5th, and 6th leaf from the top (red arrowheads) of each plant were used for the infection assay. **(B)** The representative images showing the water-soaking lesion (top) and trypan blue staining of dead cells (bottom) from four different disease severity index, ranging from 0 to 3.

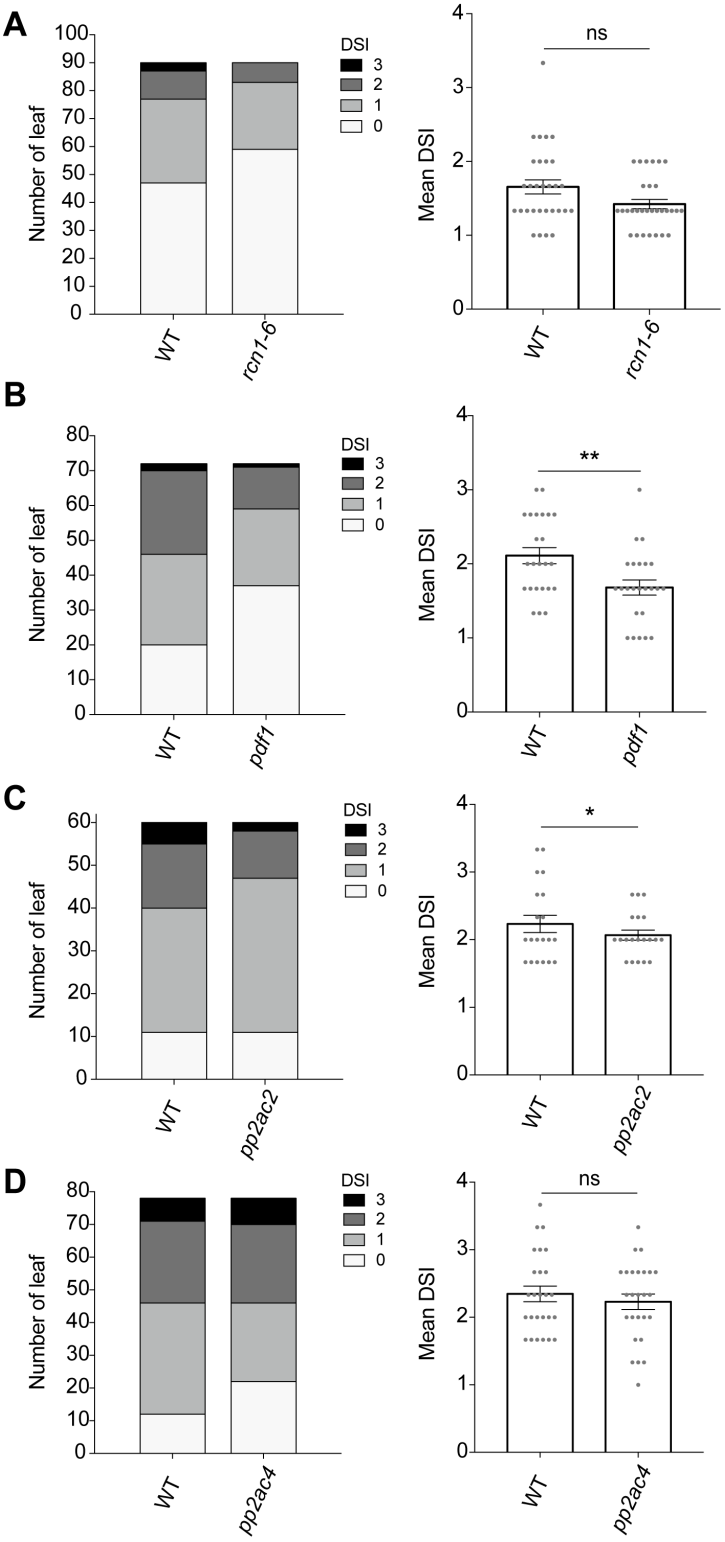
A
B
C
D
Number of leaf
DSI
3
2
1
0
Mean DSI
ns
**
*
WT
rcn1-6
pdf1
pp2ac2
pp2ac4

Figure 3.22. Disease severity of single mutant of PP2A A and C subunits upon *P. capsici* infection. The infection results of different mutants indicated were shown by both stacked bar (right) and the mean disease severity index (DSI, left). Both *pdf1-1* **(B)** and *pp2ac2* **(C)** mutants had significant reduction of disease severity compared to WT. However, *rcn1-6* **(A)** and *pp2ac4* **(D)** mutants did not show significant changes on disease phenotype compared to WT. The comparisons of Mean DSI between WT and mutants were done by unpaired t test. * $P<0.05$, ** $P<0.01$, ns, not significant.

To further examine the role of RCN1 in plant immunity against *Phytophthora*, specifically, I generated RCN1-overexpressing Arabidopsis lines (**Figure 3.23**). Genotyping PCR and western blot analyses confirmed the existence of 3×Flag-tagged RNC1 transgene and protein in these lines (**Figure 3.23A and B**). Next, I examined the disease susceptibility of RCN1-overexpressing lines, including RCN1-10-18^{OE}, RCN1-10-14^{OE}, and RCN1-9-7^{OE}, upon *Phytophthora* infection. I noticed that some individuals of the RCN1^{OE} Arabidopsis (e.g. ~30% of the RCN1-10-18^{OE} and RCN1-10-14^{OE} lines) exhibited striking developmental abnormalities, and remained small and dwarf (**Figure 3.23C**). Therefore, only the RCN1^{OE} Arabidopsis individuals with normal morphology as the wild-type were used for the infection experiments. I found that two of the three RCN1-overexpressing lines (RCN1-10-18^{OE} and RCN1-10-14^{OE}) showed significant increase in disease susceptibility (**Figure 3.24**), suggesting that RCN1 serve as a negative regulator of plant defense against *Phytophthora* infection.

3.15 PDF1 was functionally important for PSR2-mediated disease promotion

As a virulence factor, PSR2-5^{OE} Arabidopsis was known to have enhanced disease susceptibility compared to wild-type (Qiao et al., 2013, Xiong et al., 2014). To functionally evaluate whether PSR2 loses this disease promotion phenotype with genetic absence of PP2A A subunits, disease susceptibility of PSR2-5^{OE}*rcn1-6* and PSR2-5^{OE}*pdf1-1* mutant were examined upon *P. capsici* infection. Importantly, PSR2-5^{OE}*pdf1-1* mutants, both lines 23 and line 26 had more leaves with mild DSI and showed significantly reduced mean DSI compared to PSR2-5^{OE} alone (**Figure 3.25A and B**). The

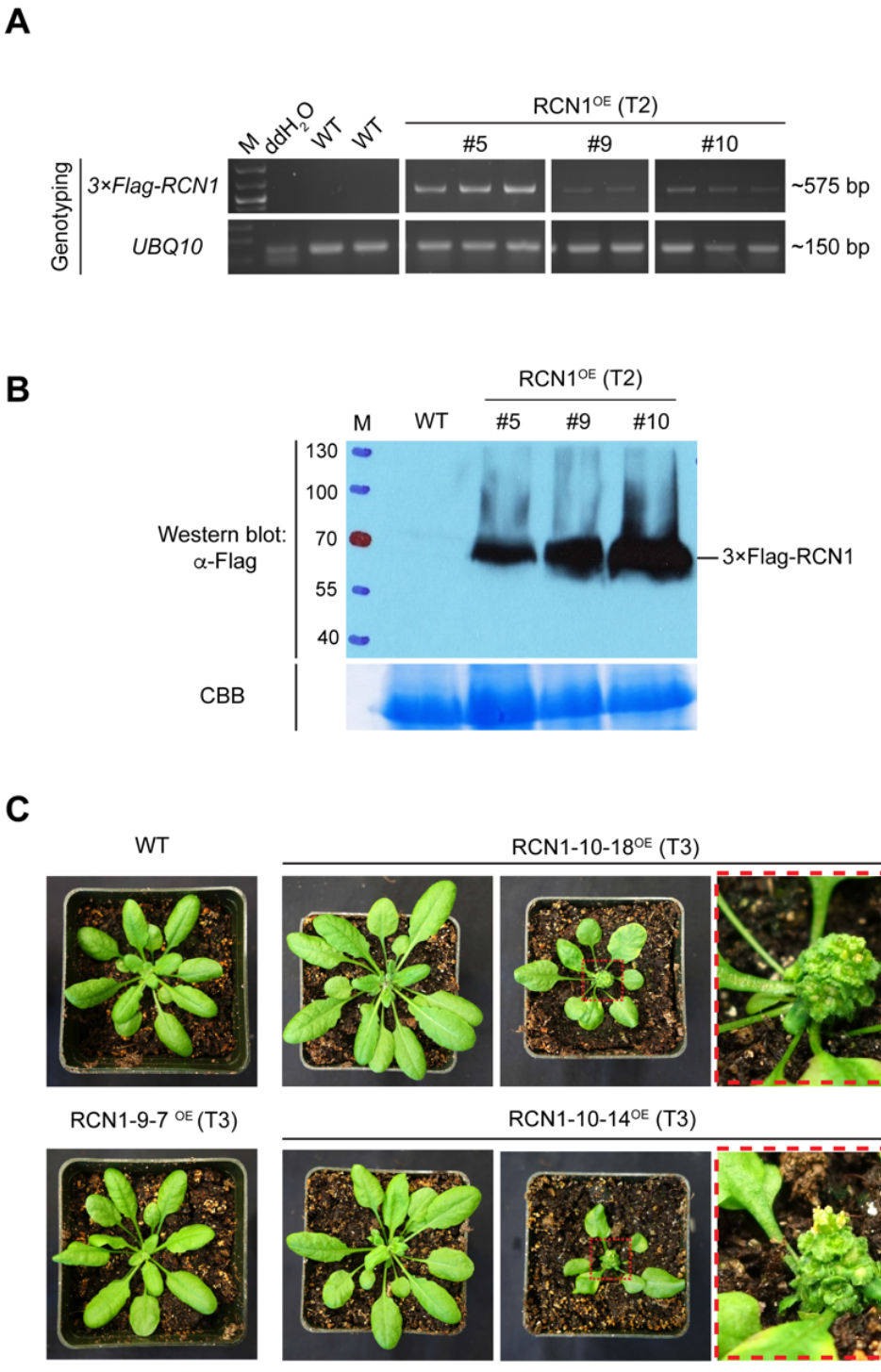
A
RCN1OE (T2)
M
ddH2O
WT
WT
#5
#9
#10
Genotyping
3×Flag-RCN1
UBQ10
~575 bp
~150 bp
B
RCN1OE (T2)
M
WT
#5
#9
#10
130
100
70
55
40
Western blot:
α-Flag
3×Flag-RCN1
CBB
C
WT
RCN1-10-18OE (T3)
RCN1-9-7 OE (T3)
RCN1-10-14OE (T3)

Figure 3.23. Characterization RCN1^{OE} transgenic lines. (A) PCR-based genotyping for three different RCN1^{OE} lines (#5, #9, and #10). PCR primers specific to *3×Flag*-tagged *RCN1* and ubiquitin 10 (UBQ10, negative control) were used. **(B)** Protein expression of RCN1 was examined in each line by western blotting using anti-Flag antibody. CBB staining was used as a loading control. **(C)** The adult plant phenotypes of WT, RCN1-9-7^{OE}, RCN1-10-18^{OE} and RCN1-10-14^{OE} lines. Note that the some of the plants of RCN1-10-18^{OE} and RCN1-10-14^{OE} lines showed abnormality of development.

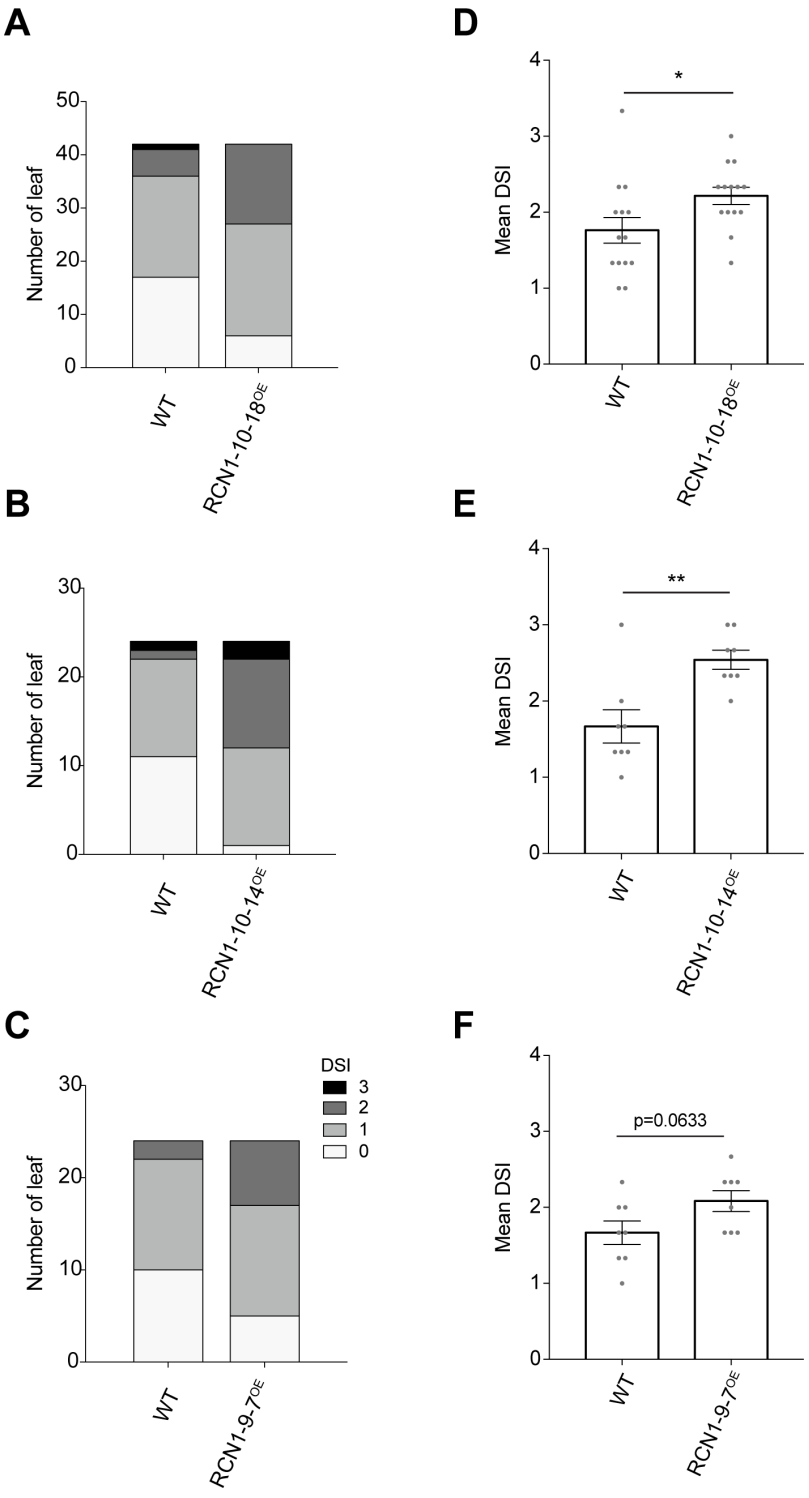
A
Number of leaf
50
40
30
20
10
0
WT
RCN1-10-18OE
B
Number of leaf
30
20
10
0
WT
RCN1-10-14OE
C
Number of leaf
DSI
3
2
1
0
WT
RCN1-9-7OE
D
Mean DSI
*
WT
RCN1-10-18OE
E
Mean DSI
**
WT
RCN1-10-14OE
F
Mean DSI
p=0.0633
WT
RCN1-9-7OE

Figure 3.24. Disease severity of RCN1^{OE} transgenic lines upon *P. capsici* infection. The infection results of different RCN1^{OE} transgenic lines, including RCN1-10-18^{OE}, RCN1-10-14^{OE} and RCN1-9-7^{OE}, were shown by both stacked bar **(A-C)** and the mean disease severity index **(D-F)**. The comparisons of Mean DSI between WT and mutants were done by unpaired t test. * $P<0.05$, ** $P<0.01$, ns, not significant.

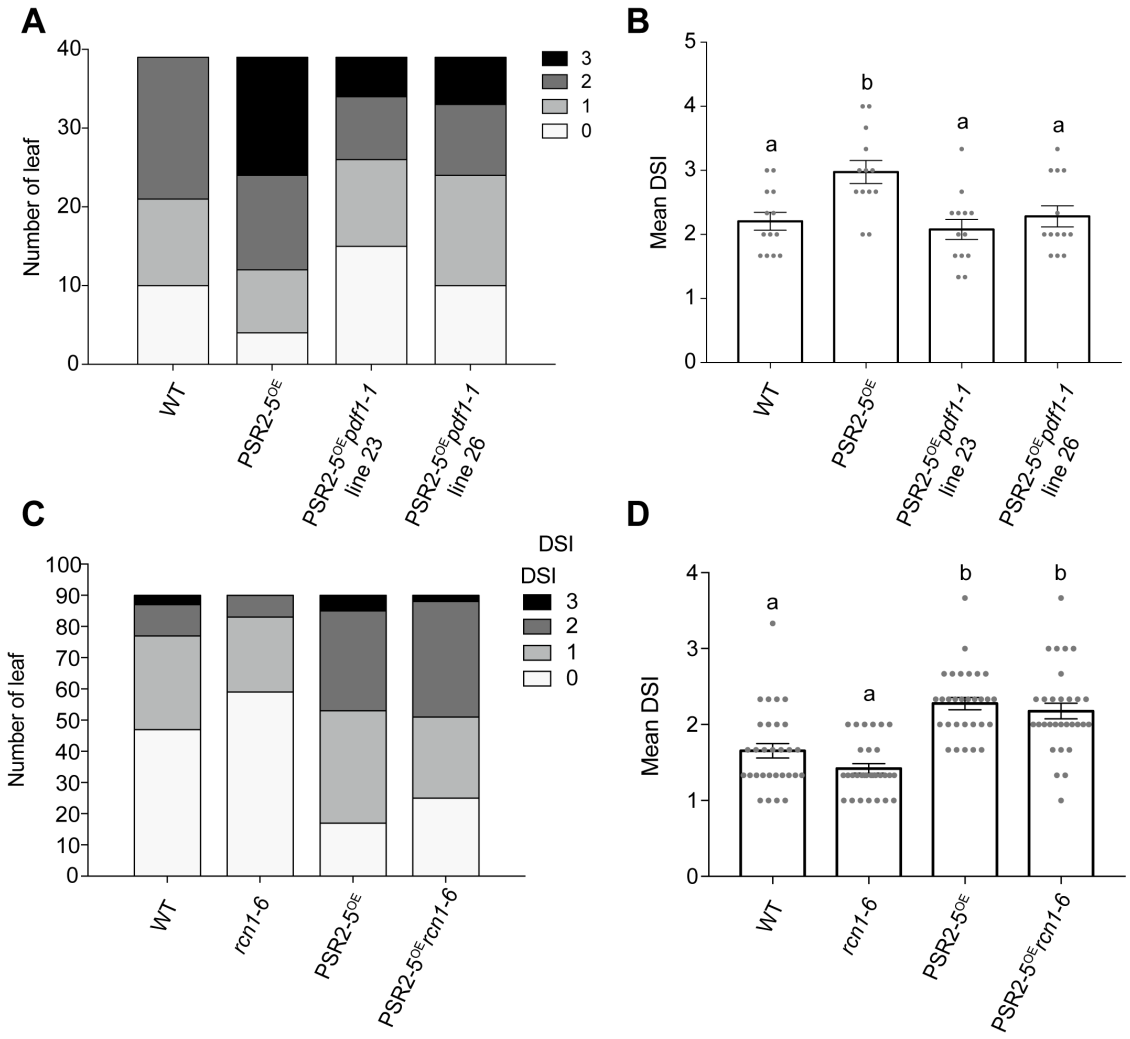
A
Number of leaf
40
30
20
10
0
3
2
1
0
WT
PSR2-5OE
PSR2-5OEpdf1-1 line 23
PSR2-5OEpdf1-1 line 26
B
Mean DSI
5
4
3
2
1
0
a
b
a
a
WT
PSR2-5OE
PSR2-5OEpdf1-1 line 23
PSR2-5OEpdf1-1 line 26
C
Number of leaf
100
90
80
70
60
50
40
30
20
10
0
DSI
DSI
3
2
1
0
WT
rcn1-6
PSR2-5OE
PSR2-5OErcn1-6
D
Mean DSI
4
3
2
1
0
a
a
b
b
WT
rcn1-6
PSR2-5OE
PSR2-5OErcn1-6

Figure 3.25. Disease severity of PSR2^{OE}*rcn1-6* and PSR2^{OE}*pdf1-1* transgenic lines upon *P. capsici* infection. Both stacked bar (A, C) and the mean disease severity index (B, D) were used to show *P. capsici* infection results on PSR2^{OE}*rcn1-6* and PSR2^{OE}*pdf1-1* transgenic lines. **(A-B)** PSR2^{OE}*pdf1-1* showed significant reduction of disease severity compared to PSR2^{OE}. Note that the result of *P. capsici* infection on *pdf1-1* mutant alone is in **Figure 3.22**. **(C-D)** *rcn1-6* mutant alone did not significantly change the disease severity compared to WT; similarly, PSR2^{OE}*rcn1-6* did not significantly change the disease severity compared to PSR2^{OE}. The comparisons of Mean DSI between different groups were done by one-way ANOVA with post-hoc Tukey test. Different letters indicate significantly different groups, $P<0.05$.

disease severity of both lines of PSR2-5^{OE}*pdf1-1* mutant were statistically indistinguishable from the wild-type. These results suggested that *PDF1* may be required for PSR2-mediated disease promotion.

I also examined the disease susceptibility of PSR2-5^{OE}*rcn1-6* mutant upon *Phytophthora* infection. Preliminary results showed that there was no significant difference in the disease symptom between PSR2-5^{OE}*rcn1-6* and PSR2-5^{OE} plants (**Figure 3.25C and D**). However, there is also variations of the short root phenotype found in the PSR2-5^{OE}*rcn1-6* population. Indeed, one preliminary infection dataset using the PSR2-5^{OE}*rcn1-6* individuals with the short root phenotype, showed a reduced mean DSI compared to PSR2-5^{OE} plants. Given the caveats that the *rcn1-6* mutant allele might not be homogeneous across whole population, the role of RCN1 in PSR2-mediated disease promotion is still inconclusive.

3.16 Functional involvement of RCN1 and PDF1 in PSR2-mediated small RNA suppression

To further understand if PSR2 loses the ability to suppress phasiRNA production when PP2A A subunit is absent, small RNA accumulation in the PSR2-5^{OE}*rcn1-6* mutant and PSR2-5^{OE}*pdf1-1* mutant was tested by Northern blotting. Total RNAs were obtained from the wild-type Arabidopsis, the crossing parental plants (PSR2-5^{OE} and *rcn1-6* or *pdf1-1* mutants), and the crossing lines (PSR2-5^{OE}*rcn1-6* and PSR2-5^{OE}*pdf1-1* mutants) and the abundance of specific small RNAs was determined by northern blot analysis (the small RNA Northern blot was done by Dr. Yingnan Hou). Here, miR173 was used to

represent microRNA species; while the secondary siRNA species, TAS1-tasiR255 and TAS2-tasiR1511, which are derived from *miR173*/*TAS1*/*TAS2* non-coding mRNAs, were used to represent phasiRNA species (**Figure 3.26A**). In addition, miR390 and it downstream phasiRNA, TAS3-5'D8 tasiRNA, was also analyzed (**Figure 3.26B**).

Consistent with the published results from the lab (Qiao et al., 2013), PSR2-5^{OE} had no effect on miRNA production but showed largely reduced phasiRNA levels compared to wild-type (WT) plants. Interestingly, PSR2-mediated reduction of phasiRNAs (tasiR255, tasiR1511, and 5'D8) was abolished in the PSR2-5^{OE}*rcn1-6* mutant, while *rcn1-6* mutant alone had no effect on the small RNA biogenesis (**Figure 3.26**). PhasiRNA accumulation was also rescued in two independent lines of PSR2-5^{OE}*pdf1-1* (line 23 and 26), but was slightly increased in *pdf1-1* single mutant (**Figure 3.27**). These genetic results suggested that RCN1 and PDF1 are required for PSR2-mediated phasiRNA suppression.

Given by the fact that both single mutant of *rcn1-6* and *pdf1-1* did not significantly alter the phasiRNA accumulation compared to wild-type plants, a hijack model of *Phytophthora* PSR2 in phasiRNA regulation by hijacking PP2A scaffold was proposed. In the absence of PSR2, cellular PP2A scaffolds did not participate in the regulation of phasiRNA biogenesis. However, with the presence of PSR2, they were hijacked by PSR2 and mediated the function of PSR2 in suppressing phasiRNA production.

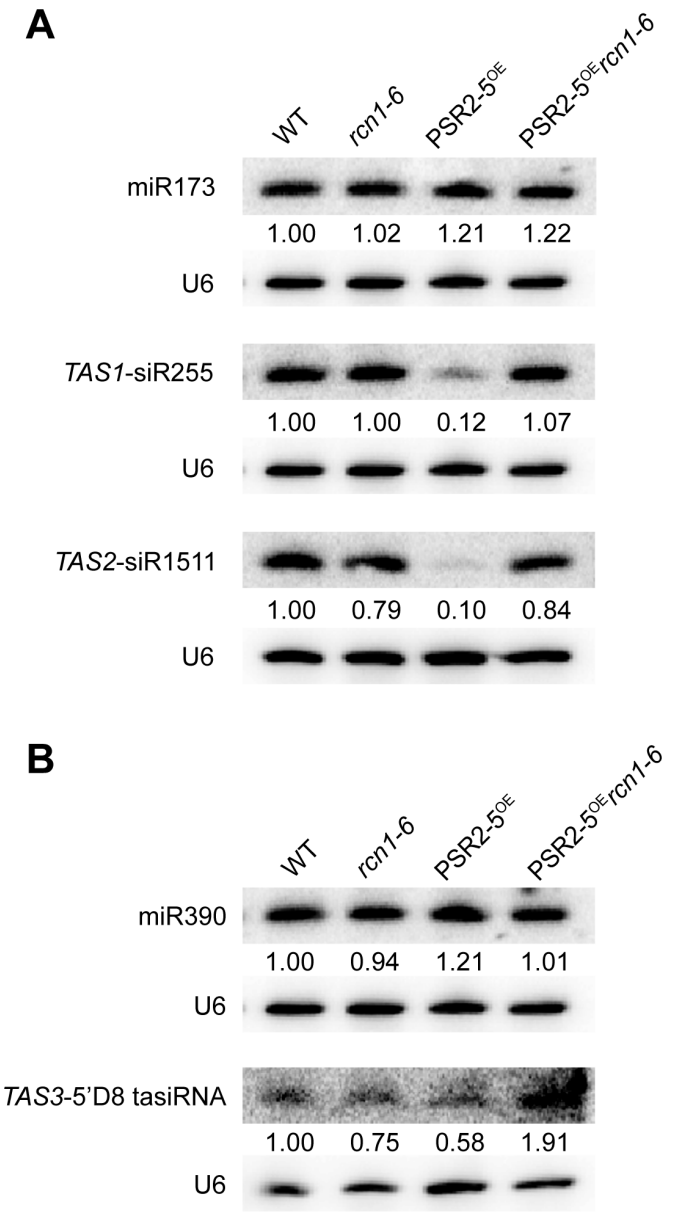
A
WT
rcn1-6
PSR2-5OE
PSR2-5OErcn1-6
miR173
1.00 1.02 1.21 1.22
U6
TAS1-siR255
1.00 1.00 0.12 1.07
U6
TAS2-siR1511
1.00 0.79 0.10 0.84
U6
B
WT
rcn1-6
PSR2-5OE
PSR2-5OErcn1-6
miR390
1.00 0.94 1.21 1.01
U6
TAS3-5'D8 tasiRNA
1.00 0.75 0.58 1.91
U6

Figure 3.26. RCN1 was required for PSR2-mediated phasiRNA suppression (small RNA Norther blotting performed by Dr. Yingnan Hou). Small RNA Northern blotting revealed the expression levels of microRNA (miR173 and miR390) and phasiRNA (*TAS1*-siR255, *TAS2*-siR1511, and *TAS3*-5′D8) in WT, *rcn1-6*, PSR2^{OE}, and PSR2^{OE}*rcn1-6* Arabidopsis lines. Blots were imaged using a PhosphorImager and each small RNA species were quantified using ImageQuant software, with normalization to the amount of U6 RNA (internal control). The numbers below each blot indicated the relative amount of each small RNA species as compared to the corresponding WT control. **(A)** Accumulations of *TAS1*-siR255 and *TAS2*-siR1511 were suppressed in PSR2^{OE} line, but not in the rescue line PSR2^{OE}*rcn1-6*. miR173 functions upstream the biogenesis pathway of *TAS1*-siR255 and *TAS2*-siR1511. **(B)** The suppression of *TAS3*-5′D8 could be seen in PSR2^{OE} line but not in PSR2^{OE}*rcn1-6* line. miR393 functions upstream the biogenesis pathway of *TAS3*-5′D8.

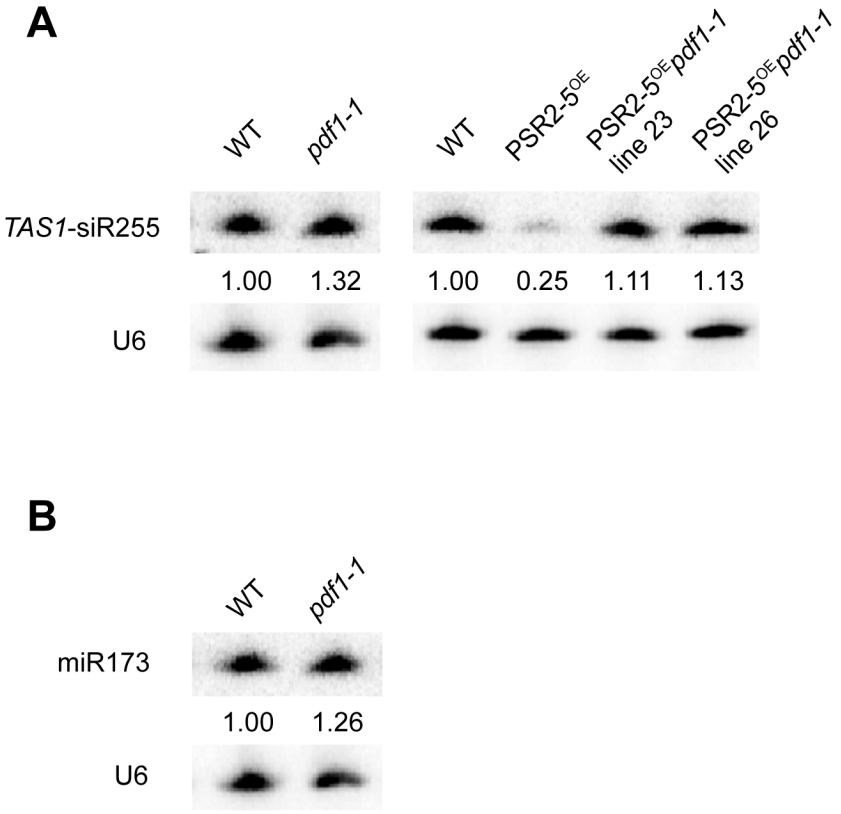
A
WT
pdf1-1
WT
PSR2-5OE
PSR2-5OE pdf1-1 line 23
PSR2-5OE pdf1-1 line 26
TAS1-siR255
1.00
1.32
1.00
0.25
1.11
1.13
U6
B
WT
pdf1-1
miR173
1.00
1.26
U6

Figure 3.27. PDF1 is required for PSR2-mediated phasiRNA suppression. This small RNA Norther blotting was performed with the support from Dr. Yingnan Hou. The expression levels of microRNA (miR173) and phasiRNA (*TAS1*-siR255) in WT, *pdf1-1*, PSR2^{OE}, and PSR2^{OE}*pdf1-1* Arabidopsis lines were shown by small RNA Northern blot analysis. Blots were imaged using a PhosphorImager and each small RNA species were quantified using ImageQuant software, with normalization to the amount of U6 RNA (internal control). The numbers below each blot indicate the relative amount of each small RNA species as compared to the corresponding wild-type control. **(A)** *TAS1*-siR255 production was suppressed in PSR2^{OE} line, but not in the PSR2^{OE}*rcn1-6* line 23 and line 26. *pdf1-1* mutant alone did not change *TAS1*-siR255 abundance compared to WT. **(B)** miR173 functions upstream the *TAS1*-siR255 biogenesis pathway and induces the production of *TAS1*-siR255. *pdf1-1* mutant did not alter the abundance of miR173 compared to WT.

3.17 Identification of PSR2 truncates that lose interactions with PP2A A subunits

To further investigate whether PP2A A subunits are required for PSR2-mediated phasiRNA suppression and disease promotion, I identified PSR2 domains that are important for interaction with RCN1/PDF1 and tested the functional consequence of these PSR2 truncates. The PSR2 family effectors exhibit multiple repeat units and each repeat unit is consisted of conserved W-Y or L-W-Y motifs (Ye & Ma, 2016). In PSR2, there is one WY motif followed by six LWY motifs (**Figure 3.28**). Previous members in the lab (M.S. Shuyi Duan and Dr. Duseok Choi) have generated a series of deletion mutants of PSR2, including the mutants lack one single repeat unit ($PSR2^{\Delta N}$, $PSR2^{\Delta WY1}$, $PSR2^{\Delta LWY2}$, $PSR2^{\Delta LWY3}$, $PSR2^{\Delta LWY4}$, $PSR2^{\Delta LWY5}$, $PSR2^{\Delta LWY6}$, and $PSR2^{\Delta LWY7}$) and several mutants lacking two repeat units (**Figure 3.28**)

To investigate which repeat(s) are required for the interaction with PP2A, I first tested interactions between these PSR2 deletion mutants and PP2A A subunits using Y2H (**Figure 3.29**). Eight single-deletion mutants and one double-deletion mutant were cloned into the Y2H BD vector, and their interactions were tested with AD-RCN1 and AD-PDF1 on the $SD^{Trp-Leu-His-}$ and $SD^{Trp-Leu-His-Ade-}$ selective media. RCN1 and PDF1 showed the same results in that they lost the interactions with $PSR2^{\Delta LWY2}$, $PSR2^{\Delta LWY3}$, $PSR2^{\Delta LWY4}$, $PSR2^{\Delta LWY5}$, $PSR2^{\Delta LWY6}$, and $PSR2^{\Delta LWY3+\Delta LWY4}$; however, they still interacted with $PSR2^{\Delta N}$, $PSR2^{\Delta WY1}$, and $PSR2^{\Delta LWY7}$ (**Figure 3.29A and B**). No yeast cell of the empty vector control grew on the selective media (**Figure 3.29C**). These results suggested that the LWY2, LWY3, LWY4, LWY5, LWY6 motifs of PSR2 are required for binding to

RCN1 and PDF1 in yeast. Note that the protein expression of these BD-PSR2 deletion mutant constructs in yeast was not yet tested.

To investigate if PSR2$^{\Delta LWY2}$, PSR2$^{\Delta LWY3}$, PSR2$^{\Delta LWY4}$, PSR2$^{\Delta LWY5}$, PSR2$^{\Delta LWY6}$ also lose the association with RCN1 in plant cells, the *in planta* co-IP was performed (**Figure 3.30**). These potential loss-of-interaction PSR2 deletion mutants were tagged with 3×Flag (the 3×Flag-PSR2 deletion mutants were cloned by Ms. Shuyi Duan and Dr. Duseok Choi) and served as the baits. The bacterial effector HopZ1a^{C216A} was used as a negative control. Consistent with the Y2H results, PSR2$^{\Delta LWY2}$, PSR2$^{\Delta LWY3}$, PSR2$^{\Delta LWY4}$, and PSR2$^{\Delta LWY6}$ showed nearly no interaction with RCN1 compared to the full-length PSR2 in the co-IP assay (**Figure 3.30**). Although PSR2$^{\Delta LWY5}$ was not tested in co-IP, my current co-IP results suggested that the LWY repeats in the middle region (LWY2, LWY3, LWY4, and LWY6) of PSR2 are critical for interacting with PP2A A subunits.

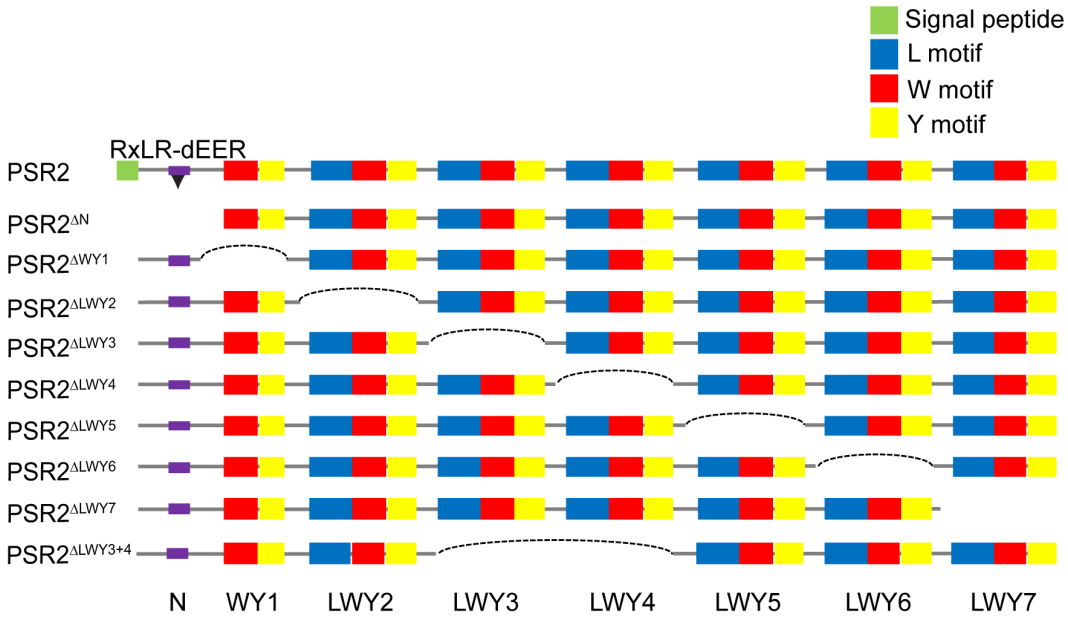

Figure 3.28. The protein structure of full-length PSR2 and PSR2 deletion mutants (figure adapted from Dr. Duseok Choi). Schematic cartoon showing the PSR2 protein structure with the repeated WY and LWY motifs. Full length PSR2 protein has a signal peptide at the N terminal (green box) followed by a signature RxLR-dEER motif (purple box) of RxLR effectors. Full length PSR2 which contains one WY and six LWY motifs is shown on top, following by seven different PSR2 deletion mutants, including $PSR2^{\Delta N}$, $PSR2^{\Delta WY1}$, $PSR2^{\Delta LWY2}$, $PSR2^{\Delta LWY3}$, $PSR2^{\Delta LWY4}$, $PSR2^{\Delta LWY5}$, $PSR2^{\Delta LWY6}$, and $PSR2^{\Delta LWY7}$.


SD Trp-Leu-
SD Trp-Leu-His-
SD Trp-Leu-His-Ade-
A
10 mM 3AT
AD-RCN1 + BD-PSR2
AD-RCN1 + BD-PSR2ΔN
AD-RCN1 + BD-PSR2ΔWY1
AD-RCN1 + BD-PSR2ΔLWY2
AD-RCN1 + BD-PSR2ΔLWY3
AD-RCN1 + BD-PSR2ΔLWY4
AD-RCN1 + BD-PSR2ΔLWY5
AD-RCN1 + BD-PSR2ΔLWY6
AD-RCN1 + BD-PSR2ΔLWY7
AD-RCN1 + BD-PSR2ΔLWY3+4
AD-RCN1 + BD-EV
B
1 mM 3AT
AD-PDF1 + BD-PSR2
AD-PDF1 + BD-PSR2ΔN
AD-PDF1 + BD-PSR2ΔWY1
AD-PDF1 + BD-PSR2ΔLWY2
AD-PDF1 + BD-PSR2ΔLWY3
AD-PDF1 + BD-PSR2ΔLWY4
AD-PDF1 + BD-PSR2ΔLWY5
AD-PDF1 + BD-PSR2ΔLWY6
AD-PDF1 + BD-PSR2ΔLWY7
AD-PDF1 + BD-PSR2ΔLWY3+4
AD-PDF1 + BD-EV
C
1 mM 3AT
AD-EV + BD-PSR2
AD-EV + BD-PSR2ΔN
AD-EV + BD-PSR2ΔWY1
AD-EV + BD-PSR2ΔLWY2
AD-EV + BD-PSR2ΔLWY3
AD-EV + BD-PSR2ΔLWY4
AD-EV + BD-PSR2ΔLWY5
AD-EV + BD-PSR2ΔLWY6
AD-EV + BD-PSR2ΔLWY7
AD-EV + BD-PSR2ΔLWY3+4
AD-EV + BD-EV

Figure 3.29. The region LWY2–LWY6 of PSR2 protein is required for interacting with PP2A A subunits in Y2H assays. PP2A A subunits RCN1 and PDF1 were used in this experiment. The protein interactions in Y2H assay were selected by the nutrient-deficient SD media, including $SD^{Trp-Leu-His-}$ and $SD^{Trp-Leu-His-Ade-}$. The $SD^{Trp-Leu-His-}$ agar plates were supplemented with 10 mM 3-AT while using AD-RCN1 construct for experiments **(A)**, but were only supplemented with 1 mM 3-AT while using other constructs **(B, C)**. **(A-B)** Both AD-RCN1 and AD-PDF1 could not interact with BD-$PSR2^{\Delta LWY2}$, BD-$PSR2^{\Delta LWY3}$, BD-$PSR2^{\Delta LWY4}$, BD-$PSR2^{\Delta LWY5}$, and BD-$PSR2^{\Delta LWY6}$. **(C)** the AD empty vector control.

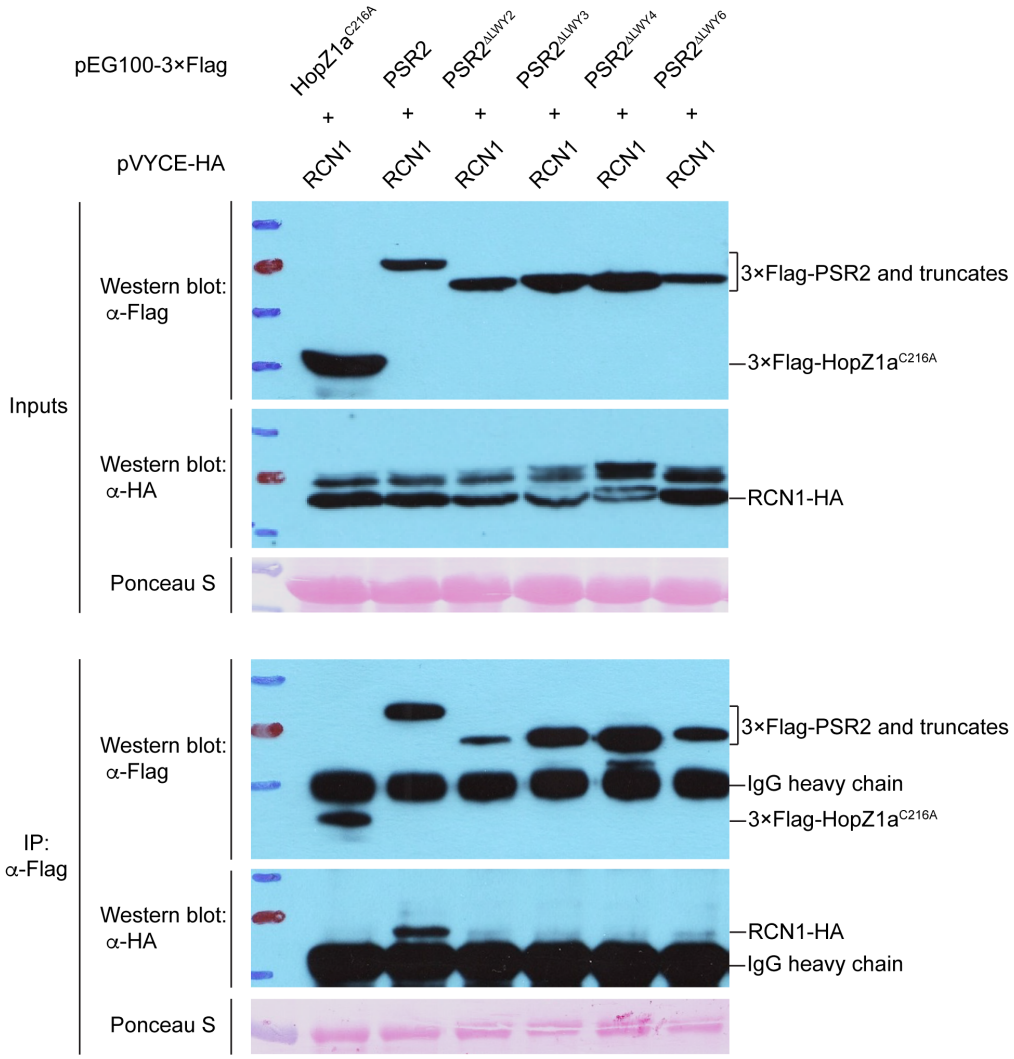
pEG100-3×Flag
HopZ1a^C216A
PSR2
PSR2^ΔLWY2
PSR2^ΔLWY3
PSR2^ΔLWY4
PSR2^ΔLWY6
+
pVYCE-HA
RCN1
Inputs
Western blot: α-Flag
3×Flag-PSR2 and truncates
3×Flag-HopZ1a^C216A
Western blot: α-HA
RCN1-HA
Ponceau S
IP: α-Flag
IgG heavy chain

Figure 3.30. The LWY2, LWY3, LWY4, and LWY6 motifs of PSR2 protein are required for interacting with PP2A A subunits in co-IP assay (LWY5 was not tested). 3×Flag tagged PSR2 and its truncates were co-expressed with HA-tagged RCN1 in *N. benthamiana* (inputs). Immunoprecipitates of the anti-Flag resin (IP: α-Flag) were analyzed by western blotting using anti-Flag and anti-HA antibodies, respectively. RCN1-HA had no if any interaction with 3×Flag-PSR2$^{\Delta LWY2}$, 3×Flag-PSR2$^{\Delta LWY3}$, 3×Flag-PSR2$^{\Delta LWY4}$, and 3×Flag-PSR2$^{\Delta LWY6}$. A non-interacting protein of RCN1 (3×Flag-HopZ1a^{C216A}) was used as a negative control of co-IP. Ponceau S staining was used as a loading control.

3.18 The loss-of-interaction PSR2 deletion mutants partially lost the phasiRNA suppression activity

Upon identifying the loss-of-interaction PSR2 deletion mutants with PP2A (PSR2$^{\Delta LWY2\text{-}OE}$ PSR2$^{\Delta LWY3\text{-}OE}$, PSR2$^{\Delta LWY4\text{-}OE}$, PSR2$^{\Delta LWY5\text{-}OE}$ and PSR2$^{\Delta LWY6\text{-}OE}$), I next examined whether these PSR2 deletion mutants lose the ability to suppress phasiRNA biogenesis in Arabidopsis. To test this hypothesis, I generated transgenic Arabidopsis overexpressing these loss-of-interaction PSR2 truncates by *Agrobacterium*-mediated plant transformation, and successfully obtain the transgenic lines of PSR2$^{\Delta LWY2\text{-}OE}$, PSR2$^{\Delta LWY3\text{-}OE}$, and PSR2$^{\Delta LWY6\text{-}OE}$. Genotyping and western blot were used to validate the gene insertion and protein expression of the PSR2 mutants in transgenic lines (**Figure 3.31**). No obvious developmental abnormity was observed in the PSR2$^{\Delta LWY2\text{-}OE}$ PSR2$^{\Delta LWY3\text{-}OE}$, and PSR2$^{\Delta LWY6\text{-}OE}$ lines.

PSR2-5^{OE}, which expresses the full-length PSR2, showed significant reduced amount of phasiRNA accumulation in plants compared to the wild-type, consistent with the previous study (Qiao et al., 2013). Here, *TAS1*-tasi255 was used as a representative of phasiRNA family, and its accumulation in transgenic plants was analyzed by small RNA Northern blot (small RNA Northern blot was done with the assistance from Dr. Yingnan Hou). Notably, Arabidopsis lines expressing PSR2 truncates, including PSR2$^{\Delta LWY2\text{-}OE}$ PSR2$^{\Delta LWY3\text{-}OE}$, and PSR2$^{\Delta LWY6\text{-}OE}$, partially lost the ability to suppress phasiRNA biogenesis, shown by the higher amount of *TAS1*-tasi255 accumulation compared to PSR2-5 (**Figure 3.32**). The relative signal intensities for *TAS1*-tasi255/U6 ratio for these four PSR2 deletion mutants were around 0.55-0.63 with wild-type normalized to 1,

indicating these deletion mutants partially rescued the phasiRNA biogenesis. These results supported that the phasiRNA suppression activity of PSR2 depended on the binding of PSR2 to RCN1 and PDF1. Given that the amount of *TAS1*-tasi255 detected in these mutants was still lower than in wild-type, it suggested that factors other than RCN1 and PDF1 might be involved in mediating the small RNA suppression of PSR2.

3.19 Systematic analysis of PP2A-associating protein complexes in plants

My results suggest that *Phytophthora* effector PSR2 targets plant PP2A proteins, and the A subunits of PP2A are required for PSR2-mediated small RNA suppression. Since PP2As are serine/threonine phosphatases, their biological functions are likely accomplished by manipulating specific cellular substrate(s). To further elucidate how PSR2 and PP2A may regulate plant RNA silencing, I aim to identify potential substrates associated with PSR2 and PP2A using mass spectrometry-based IP analysis in *N. benthamiana*. Given that PSR2 suppresses small RNA biogenesis, I performed the mass spectrometry-based IP analysis while RNA silencing was actively induced. Specifically, *N. benthamiana* line 16c with constitutively GFP expression was used. Transgene-induced RNA silencing was achieved by transiently express exogenous GFP via agroinfiltration. In this case, it might increase the chance to identify proteins that are involved in regulating RNA silencing processes. Here, Arabidopsis PP2A scaffold RCN1 was used as the bait of this experiment.

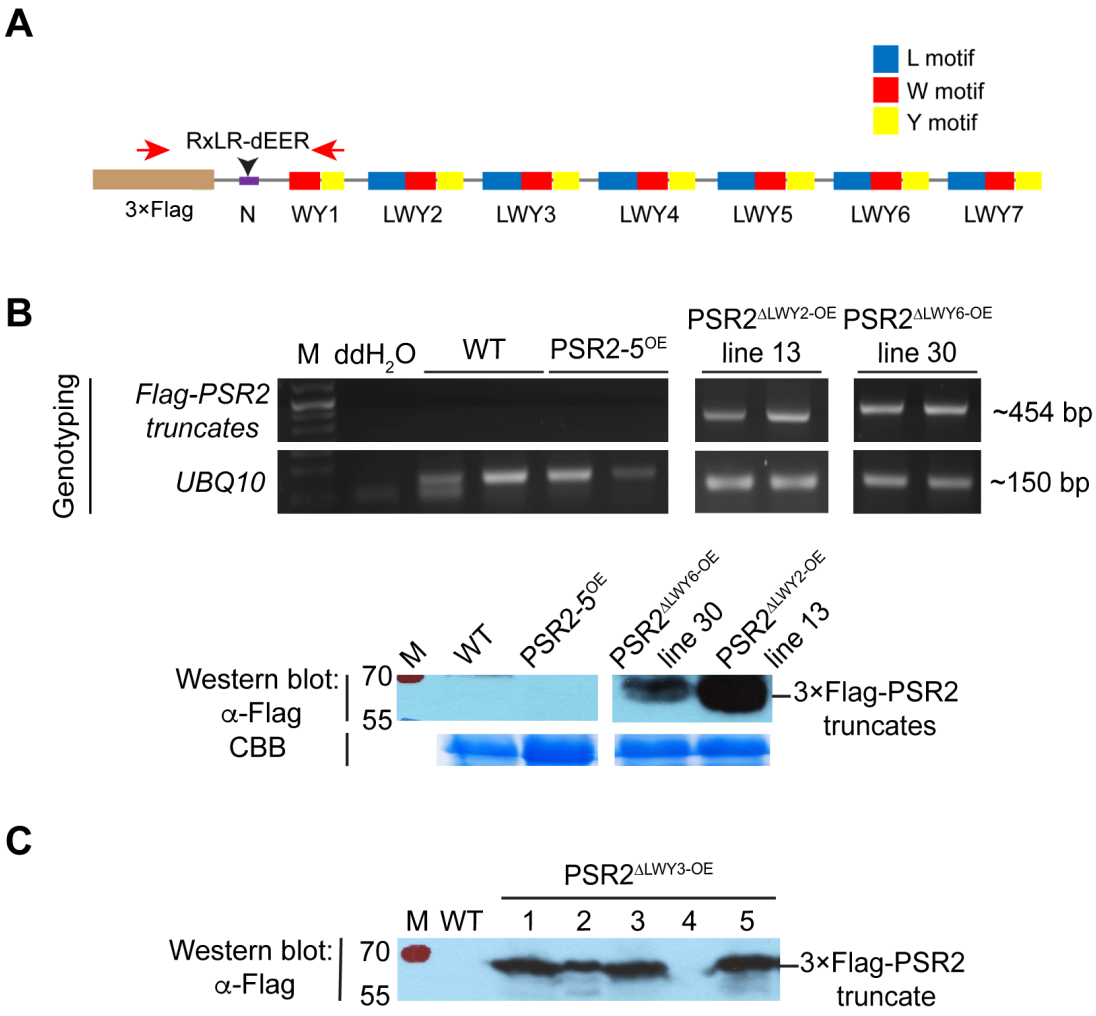
A
L motif
W motif
Y motif
RxLR-dEER
3×Flag
N
WY1
LWY2
LWY3
LWY4
LWY5
LWY6
LWY7
B
M
ddH2O
WT
PSR2-5OE
PSR2ΔLWY2-OE line 13
PSR2ΔLWY6-OE line 30
Genotyping
Flag-PSR2 truncates
UBQ10
~454 bp
~150 bp
Western blot: α-Flag
CBB
70
55
3×Flag-PSR2 truncates
C
PSR2ΔLWY3-OE
M WT 1 2 3 4 5
Western blot: α-Flag
70
55
3×Flag-PSR2 truncate

Figure 3.31. Characterization of Arabidopsis transgenic plants overexpressing PSR2 deletion mutants. Arabidopsis transgenic mutants PSR2$^{\Delta LWY2\text{-}OE}$, PSR2$^{\Delta LWY3\text{-}OE}$, PSR2$^{\Delta LWY4\text{-}OE}$, and PSR2$^{\Delta LWY6\text{-}OE}$ were generated (PSR2$^{\Delta LWY5\text{-}OE}$ was not obtained). PCR-based genotyping and western blotting were used to validate the gene insertion and protein expression of these lines. **(A)** A schematic picture modified from Dr. Duseok Choi shows PSR2 protein structure and the primers used in genotyping. **(B)** PSR2$^{\Delta LWY2\text{-}OE}$ and PSR2$^{\Delta LWY6\text{-}OE}$ lines were confirmed to have their transgenes and protein expression examined by PCR and anti-Flag western blotting. UBQ10 and CBB staining were used as loading controls for PCR and western blotting, respectively. Note that the PSR2 protein expression of PSR2-5^{OE} line was not recognized by anti-Flag antibody might due to unknown cellular processes trimming off the Flag-tag (see Discussion for details). **(C)** PSR2$^{\Delta LWY3}$ protein expression in five different PSR2$^{\Delta LWY3\text{-}OE}$ lines was examined by anti-Flag western blotting.

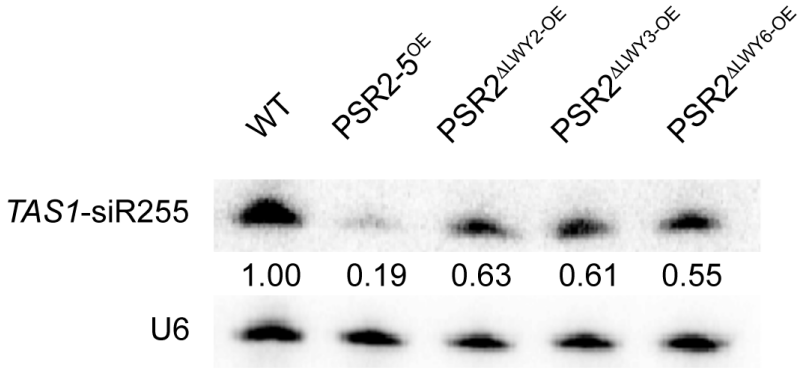

Figure 3.32. The loss-of-interaction PSR2 deletion mutants partially lost their activities in phasiRNA suppression. This small RNA Norther blotting was performed with the support from Dr. Yingnan Hou. The expression levels of phasiRNA (*TAS1*-siR255) was examined in WT, PSR2-5^{OE}, PSR2$^{\Delta LWY2\text{-}OE}$, PSR2$^{\Delta LWY3\text{-}OE}$, and PSR2$^{\Delta LWY6\text{-}OE}$ Arabidopsis lines using small RNA Northern blotting. Blots were imaged using a PhosphorImager and each small RNA species were quantified using ImageQuant software, with normalization to the amount of U6 RNA (internal control). The numbers below each blot indicate the relative amount of each small RNA species as compared to the corresponding WT control. Result showed that *TAS1*-siR255 production could not be fully suppressed in the plants overexpressing PSR2 deletion mutants who lose their associations with PP2A A subunits. However, *TAS1*-siR255 production was fully suppressed in PSR2-5^{OE} lines.

To identify additional proteins that might associate with PSR2 and PP2A in *N. benthamiana* line 16c, exogenous GFP, PSR2 and Flag-tagged RCN1 were transiently expressed in 16c plants. 3×Flag-RCN1-associating protein complexes were immunoprecipitated with anti-Flag resins, and the IP complexes were analyzed by the LTQ-Orbitrap Fusion mass spectrometry. The mass spectrometry results showed that RCN1 was associated with other PP2A subunits, including the B″family (4 hits), the B′ family (8 hits), the B family (8 hits), the C subunits (7 hits), and the A subunits (3 hits). In addition, RCN1 also associated with plenty of late blight resistance proteins (19 hits), other serine/threonine protein phosphatases SIT4 (6 hits) which were known to associate with PP2A, and few RNA silencing regulators (4 hits) (**Table 3.4**).

To understand whether these potential targets of RCN1 were found specifically in the presence of PSR2, I also performed mass spectrometry-based IP analysis with transiently expression of GFP and 3×Flag-RCN1 (**Figure 3.33**). Comparison of mass spectrometry results with the presence or the absence of PSR2 showed a high degree of overlap in both samples, suggesting either PSR2 might utilize similar RCN1 protein networks to regulate small RNA biogenesis, or there might be other non-PSR2 associated RCN1 protein complexes masking the identification of PSR2/RCN1 associated proteins.

3.20 PSR2 bound to PP2A core enzymes probably by acting as a PP2A B subunit

Although there was no protein candidate that specifically associated with RCN1 in the presence of PSR2, it is intriguing that many PP2A B subunits were immunoprecipitated when using RCN1 as the bait (**Table 3.4**), while none of the PP2A B subunits showed up

when using PSR2 as the bait (**Figure 3.33 and Table 3.5**). In Arabidopsis, there are 17 different B subunits classified in three B subunit families: six in the B″ family, nine in the B′ family, and two in the B family. The mass spectrometry data suggested that 3×Flag-RCN1 was associated with a number of PP2A B subunits in *N. benthamiana* 16c, and the phylogenetic relationship of these PP2A B subunits in *N. benthamiana* and Arabidopsis was analyzed. The phylogenetic tree revealed that 3×Flag-RCN1 may be associated with B subunits from all three families in Arabidopsis, including the ATB″δ, ATB″ε, ATB″γ, ATB′α, ATB′β, ATB′γ, ATB′η, ATB′κ, and ATBβ (**Figure 3.33**). Since PP2A B subunits are known as regulatory subunits for regulating substrate specificity and subcellular localization of the core enzyme (A and C subunits), the lack of all PP2A B subunit when using PSR2 as a bait for IP analysis indicated that PSR2 might act as a PP2A B subunit.

3.21 PSR2 had similar protein structure and binding properties with B′ subunits of PP2A

To explore the possibility that PSR2 might act as a PP2A B subunit, I first compared the published crystal structures of the PP2A from *Homo sapiens* (**Figure 3.34A**) with the PSR2 protein structure (**Figure 3.34B**, unpublished work in Dr. Wenbo Ma lab and Dr. Jinbiao Ma lab). Notably, both the B′ subunit and PSR2 had similar superhelical structures.

Table 3.4 Potential RCN1-associated proteins identified from *N. benthamiana* 16c under a RNA silencing-induced condition.

Nb accession number	Best match in *At*	Description
Serine/threonine protein phosphatase 2A (PP2A) B" family subunits		
NbS00023313g0035.1	AT5G28850.2	ATB" ε, Serine/threonine protein phosphatase 2A regulatory subunit B
NbS00011191g0017.1	AT5G28850.2	ATB" ε, Serine/threonine protein phosphatase 2A regulatory subunit B
NbS00002953g0001.1	AT1G54450.1	ATB" γ, Serine/threonine protein phosphatase 2A regulatory subunit B
NbC25940621g0002.1	AT5G28900.1	ATB" δ, Serine/threonine protein phosphatase 2A regulatory subunit B
Serine/threonine protein phosphatase 2A (PP2A) B' family subunits		
NbS00004881g0002.1	AT3G26020.2	ATB' η, Serine/threonine protein phosphatase 2A 59 kDa regulatory subunit B'
NbS00004393g0002.1	AT3G26020.2	ATB' η, Serine/threonine protein phosphatase 2A 59 kDa regulatory subunit B'
NbS00018995g0001.1	AT3G26020.2	ATB' η, Serine/threonine protein phosphatase 2A 59 kDa regulatory subunit B'
NbS00048529g0001.1	AT3G26020.2	ATB' η, Serine/threonine protein phosphatase 2A 59 kDa regulatory subunit B'
NbS00010073g0012.1	AT3G09880.1	ATB' β, Serine/threonine protein phosphatase 2A 57 kDa regulatory subunit B'
NbS00046550g0008.1	AT3G09880.1	ATB' β, Serine/threonine protein phosphatase 2A 57 kDa regulatory subunit B'
NbS00009603g0009.1	AT5G03470.1	ATB' α, Serine/threonine protein phosphatase 2A 57 kDa regulatory subunit B'
NbS00016621g0008.1	AT4G15415.1	ATB' γ, Serine/threonine protein phosphatase 2A 59 kDa regulatory subunit B'
Serine/threonine protein phosphatase 2A (PP2A) B family subunits		
NbS00020897g0013.1	AT1G17720.2	ATB β, Serine/threonine protein phosphatase 2A 55 kDa regulatory subunit B
NbS00001706g0008.1	AT1G17720.2	ATB β, Serine/threonine protein phosphatase 2A 55 kDa regulatory subunit B
NbS00042956g0009.1	AT1G17720.1	ATB β, Serine/threonine protein phosphatase 2A 55 kDa regulatory subunit B
NbS00009648g0006.1	AT1G17720.1	ATB β, Serine/threonine protein phosphatase 2A 55 kDa regulatory subunit B
NbS00015567g0011.1	AT1G17720.2	ATB β, Serine/threonine protein phosphatase 2A 55 kDa regulatory subunit B
NbS00044649g0001.1	AT1G17720.1	ATB β, Serine/threonine protein phosphatase 2A 55 kDa regulatory subunit B
NbS00008999g0022.1	AT1G17720.2	ATB β, Serine/threonine protein phosphatase 2A 55 kDa regulatory subunit B
NbS00052687g0004.1	AT1G17720.2	ATB β, Serine/threonine protein phosphatase 2A 55 kDa regulatory subunit B
Serine/threonine protein phosphatase 2A (PP2A) C subunits		
NbS00010634g0008.1	AT2G42500.1	Protein phosphatase 2A-3 (PP2A-3), serine/threonine protein phosphatase 2A catalytic subunit
NbS00052644g0005.1	AT2G42500.1	Protein phosphatase 2A-3 (PP2A-3), serine/threonine protein phosphatase 2A catalytic subunit
NbS00020903g0004.1	AT3G58500.1	Protein phosphatase 2A-4 (PP2A-4), serine/threonine protein phosphatase 2A catalytic subunit
NbS00009650g0005.1	AT3G58500.1	Protein phosphatase 2A-4 (PP2A-4), serine/threonine protein phosphatase 2A catalytic subunit
NbS00043074g0007.1	AT3G58500.1	Protein phosphatase 2A-4 (PP2A-4), serine/threonine protein phosphatase 2A catalytic subunit
NbS00051180g0008.1	AT1G10430.1	Protein phosphatase 2A-4 (PP2A-2), serine/threonine protein phosphatase 2A catalytic subunit
NbS00040706g0007.1	AT1G10430.1	Protein phosphatase 2A-4 (PP2A-2), serine/threonine protein phosphatase 2A catalytic subunit

Table 3.4 (Continued)

Nb accession number	Best match in *At*	Description
Serine/threonine protein phosphatase 2A (PP2A) A subunits		
NbS00006732g0010.1	AT3G25800.1	PDF1, protein phosphatase 2A subunit A2 (PP2AA2), protein phosphatase 2A 65 kDa regulatory subunit
NbS00031201g0004.1	AT3G25800.1	PDF1, protein phosphatase 2A subunit A2 (PP2AA2), protein phosphatase 2A 65 kDa regulatory subunit
NbS00023637g0006.1	AT3G25800.2	PDF1, protein phosphatase 2A subunit A2 (PP2AA2), protein phosphatase 2A 65 kDa regulatory subunit
Resistance proteins		
NbC24350532g0001.1	AT1G58400.1	Late blight resistance protein homolog R1B-8, disease resistance protein (CC-NBS-LRR class) family
NbS00016103g0004.1	AT1G53350.1	NRC1, late blight resistance protein homolog R1A-6, disease resistance protein (CC-NBS-LRR class) family
NbS00002971g0007.1	AT1G53350.1	NRC1, late blight resistance protein homolog R1A-6, disease resistance protein (CC-NBS-LRR class) family
NbS00030243g0001.1	AT1G53350.1	NRC1, late blight resistance protein homolog R1A-6, disease resistance protein (CC-NBS-LRR class) family
NbS00018282g0007.1	AT1G53350.1	NRC1, disease resistance RPP8-like protein 2 (CC-NBS-LRR class) family
NbS00031134g0006.1	AT1G53350.1	NRC1, late blight resistance protein homolog R1A-12, disease resistance protein (CC-NBS-LRR class) family
NbS00049598g0001.1	AT5G47280.1	NRC1, disease resistance protein (CC-NBS-LRR class) family, ADR1-LIKE 3
NbS00002627g0014.1	AT1G59780.1	Late blight resistance protein homolog R1B-12, NB-ARC domain-containing disease resistance protein
NbS00026706g0016.1	AT5G35450.1	NRC1, late blight resistance protein homolog R1A-12, disease resistance protein (CC-NBS-LRR class) family
NbS00002946g0006.1	AT5G35450.1	Late blight resistance protein homolog R1C-3, NB-ARC domain-containing disease resistance protein
NbS00033032g0022.1	AT5G35450.1	Prf, late blight resistance protein homolog R1B-16, disease resistance protein (CC-NBS-LRR class) family
NbS00018399g0005.1	AT5G35450.1	Prf, late blight resistance protein homolog R1B-16, disease resistance protein (CC-NBS-LRR class) family
NbS00004802g0023.1	AT3G07040.1	Disease resistance protein RPM1, RPS3, NB-ARC domain-containing disease resistance protein
NbS00002627g0004.1	AT3G46530.1	Late blight resistance protein homolog R1B-17, RPP13, NB-ARC domain-containing disease resistance protein
NbS00005888g0018.1	AT3G46530.1	Late blight resistance protein homolog R1B-12, RPP13, NB-ARC domain-containing disease resistance protein
NbS00031132g0007.1	AT3G46530.1	Late blight resistance protein homolog R1B-12, RPP13, NB-ARC domain-containing disease resistance protein
NbS00002627g0020.1	AT3G46530.1	Late blight resistance protein homolog R1B-13, RPP13, NB-ARC domain-containing disease resistance protein
NbS00005032g0004.1	AT3G46530.1	Late blight resistance protein homolog R1B-12, RPP13, NB-ARC domain-containing disease resistance protein
NbC25252651g0002.1	AT3G14470.1	N' tobamovirus resistance protein, disease resistance RPP13-like protein 1, NB-ARC domain-containing disease
Other serine/threonine protein phosphatases		
NbS00050068g0005.1	AT3G45190.1	Serine/threonine-protein phosphatase 6 regulatory subunit 3, SIT4 phosphatase-associated family protein
NbS00017033g0010.1	AT3G45190.1	Serine/threonine-protein phosphatase 6 regulatory subunit 3, SIT4 phosphatase-associated family protein
NbS00019018g0007.1	AT3G45190.1	Serine/threonine-protein phosphatase 6 regulatory subunit 3, SIT4 phosphatase-associated family protein
NbS00013645g0005.1	AT1G07990.1	Serine/threonine-protein phosphatase 6 regulatory subunit 3, SIT4 phosphatase-associated family protein
NbS00012513g0007.1	AT1G07990.1	Serine/threonine-protein phosphatase 6 regulatory subunit 3, SIT4 phosphatase-associated family protein
NbS00004831g0017.1	AT1G07990.1	Serine/threonine-protein phosphatase 6 regulatory subunit 3, SIT4 phosphatase-associated family protein
RNA silencing regulators		
NbS00008430g0013.1	AT1G48410.1	AGO1, stabilizer of iron transporter SufD, polynucleotidyl transferase, stem cell self-renewal protein Piwi
NbS00014977g0008.1	AT1G48410.1	AGO1, stabilizer of iron transporter SufD, polynucleotidyl transferase, stem cell self-renewal protein Piwi
NbS00007950g0008.1	AT2G27040.2	AGO4, argonaute family protein, stem cell self-renewal protein Piwi
NbS00022154g0003.1	AT3G03300.3	DCL2, dicer-like 2, ribonuclease 3-like protein 3, ribonuclease III

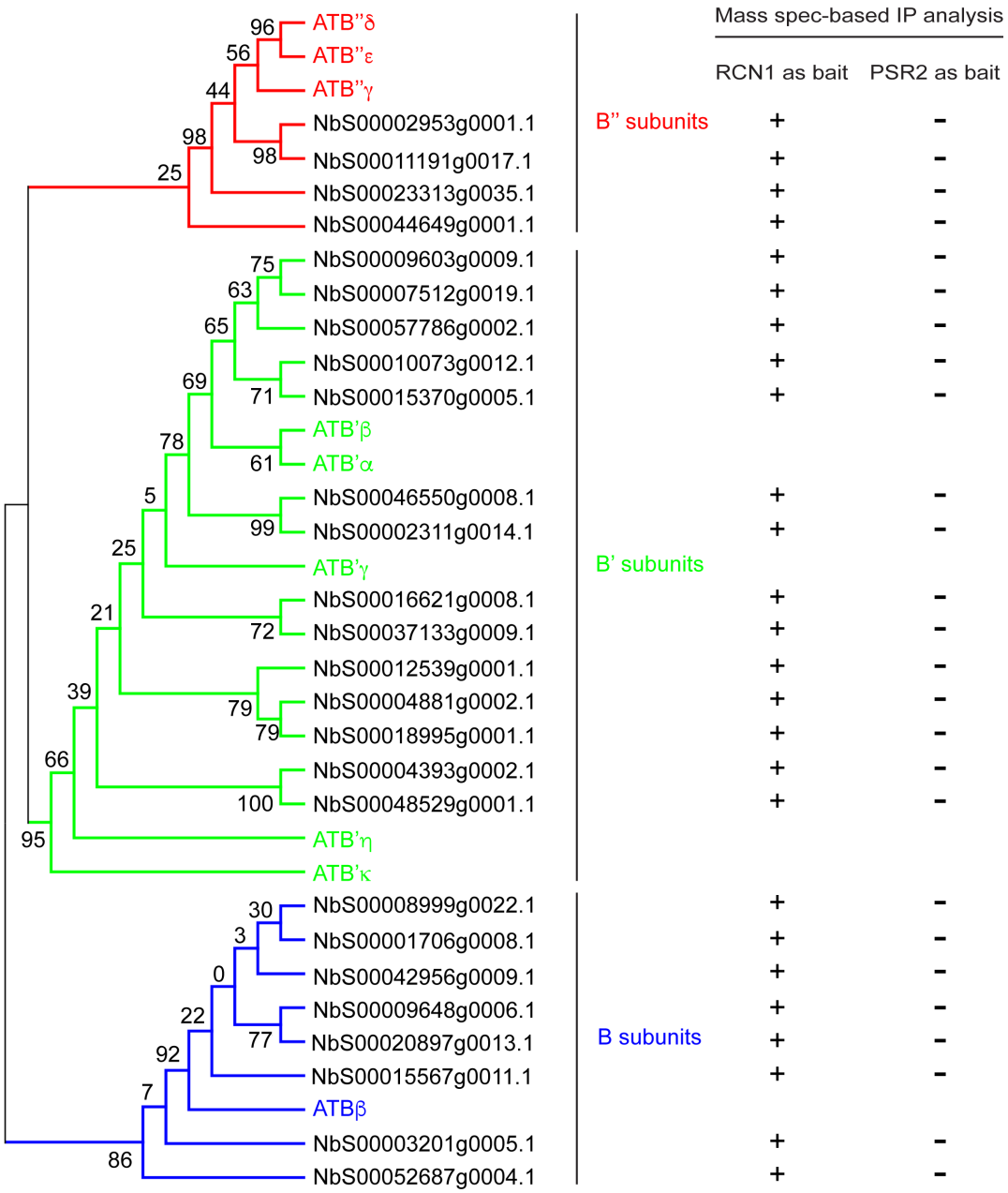
Mass spec-based IP analysis
RCN1 as bait
PSR2 as bait
ATB"δ
ATB"ε
ATB"γ
NbS00002953g0001.1
NbS00011191g0017.1
NbS00023313g0035.1
NbS00044649g0001.1
B" subunits
NbS00009603g0009.1
NbS00007512g0019.1
NbS00057786g0002.1
NbS00010073g0012.1
NbS00015370g0005.1
ATB'β
ATB'α
NbS00046550g0008.1
NbS00002311g0014.1
ATB'γ
NbS00016621g0008.1
NbS00037133g0009.1
NbS00012539g0001.1
NbS00004881g0002.1
NbS00018995g0001.1
NbS00004393g0002.1
NbS00048529g0001.1
ATB'η
ATB'κ
B' subunits
NbS00008999g0022.1
NbS00001706g0008.1
NbS00042956g0009.1
NbS00009648g0006.1
NbS00020897g0013.1
NbS00015567g0011.1
ATBβ
NbS00003201g0005.1
NbS00052687g0004.1
B subunits
96
56
44
98
98
25
75
63
65
69
71
78
61
5
99
25
21
72
39
79
79
66
100
95
30
3
0
22
77
92
7
86

Figure 3.33. Phylogenetic analysis of PP2A B subunits. Phylogenetic tree of PP2A B subunits amino acid sequences of *N. benthamiana* mass spectrometry hits (*Nb* accession numbers) and all Arabidopsis PP2A B subunits (in colors) was constructed in the MEGA6 software using Maximum Likelihood methods. The numbers shown at the branches of the phylogenetic tree were bootstrap numbers. Arabidopsis B subunits are encoded in three subfamilies: B (shown in blue), B' (shown in green), and B'' (shown in red). The column on the right was the detection results by either using RCN1 or PSR2 as a bait for mass spec-based IP analysis. "+" and "–" indicate the presence or absence of protein detection in the mass spec-based IP analysis, respectively. B subunits was only present in the RCN1 immunocomplexes, but not in the PSR2 immunocomplexes.

Table 3.5 Potential PSR2-associated proteins identified from *N. benthamiana* 16c under a RNA silencing-induced condition.

Nb accession number	Description
Serine/threonine protein phosphatase 2A (PP2A)	
NbS00006732g0010.1	Serine/threonine-protein phosphatase 2A subunit A2, PP2AA2, PDF1, PR65
NbS00023637g0006.1	Serine/threonine-protein phosphatase 2A subunit A2, PP2AA2, PDF1, PR65
NbS00020903g0004.1	Serine/threonine-protein phosphatase PP2A catalytic subunit, PP2A-4
NbS00043074g0007.1	Serine/threonine-protein phosphatase PP2A catalytic subunit, PP2A-4
NbS00010634g0008.1	Serine/threonine-protein phosphatase PP2A catalytic subunit, PP2A-3
NbS00040706g0007.1	Serine/threonine-protein phosphatase PP2A catalytic subunit, PP2A-2
NbS00007440g0018.1	Serine/threonine-protein phosphatase PP2A catalytic subunit, PP2A-2
NbS00013026g0010.1	Serine/threonine-protein phosphatase PP2A catalytic subunit, PP2A-2
NbS00031201g0004.1	Serine/threonine-protein phosphatase 2A subunit A2, PP2AA2, PDF1, PR65
NbS00051180g0008.1	Serine/threonine-protein phosphatase PP2A catalytic subunit, PP2A-2
Kinases	
NbS00024829g0011.1	Serine/threonine-protein kinase WNK4, NN mitogen-activated protein kinase
NbS00031309g0007.1	Serine/threonine-protein kinase WNK4, NN mitogen-activated protein kinase
NbS00014198g0009.1	Uridine kinase-like protein 4
Methyltransferase	
NbS00027670g0006.1	Serine hydroxymethyltransferase
NbS00042478g0005.1	Serine hydroxymethyltransferase
NbS00012972g0007.1	Serine hydroxymethyltransferase
NbS00010831g0013.1	Serine hydroxymethyltransferase
NbS00012577g0009.1	5-methyltetrahydropteroyltriglutamate, homocysteine methyltransferase
NbS00003479g0020.1	Catechol O-methyltransferase
NbS00045109g0006.1	Catechol O-methyltransferase
NbS00009739g0005.1	Serine hydroxymethyltransferase
NbS00047057g0006.1	Serine hydroxymethyltransferase
NbS00012020g0003.1	Serine hydroxymethyltransferase
Aminotransferase	
NbS00004472g0004.1	Hop-interacting protein THI032, serine-glyoxylate aminotransferase
NbS00039057g0010.1	Aminomethyltransferase, glycine cleavage system T protein
NbS00013023g0001.1	Aminomethyltransferase, glycine cleavage system T protein
NbS00019758g0008.1	Hop-interacting protein THI032, serine-glyoxylate aminotransferase

Table 3.5 (Continued)

Nb accession number	Description
RNA editing/helicase/binding	
NbS00001653g0010.1	Pre-mRNA-processing factor 39-like
NbS00017354g0008.1	Pre-mRNA-processing factor 39-like
NbS00025364g0011.1	ATP-dependent RNA helicase eIF4A-9
NbS00032509g0005.1	DEAD-box RNA helicase-like protein
NbS00060849g0001.1	Uncharacterized RNA-binding protein, polyadenylate-binding protein RBP47B'
NbS00027114g0020.1	RNA-binding glycine-rich protein
RNA silencing regulators	
NbS00007950g0008.1	AGO4-2
NbS00034990g0010.1	AGO1-1
NbS00008430g0013.1	AGO1-2

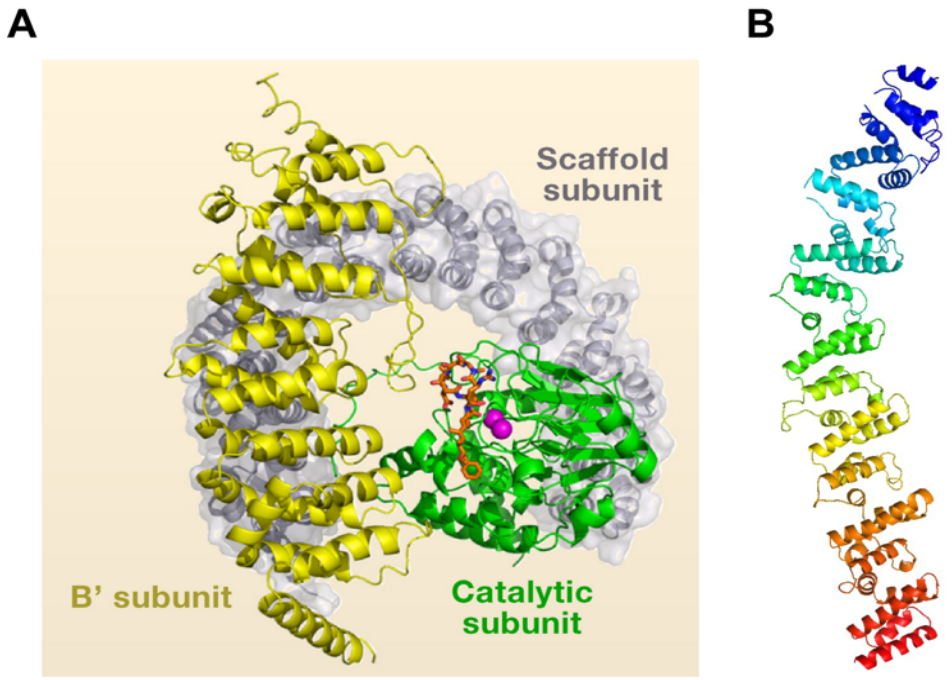

Figure 3.34. Structural similarity between PP2A B′ subunit and PSR2. (A) Structure of the human PP2A heterotrimeric holoenzyme, consisting of the scaffold (gray), B′ regulatory (yellow), and catalytic (green) subunits. In human, the B′ regulatory subunit recognizes HEAT repeats 2–8 of the scaffold subunit at the N′ terminal, while the catalytic subunit binds to HEAT repeat 11–15 at C′ terminal. This image is adapted from (Shi, 2009). **(B)** The crystal structure of PSR2 protein with seven WY/LWY repeats in different colors (unpublished protein structure data from Drs. Jinbiao Ma and Wenbo Ma labs).

Next, I asked whether PSR2 binds the PP2A scaffold subunit (A subunit) in the same way as B subunits do. The crystal structures of human PP2A holoenzyme revealed that the scaffold A subunit contains 15 tandem HEAT (huntingtin-elongation-A subunit-TOR) repeats, where the repeats 2~8 are recognized by the B′ subunit and repeats 11~15 are recognized by the catalytic C subunit. In Arabidopsis, RCN1 was predicted to have around 12 to 14 tandem HEAT repeats by the online protein searching engines/database such as UniProtKB, Prosite, and InterPro. Thus, I generated a truncated $RCN1^{396\text{-}588}$ (from amino acid 396 to 588) which only contains the last 4~5 HEAT repeats that were responsible for the binding of catalytic subunits, but presumably could not interact with B subunits (**Figure 3.35A**).

As expected, PSR2 interact with full length RCN1 but not with this truncated $RCN1^{396\text{-}588}$ in the Y2H assays (**Figure 3.35B and C**). However, truncated $RCN1^{396\text{-}588}$ still showed interaction with the catalytic C subunits (**Figure 3.35C**), such as PP2AC3 and PP2AC5. Altogether, these data suggested that PSR2 may act like a B′ subunit and bind to the N′-terminal region of PP2A A subunits.

3.22 PSR2 could determine the subcellular localization of PP2A

PP2A B subunits were known to determines subcellular localization of PP2A core enzyme. If PSR2 could act as the B subunits, I hypothesized that the location of PSR2 could control the subcellular localization of PP2A core enzyme. To test this hypothesis, I used either wild-type PSR2 or a PSR2 fused with NLS (nuclear localization signal) to perform BiFC assays with PP2A A subunits. The interaction between PSR2 and PP2A A

subunits was mainly in the cytoplasm and there was no fluorescence signal in the nucleus (**Figure 3.36**). If PSR2 was localized to the nucleus, I expect there will be BiFC fluorescence signals in the nucleus.

To generate a PSR2 that can be localized to the nucleus, I fused PSR2 with the NLS sequence (CCTAAAAAGAAGCGTAAGGTT) at the C′ terminus, and cloned it into pVYNE vector for BiFC assays. Subsequently, the subcellular localization where PSR2 or PSR2NLS interact with PP2A A subunits was examined. Interestingly, when the PSR2NLS was forced to be localized to the nucleus, PDF1 and PDF2, and small amount of RCN1 were also brought into the nucleus, as demonstrated by the yellow fluorescence (Venus) signal in the nucleus, suggesting the location of PSR2 could control the subcellular localization of PSR2/PP2A complex.

3.33 Preliminary data suggested PSR2 may compete out B′ subunit from the PP2A scaffold

Given that similarity between PSR2 and PP2A B subunits in terms of their protein structure and binding properties to the scaffold A subunit, it is possible that PSR2 might compete with PP2A B subunits for interacting with PP2A A and C subunits. To understand whether PSR2 and B subunit compete for the binding to scaffold A subunit, a protein competition assay was performed by using the *in vitro* GST pull-down assay.

Here, both PP2A subunits and PSR2 were cloned into the *E. coli* protein expression vectors and transformed into *E. coli* strain BL21-RIL for the protein induction upon IPTG (Isopropyl β-D-1-thiogalactopyranoside) treatment. The PP2A scaffold subunit RCN1

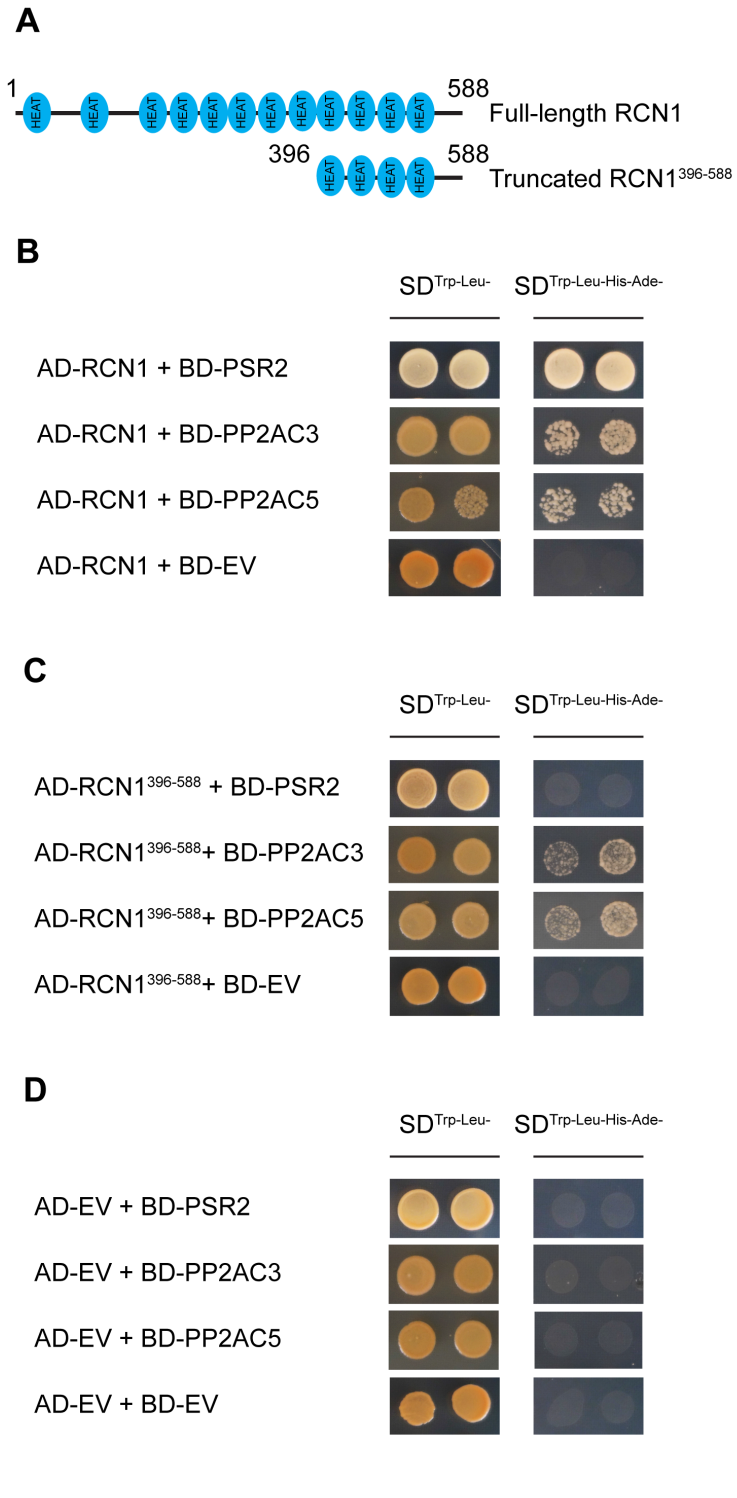
A
1
588
HEAT
Full-length RCN1
396
588
Truncated RCN1396-588
B
SDTrp-Leu-
SDTrp-Leu-His-Ade-
AD-RCN1 + BD-PSR2
AD-RCN1 + BD-PP2AC3
AD-RCN1 + BD-PP2AC5
AD-RCN1 + BD-EV
C
SDTrp-Leu-
SDTrp-Leu-His-Ade-
AD-RCN1396-588 + BD-PSR2
AD-RCN1396-588+ BD-PP2AC3
AD-RCN1396-588+ BD-PP2AC5
AD-RCN1396-588+ BD-EV
D
SDTrp-Leu-
SDTrp-Leu-His-Ade-
AD-EV + BD-PSR2
AD-EV + BD-PP2AC3
AD-EV + BD-PP2AC5
AD-EV + BD-EV

Figure 3.35. The C′ region of RCN1 (RCN1$^{396–588}$) is not important for the binding of PSR2. The C′ region of PP2A scaffold protein is known to be recognized by the catalytic subunits (e.g. HEAT repeat 11–15 of scaffold is the C subunit binding site). **(A)** Schematics of a full length RCN1 and a truncated RCN1 only expressing the last four HEAT repeats. Blue ovals indicate repeats of HEAT domains. The numbers indicate the amino acids of RCN1. **(B-D)** Full length of RCN1 (B) but not RCN1$^{396–588}$ truncate (C) interacted with PSR2; while both RCN1 and RCN1$^{396-588}$ truncate interacted with PP2A C subunits (C3 and C5). Interaction of Y2H was selected on nutrient-deficient SD media, SD$^{Trp–Leu–His–}$ and SD$^{Trp–Leu–His–Ade–}$. AD empty vector control was shown in (D).

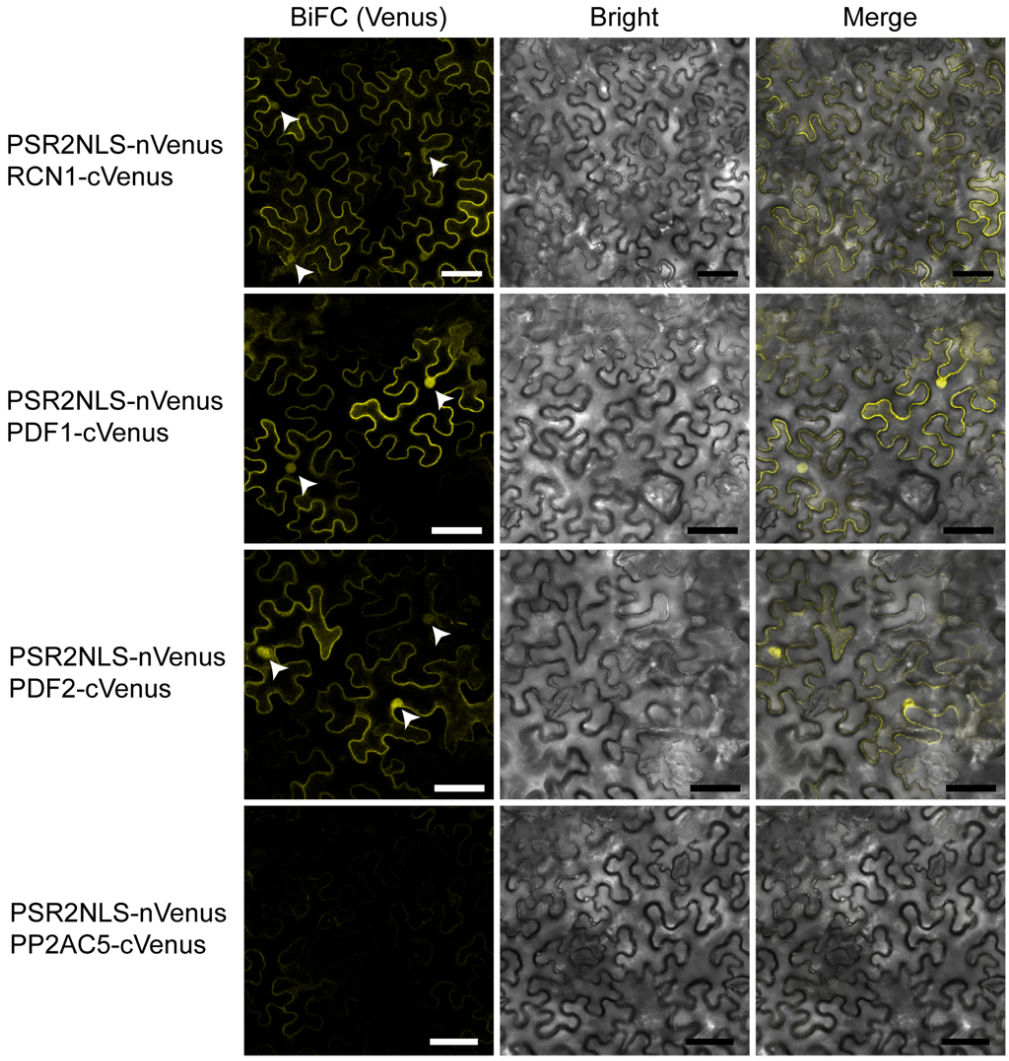
BiFC (Venus)
Bright
Merge
PSR2NLS-nVenus
RCN1-cVenus
PSR2NLS-nVenus
PDF1-cVenus
PSR2NLS-nVenus
PDF2-cVenus
PSR2NLS-nVenus
PP2AC5-cVenus
Scale bar : 50 μm

Figure 3.36. Subcellular localization of PSR2 determined the interaction location of PSR2 and PP2A. Bimolecular fluorescence complementation (BiFC) assay of PSR2NLS and PP2A A subunits in *N. benthamiana* leaves, which were infiltrated with Agrobacteria carrying indicated constructs. Fluorescence was detected in nucleus (arrowheads) when PSR2NLS interacted with PP2A A subunits (RCN1, PDF1, and PDF2). Note that there was still fluorescence detected in cytosol that likely due to the weak NLS sequence (5′-CCTAAAAAGAAGCGTAAGGTT-3′) used. PSR2NLS/PP2AC5 served as a negative control for BiFC assay. Scale bar = 50 μm.

was tagged with GST to serve as the bait in the GST pull-down system (pGEX-RCN1 was cloned by Dr. Yi Zhai). The B subunits and PSR2 were tagged with His-SUMO to serve as the prey and the competitor, respectively (pRSF-PSR2 was cloned by Dr. Yi Zhai).

I firstly aimed to ensure that PP2A B subunits could be successfully pulled down by RCN1. To test this, several B subunits were used, including ATB′α, ATB′γ, and ATBβ. However, only His-SUMO-ATB′α was successfully expressed in *E. coli* with great protein solubility after several protein induction conditions tested. Therefore, His-SUMO-ATB′α proteins was used to perform the pull-down assay with GST-RCN1, and the results confirmed that ATB′α had direct association with RCN1 (**Figure 3.37A**). A non-related protein, His-SUMO-GFP was used as a negative control here to show no interaction with RCN1 (pRSF-GFP was cloned by Dr. Yao Zhao). (**Figure 3.37A**).

With the established pull-down conditions for ATB′α/RCN1, I proceeded to perform the competition assay where increasing amount of His-SUMO-PSR2 were introduced into this ATB′α/RCN1 pull-down system by serving as the competitor of ATB′α. Specifically, I incubated the RCN1-containing GST resins with both His-SUMO-ATB′α and different concentrations of His-SUMO-PSR2. Along with the increase of PSR2 concentration, a preliminary pull-down result revealed that the amount of RCN1-bound ATB′α subunits reduced (**Figure 3.37B**), suggesting PSR2 might compete with ATB′α for binding to RCN1.

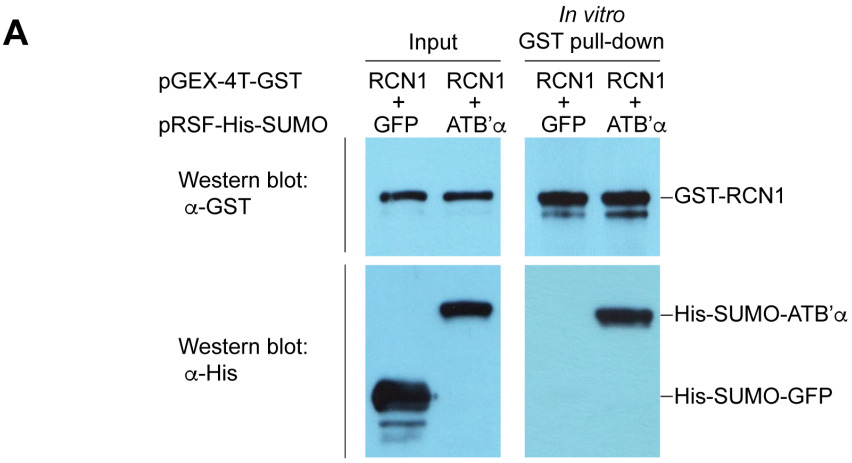
A
Input
In vitro
GST pull-down
pGEX-4T-GST
RCN1 + GFP
RCN1 + ATB'α
RCN1 + GFP
RCN1 + ATB'α
pRSF-His-SUMO
Western blot: α-GST
GST-RCN1
Western blot: α-His
His-SUMO-ATB'α
His-SUMO-GFP

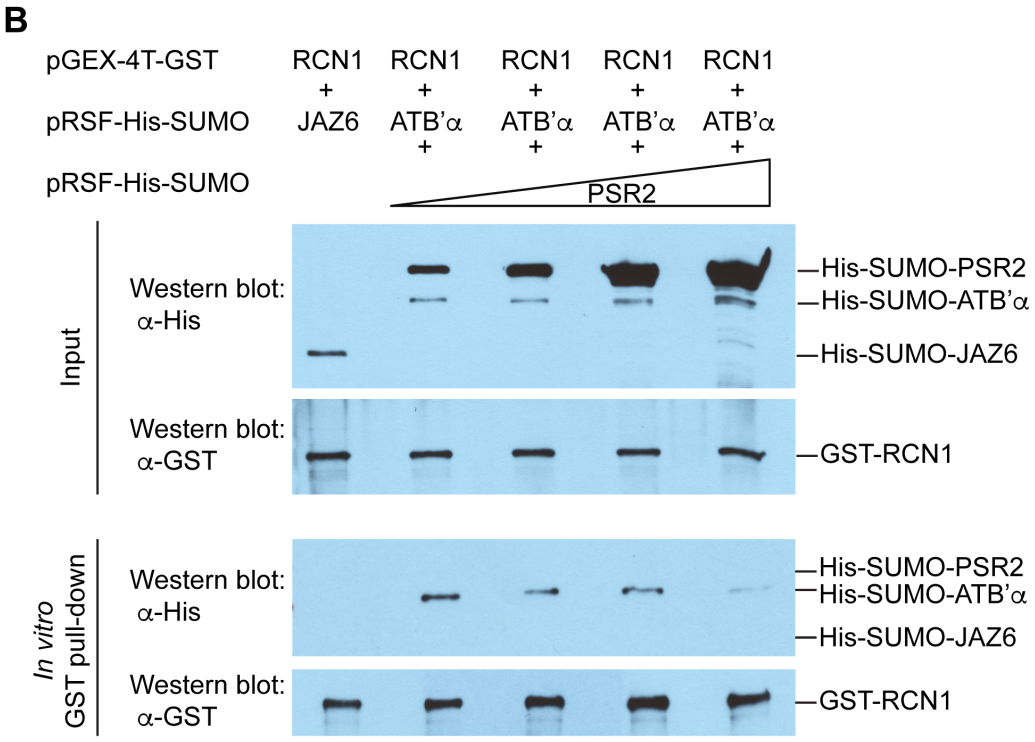
B
pGEX-4T-GST
RCN1 + JAZ6
RCN1 + ATB'α +
RCN1 + ATB'α +
RCN1 + ATB'α +
RCN1 + ATB'α +
pRSF-His-SUMO
pRSF-His-SUMO
PSR2
Input
Western blot: α-His
His-SUMO-PSR2
His-SUMO-ATB'α
His-SUMO-JAZ6
Western blot: α-GST
GST-RCN1
In vitro GST pull-down
Western blot: α-His
His-SUMO-PSR2
His-SUMO-ATB'α
His-SUMO-JAZ6
Western blot: α-GST
GST-RCN1

Figure 3.37. The binding competition between PSR2 and the regulatory subunit ATB′α on PP2A scaffold. (A) Direct interaction of between RCN1 scaffold and ATB′α subunit was confirmed by GST pull-down, where GST-RCN1 was used as the bait and His-SUMO-ATB′α was pulled down. Anti-GST and anti-His western blotting were used to detect RCN1 and ATB′α, respectively. His-SUMO-GFP was a negative control. **(B)** The PSR2-ATB′α competition assay was performed based on the GST pull-down system. GST resins bound by GST-RCN1 were incubated with His-SUMO-ATB′α and increased concentrations of His-SUMO-PSR2. In the pull-down output, reduced amount of His-SUMO-ATB′α bound by RCN1 were detected along with the increased amount of His-SUMO-PSR2. His-SUMO-JAZ6 (pRSF-JAZ6 construct provided by Ms. Eva Hawara) was a negative control that cannot interact with PP2A scaffold.

Chapter IV

DISCUSSION

This thesis research provides mechanistic insights into the virulence function of *Phytophthora* sojae PSR2 effector, which associates with the plant PP2A core enzyme and suppress specific small RNA accumulation, probably by serving as a regulatory subunit of PP2A. The functional roles and molecular mechanisms of the PSR2-PP2A interactions were demonstrated by using Arabidopsis transgenic plants overexpressing PSR2 along with different PP2A mutations. My results showed that hijacking of plant PP2A core enzyme is required for the PSR2 function in suppressing phasiRNA accumulation in Arabidopsis. Meanwhile, the role of PP2A as a negative regulator of the anti-*Phytophthora* defense regulation was firstly reported. Finally, the PSR2 homolog of *Phytophthora infestans*, PiPSR2, also associates with PP2A, suggesting the forming of PSR2/PP2A holoenzyme in hosts may be a conserved pathogenic mechanism of the PSR2 family effectors. Thus, the plant PP2A may be a novel target for developing effective disease management methods to control *Phytophthora* diseases.

4.1 PSR2 associates with PP2A core enzyme in plants

PP2A is a heterotrimeric enzyme consisting of a scaffold A subunit, a regulatory B subunit, and a catalytic C subunit (Farkas et al., 2007, Uhrig et al., 2013). Cellular PP2As were found to exist in two forms: one is the heterodimeric core enzyme that consists of only A and C subunits; another is the heterotrimeric holoenzyme with all A, B and C

subunits (Janssens & Goris, 2001, Shi, 2009). The core enzyme form of PP2A is abundant in the cells, which serves as an enzyme pool ready for loading different B subunits to recruit diverse substrates for functions (Kremmer et al., 1997).

It is interesting that none of the PP2A B subunits was found in both UPLC/Q-TOF-MS and LTQ-Orbitrap Fusion mass spectrometry analyses (**Tables 3.1, 3.2**, and **3.5**). Especially, the LTQ-Orbitrap Fusion is an advanced mass spectrometer with powerful resolution and accuracy in protein detection, and 1500~4000 protein hits were identified in each of my samples. With such high sensitivity, plenty of PP2A A and C subunit hits were identified; however, no any B subunit was found in the PSR2-associating protein complexes, implying a very specific binding of PSR2 to PP2A A and C subunits.

4.2 The interaction between PSR2 and Arabidopsis PP2A core enzyme subunits

PP2A is an evolutionally conserved protein phosphatase that play important roles in diverse cellular pathways (Farkas et al., 2007, Uhrig et al., 2013). The core enzyme subunits are encoded by gene families with multiple members that some of which have functional redundancy. The model plant Arabidopsis was used in this thesis research for the mechanistic study of PSR2. In Arabidopsis, each PP2A gene family member was found to produce different mRNA splice variants and protein isoforms (**Table 3.3** and **Figure 3.3**). All Arabidopsis PP2A constructs used in this research thesis were cloned using cDNA of isoform 1 (except for the AD-PDF2 construct used in Y2H assays where cDNA of isoform 2, At1g13320.2, was used). Isoform 1 is the default cDNA sequence of

each locus on TAIR (The Arabidopsis Information Resource) website, and is considered as a more dominant version in the cell.

To gain insights how PSR2 regulates plant small RNA biogenesis and infection via interacting with plant PP2A, the exact PP2A A and C subunit members that targeted by PSR2 were investigated by different protein interaction assays, including Y2H, BiFC, and co-IP. The interaction results of PSR2 and Arabidopsis PP2A subunits are summarized in **Table 4.1**. It is shown that PSR2 interacted with PP2A A subunits in three types of interaction assays (**Figures 3.6**, **3.8**, and **3.9**) (As described above, cloning of AD-PDF2 in Y2H assays used PDF2 isoform 2 instead of isoform 1 as the template, which might be one of the underlying reasons of the discrepancy in Y2H assay and in co-IP and BiFC assays).

PSR2 interacted with C subunits in co-IP assay (**Figure 3.12**), but showed no interaction with C subunits in yeast (**Figure 3.13**), and may have weak interaction with C subunits in BiFC assay with faint and blurry signals in cytoplasm (**Figure 3.14**). In the co-IP assay of PSR2 and C subunits, at least two of the Arabidopsis C subunits (PP2AC2 and PP2AC5) interacted with PSR2; however, PP2AC1, PP2AC3, and PP2AC4 have not been tested (**Figure 3.12** and **Table 4.1**). In general, current data support an indirect interaction between PSR2 and C subunits, probably through A subunits. The comprehensive examination of protein interaction between PSR2 and C subunits has not yet been completed. Future experiments confirming the interactions of PSR2-PP2ACs will be suggested.

Table 4.1 Summary of protein interactions of PSR2s and Arabidopsis PP2A subunits.

Proteins tested		Types of protein interaction assay		
PSR2 family	**PP2A family**	**Y2H**	**BiFC**	**Co-IP**
P. sojae PSR2	Scaffold—RCN1	+	+	+
P. sojae PSR2	Scaffold—PDF1	+	+	+
P. sojae PSR2	Scaffold—PDF2	TBD	+	+
P. sojae PSR2	Catalytic—PP2AC1	–	–	TBD
P. sojae PSR2	Catalytic—PP2AC2	–	–	+
P. sojae PSR2	Catalytic—PP2AC3	–	–	TBD
P. sojae PSR2	Catalytic—PP2AC4	–	–	TBD
P. sojae PSR2	Catalytic—PP2AC5	–	–	+
P. infestans PiPSR2	Scaffold—RCN1	TBD	TBD	TBD
P. infestans PiPSR2	Scaffold—PDF1	+	TBD	TBD
P. infestans PiPSR2	Scaffold—PDF2	TBD	TBD	TBD
P. infestans PiPSR2	Catalytic—PP2AC1	–	TBD	TBD
P. infestans PiPSR2	Catalytic—PP2AC2	–	TBD	TBD
P. infestans PiPSR2	Catalytic—PP2AC3	–	TBD	TBD
P. infestans PiPSR2	Catalytic—PP2AC4	–	TBD	TBD
P. infestans PiPSR2	Catalytic—PP2AC5	–	TBD	TBD

+: interaction positive, –: interaction negative, TBD: to be determined.

4.3 PSR2 hijacks host PP2A core enzyme for suppressing phasiRNA biogenesis

The functional significance of PSR2-PP2A interaction in PSR2-mediated RNA silencing regulation was demonstrated using genetic methods in this thesis research. It has been shown that Arabidopsis transgenic plants expressing PSR2 (PSR2-5^{OE}) suppress phasiRNA production (**Figure 1.5A**) (Qiao et al., 2013). Here, I found that mutation of either RCN1 or PDF1 did not alter phasiRNA production (**Figures 3.26** and **3.27**). However, both PSR2-5^{OE}*rcn1-6* and PSR-5^{OE}*pdf1-1* transgenic Arabidopsis lost the activity to suppress specific phasiRNA species (e.g. *TAS1*-tasi255 and *TAS2*-tasi1511). The accumulation level of these phasiRNAs in PSR2-5^{OE}*rcn1-6* and PSR-5^{OE}*pdf1-1* plants is similar to either wild-type or single mutants of *rcn1-6* and *pdf1-1*, indicating the phasiRNA suppression activity of PSR2 requires RCN1 and PDF1.

It is interesting to note that both RCN1 and PDF1 are required for PSR2-mediated suppression of phasiRNA, suggesting that PSR2/PP2A holoenzyme might work as dimers or multimers with both RCN1 and PDF1 for RNAi regulation. Alternatively, it is also possible that the single mutants of either one affect the gene expression of another. In sum, my results suggest for the first time that PP2A serves as a host factor of a pathogenic virulence protein in regulating small RNA biogenesis.

Such functional role of PSR2-PP2A interaction is further supported by the examinations of PSR2 truncated mutants (PSR2$^{\Delta LWY2\text{-}OE}$, PSR2$^{\Delta LWY3\text{-}OE}$, and PSR2$^{\Delta LWY6\text{-}OE}$) in phasiRNA biogenesis. These PSR2 deletion mutants that lose the interaction (or have greatly reduced interaction) with both RCN1 and PDF1 also showed partially reduced activity on suppressing phasiRNA biogenesis (**Figures 3.29**, **3.30**, and **3.32**),

consistent with the role of PP2A in PSR2-mediated RNA silencing regulation. Since the phasiRNA suppression effects were not fully rescued, there might be either endogenous PP2As or other factors that mediate the phasiRNA biogenesis. Protein expressions of PSR2 truncates in the Arabidopsis lines of $PSR2^{\Delta LWY2\text{-}OE}$, $PSR2^{\Delta LWY3\text{-}OE}$, and $PSR2^{\Delta LWY6\text{-}OE}$ were detactable using anti-Flag western blotting; however, I have not yet compared the protein expression levels among these Arabidopsis lines expressing PSR2 truncates and $PSR2\text{-}5^{OE}$ line. Future experiments on comparing the protein expression levels of these transgenic Arabidopsis will be needed.

In addition, the Arabidopsis $PSR2\text{-}5^{OE}$ line was used as a positive control of phasiRNA suppression for assaying the silencing suppression activity of PSR2 truncated mutants (Qiao et al., 2013). However, it would be more ideal if the PSR2 truncated mutants that still interact with RCN1 and PDF1 could be included in this assay to serve as controls as well. Future work on generating Arabidopsis transgenic line expressing PSR2 truncates (such as $PSR2^{\Delta N\text{-}OE}$, $PSR2^{\Delta WY1\text{-}OE}$, or $PSR2^{\Delta LWY7\text{-}OE}$) that still interact with PP2A A subunits will be suggested (**Figure 3.29**). The phasiRNA accumulation level in these plants may provide more information about the effects of PSR2 truncated mutants on phasiRNA biogenesis.

4.4 A potential function of phasiRNA species that are regulated by the PSR2/PP2A holoenzyme

In this thesis research, *TAS1*-tasiR255, the phasiRNA species derived from the *TAS1* loci triggered by miR173, was used as a main representative of phasiRNA family (Qiao

et al., 2013). *TAS1*-tasiR255 was suppressed in PSR2-5^{OE} line, but the suppression of *TAS1*-tasiR255 was rescued by *pp2a* mutation or PSR2 truncates that lost interaction with PP2A (**Figures 3.26**, **3.27**, and **3.32**). In addition, *TAS2*-tasiR1511 and *TAS3*-5′D8 were also rescued in the PSR2-5^{OE}*rcn1-6*.

An immediate next step in the future is to systematically examine what other phasiRNA species are regulated by PSR2/PP2A complex using small RNA-sequencing of PSR2-5^{OE} and PSR2-5^{OE}*pdf1-1* or PSR2-5^{OE}*rcn1-6*. The function of individual small RNA species that are regulated by PSR2/PP2A complex in plant immunity against *Phytophthora* is also an important question to pursue by both prediction of their potential mRNA targets and generating plants that overexpressing/knocking-down these phasiRNA under a PSR2-5^{OE} genetic background for infection assays.

4.5 Functional involvement of PP2A in plant defense against Phytophthora

PP2A is known to play roles in diverse cellular mechanisms, including both abiotic and biotic stress responses in plants (Farkas et al., 2007, Janssens & Goris, 2001, Uhrig et al., 2013). Arabidopsis PP2A was reported to be a negative regulator of plant defense against bacterial pathogen (Segonzac et al., 2014). In this thesis research, specific Arabidopsis PP2A subunits were also found to negatively regulate immune response against *Phytophthora*, where mutant lines (e.g. *pdf1-1* and *pp2ac2*) were more resistant and overexpressing lines (e.g. RCN1^{OE}) were more susceptible to *Phytophthora* infection (Figures **3.22** and **3.24**).

As a negative defense regulator against *Phytophthora*, RCN1^{OE} lines had more severe *Phytophthora* infection phenotype (**Figure 3.24**); however, *rcn1-6* mutant had no effect on disease severity (**Figure 3.22**). This discrepancy may not be caused by the low basal expression level of RCN1 in cells, since PP2A is an abundant enzyme in eukaryotic cells expressed ubiquitously. Instead, previous research suggests that RCN1 performs a dominant role in regulation of phosphatase activity and that PDF1 and PDF2 functions are unmasked with the absence of RCN1 (Zhou et al., 2004). Thus, it is more likely that other scaffolds (PDF1 and/or PDF2) compensate for the function of RCN1 on defense regulation in *rcn1-6* mutant.

Arabidopsis transgenic plants PSR2-5^{OE} was also known to have enhanced disease severity upon *Phytophthora* infection (Xiong et al., 2014). This disease promotion phenotype was partially reduced in the PSR2-5^{OE}*pdf1-1* lines (**Figure 3.25A** and **B**). Since *pdf1-1* single mutant alone has an effect on plant defense against *Phytophthora* (**Figure 3.24B**), it is still unclear whether the rescue effect seen in the PSR2-5^{OE}*pdf1-1* lines was due to simple summation of two independent effects of *pdf1* mutation and PSR2 overexpression, or was because PDF1 indeed act downstream PSR2 in the same pathway against *Phytophthora*.

Since infection assays measure the downstream effects of all the cellular events related to plant immunity, it is challenging to parse out these two possibilities. However, phasiRNA suppression, a more targeted cellular event at immediate downstream of PSR2 function, was rescued in different PSR-5^{OE}*pdf1-1* lines while there was no effect in *pdf1-1* mutant lines (**Figure 3.27**), suggesting that the PP2A is required for PSR2-mediated

small RNA regulation. Future experiments linking the function of these altered small RNAs to plant immunity against *Phytophthora* will be needed.

4.6 Potential substrate(s) of PSR2/PP2A holoenzyme for RNA silencing and defense regulation

PP2A is known to have broad substrate specificity and participate in diverse cellular functions, including development, cell proliferation and death, cell mobility, cytoskeleton dynamics, cell cycle, and abiotic and biotic stress responses, etc (Janssens & Goris, 2001, Shi, 2009, Uhrig et al., 2013). This broad substrates specificity of PP2A is attributed to its diverse and large number of regulatory B subunits, who bind to core enzyme in a variety of combinations, contributing to temporal and spatial specificity for the dephosphorylating activity (Uhrig et al., 2013).

The small RNA Northern blotting data in this thesis research suggested no change of miRNA and phasiRNA abundance in *pp2a* mutants (*rcn1-6* and *pdf1-1*). However, PP2A (e.g. PDF1 and RCN1) was functionally required for PSR2 in suppressing phasiRNA biogenesis (**Figures 3.26** and **3.27**). Together with the evidence that PSR2 might act as a regulatory subunit of PP2A (**Figures 3.33**, **3.34**, **3.35**, **3.36**, and **3.37**), it is proposed that PSR2 may determine the substrate(s) of PP2A to function in RNA silencing regulation. To identify the potential substrate(s) associated with PSR2/PP2A holoenzyme, I used LTQ-Orbitrap Fusion mass spectrometry in the *N. benthamiana* 16c system and found several the important RNA silencing effector proteins, such as AGO1 and AGO4 (**Tables 3.4** and **3.5**).

However, further investigation of interactions between PSR2 and Arabidopsis AGOs showed negative results in Y2H, co-IP, and BiFC (**see Appendix**, **Figures A.1**, **A.2**, **A.3**, **A.4**, and **A.5**), suggesting that a) AGOs may be false-positive results of mass spectrometry, seen by their low mascot ranking 2081 (AGO1) and 2720 (AGO4) out of 4266 in mass spectrometry, or b) the dephosphorylating enzymatic association may be fast and unstable which was not properly revealed by protein-protein interaction assays.

To further elucidate the potential substrates of PSR2/PP2A holoenzyme and to confirm PP2A regulates RNA silencing pathways with the presence of PSR2, a systematic phosphoproteome analysis (such as the TiO2-based phosphoproteome screening) by comparing PSR2-5^{OE} and PSR2-5^{OE}*pdf1-1* (or PSR2-5^{OE}*rcn1-6*) could be done in the future. In addition, there is also a possibility that PSR2 itself might be a substrate of PP2A; therefore, the phosphorylation status of PSR2 should be examined by the systematic phosphoproteome assay.

4.7 A number of the late blight resistance proteins are found to associate with PP2A

While working on the substrate hunting for PSR2/PP2A holoenzyme, 19 hits related to the late blight resistance proteins (NB-LRR family resistance proteins) were identified to associate with the scaffold subunit RCN1 (**Table 3.4**). Late blight is a common disease symptom induced by *Phytophthora* species. Amino acid sequence analysis revealed that these late blight resistance protein hits have close relationship with the NRC1 and the Prf resistance proteins of *Solanum lycopersicum* (tomato) and the RPP13 resistance protein of Arabidopsis (**Table 3.4**).

NB-LRRs are well known for their roles as immune receptors for microbial recognition as well as immune signal transduction and amplification (DeYoung & Innes, 2006, Eitas & Dangl, 2010, McHale et al., 2006). In *Solanaceae* plant species, Prf recognition complex (composed of Prf and a protein kinase Pto) is known to confer resistance to bacterial pathogen *Pseudomonas syringae*. NRC1 is a signaling hub downstream immune receptors for defense regulation (Wu et al., 2016, Wu et al., 2017). Besides, RPP13 family genes are critical for Arabidopsis resistance against various diseases including the downy mildew disease caused by oomycete *Peronospora parasitica* (Bittner-Eddy et al., 2000).

The association of PP2A with these late blight related NB-LRR proteins suggests that PP2A may regulate the anti-*Phytophthora* immune signaling. Although the protein-protein interaction of RCN1 and late blight resistance protein have not been validated by experiments, the high mascot rankings of late blight resistance proteins (e.g. the top hit of late blight resistance proteins, NbC24350532g0001.1, ranks 168 out of 4266) strongly suggested that RCN1 might interact with them (**Table 3.4**). Future experiments confirming their interactions as well as the function of these targeted late blight resistance proteins will provide a novel mechanism underlying PP2A-mediated defense regulation against *Phytophthora*.

4.8 PSR2 may act as a regulatory B subunit of PP2A in plants

Since only A and C subunits were detected in the PSR2-associating protein complex, two hypothetical models of how PSR2 binds to the cellular PP2As were proposed. PSR2

may either 1) directly recruit the free-living PP2A core enzyme, or 2) target to PP2A holoenzymes by competing with B subunits. The PP2A core enzyme alone possesses enzymatic activity for substrate processing (Janssens & Goris, 2001, Shi, 2009, Uhrig et al., 2013). Binding to PP2A core enzyme further implies that PSR2 may either be a substrate of PP2A or be a regulatory subunit of PP2A. Given that PSR2 had higher affinity with the scaffold subunits than the catalytic subunits in interaction assays (**Table 4.1**), and the crystal structure data supported that PSR2 structural mimicked B′ family regulatory subunits and may share similar binding sites on scaffold subunits (**Figures 3.34** and **3.35**), PSR2 is more likely to act as regulatory subunits of PP2A.

The scaffold-binding competition between PSR2 and B subunit was further examined using *in vitro* pull-down system. A very preliminary result suggested that less B subunits (B′ family) were bound on the scaffold with increased amount of PSR2 (**Figure 3.37B**), supporting the idea of competition between PSR2 and B subunit. To strengthen the competition hypothesis, future experiments with a non-related protein (e.g. GFP) or the loss-of-interaction PSR2 truncates (e.g. $PSR2^{\Delta LWY2}$, $PSR2^{\Delta LWY3}$, $PSR2^{\Delta LWY4}$, $PSR2^{\Delta LWY5}$, $PSR2^{\Delta LWY6}$) that serve as negative controls will be needed to test if the competition effect between PSR2 and B subunit is specific.

In addition to PSR2, the viral protein small t (ST) and medium T (MT) antigens were also found to form complexes with PP2A by acting as regulatory B subunits (Cho et al., 2007, Chen et al., 2007, Pallas et al., 1990, Ruediger et al., 1994, Ruediger et al., 1992). ST and MT are important oncoproteins of the animal viruses including simian virus 40 (SV40), polyomavirus, and BK virus, etc. Targeting host PP2A is important for their

oncogenic functions in hosts. Like PSR2, ST and MT only associate with the PP2A A and C core enzymes but not the holoenzymes. They bind to N′-terminal region (HEAT repeat 3−6 or HEAT repeat 2−8) of scaffold A subunits, similar binding sites as B subunits and PSR2. Thus, it is conceivable that PSR2 might serve as regulatory B subunits to exert its function as previously described for viral virulence proteins (ST/MT). However, PSR2 and ST/MT may regulate PP2A core enzyme in an opposite way, where the binding of ST/MT inhibits PP2A function, while PSR2 is proposed in this thesis to hijack PP2A core enzyme for functions.

4.9 PP2A core enzyme may be a conserved target of PSR2-family effectors

PSR2 was originally found in *P. sojae* genome, , but it is evolutionarily conserved that other related *Phytophthora* species also encode PSR2 family effectors (Qiao et al., 2013, Xiong et al., 2014). The PSR2 homolog of *P. infestans*, PiPSR2, also has RNA silencing suppression and disease promotion activities (Xiong et al., 2014). In my thesis research, I found that PiPSR2 also interacts with PP2A scaffold subunit PDF1 in Y2H assays (**Figure 3.11** and **Table 4.1**), suggesting that targeting to PP2A may be an evolutionary conserved mechanism for the PSR2-family effectors to exert functions. Studying the molecular mechanisms and biological functions of PSR2-PP2A interaction may provide insights on how other PSR2-family effectors may alter the cellular events in plants.

Chapter V

CONCLUSION AND FUTURE PERSPECTIVES

Phytophthora greatly destruct the agricultural and natural environment worldwide. It evolved efficient strategies to achieve successful infection by producing numerous effectors to regulate host cellular machineries and suppress immunity. The RxLR family effectors, a large family of cytoplasmic effecters of *Phytophthora*, has been the subject to much research interest in recent years. The RxLR effector PSR2 derived from *Phytophthora sojae* is one of the first found eukaryotic pathogen RNA silencing suppressors (Qiao et al., 2013).

The molecular mechanisms of *Phytophthora* PSR2 in regulating plant cellular events were elucidated in this thesis research, and a summary model of this dissertation study is shown in **Figure 5.1**. In this study, I identified protein phosphatase 2A (PP2A) as an important factor in plants that is targeted by *Phytophthora* PSR2 effector through mass spectrometry-based IP proteomic analysis (**Tables 3.1** and **3.2**). The protein-protein interaction assays further confirmed that both scaffold A subunits and catalytic C subunits of PP2A are associated with PSR2 (**Table 4.1**), while regulatory B subunits of PP2A are not.

The functional significance of PP2A/PSR2 interaction was further demonstrated by examining the small RNA levels. The hallmark of PSR2 as a RNA silencing suppressor is that PSR2 overexpression in plants specifically suppresses phasiRNA accumulation (Qiao et al., 2013). Importantly, such suppression of phasiRNA can be rescued in the

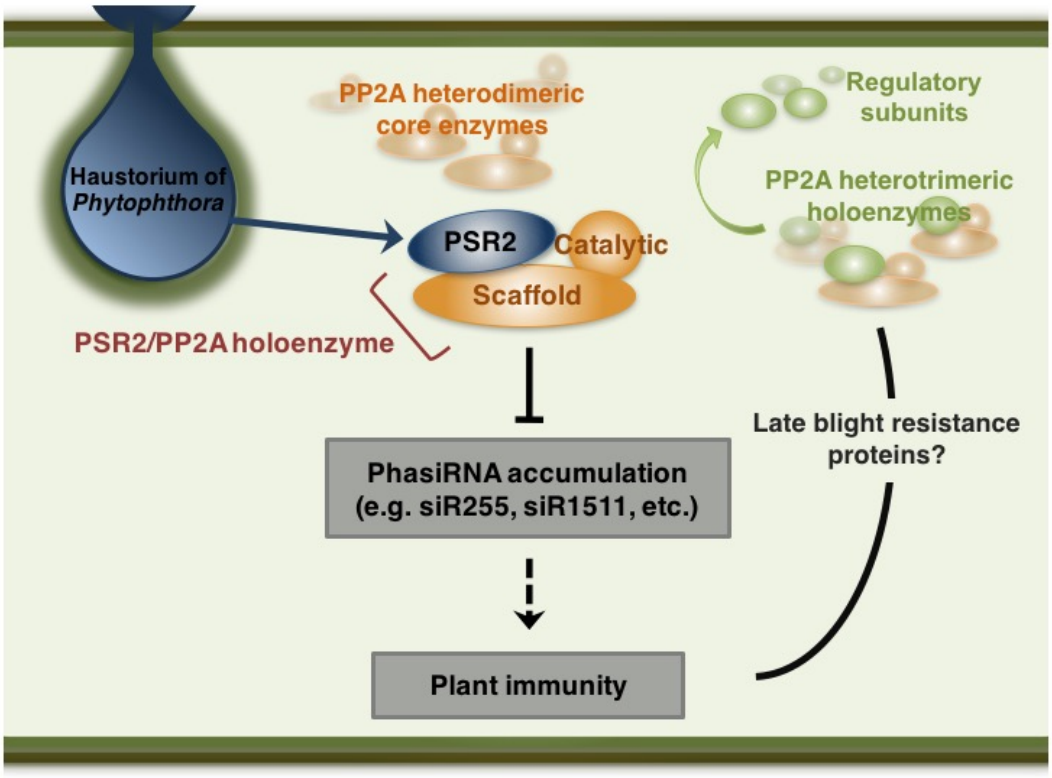

Figure 5.1 A proposed model of molecular pathogenic mechanisms of PSR2. Two forms of PP2A enzymes exist in the plant cell. One is the core enzyme form (orange), another is the holoenzyme form. When *Phytophthora* PSR2 (blue) presents in host cell, it associates with PP2A core enzyme by either 1) directly recruiting core enzyme or 2) competing with regulatory B subunits to bind core enzyme. PSR2 and core enzyme form PSR2/PP2A holoenzyme (red) to exert functions, probably by acting as a regulatory subunit. Hijacking PP2A is required for the phasiRNA suppression activity of PSR2, but need further experiments to confirm its contribution to immune suppression. PP2A alone is able to regulate the anti-*Phytophthora* defense in Arabidopsis, probably by regulating resistance proteins.

mutant backgrounds of PP2A A subunits (e.g. PSR2-5^{OE}*rcn1-6* and PSR2-*5^{OE}pdf1-1*), suggesting PP2A A subunits are required for PSR2-mediated phasiRNA suppression (**Figures 3.26** and **3.27**). In addition, structural and binding properties of PSR2 and regulatory B subunits of PP2A as well as preliminary competition assay provide hints that PSR2 might act as regulatory subunits to mediate the downstream function of PP2A/PSR2 complex (**Figures 3.34**, **3.35**, and **3.37**). Overall, the results of this research thesis provide a novel mechanistic insight into how *Phytophthora* RNA silencing suppressor mediate its effects in the plants.

PP2A has diverse functions in plant growth and development as well as in response to biotic and abiotic stresses. Although the functional involvement of PP2A in PSR2-mediated phasiRNA suppression is shown in this study, it remains unclear how PP2A regulate small RNA biogenesis. Identification of the substrate of PP2A/PSR2 complex will be of interest to elucidate the molecular mechanisms of PSR2 in RNA silencing regulation. In addition, there are many questions remain to be answered. For example, what other small RNA species might be regulated by PSR2/PP2A complex? What is the function of the specific phasiRNA species (e.g. *TAS1*-siR255 and *TAS2*-siR1511) regulated by PSR2/PP2A complex? How these small RNA species contribute to plant immunity against *Phytophthora*? Future experiments addressing these questions will significantly advance of understanding of the PSR2-mediated *Phytophthora* pathogenesis.

APPENDIX

(See DISCUSSION 4.6, page 157)

A.1 Systematic analysis of PSR2-associating proteins in the RNA silencing-induced plants

The expression of PSR2 in Arabidopsis leads to the reduced accumulation of phsiRNAs, probably by targeting to the plant PP2A enzymes and manipulating specific cellular substrate(s). Therefore, I aimed to identify potential substrate(s) presenting in the PSR2/PP2A-asscociating protein complexes that may play roles in RNA silencing regulation. To identify possible RNA silencing regulators associated with PSR2, I isolated the PSR2-associating protein complexes from *N. benthamiana* line 16c where the transgene-induced RNA silencing was actively induced. The LTQ-Orbitrap Fusion mass spectrometry was then used for screening possible RNA silencing related candidates.

Similar to the previous dataset of wild-type plants (**Table 3.1**), this 16c mass spectrometry data showed that PSR2 was still associated with PP2A core enzymes (the A and C subunits), serine/threonine-protein kinases, pre-mRNA-processing factors, pentatricopeptide repeat-containing proteins, serine hydromethyltransferases, and aminotransferases (**Table 3.5**). Notably, more RNA regulation-related proteins were found in this RNA silencing-induced system, including the RNA helicases, RNA binding proteins, and the argonaut proteins (AGOs). The control of this mass spectrometry-based IP analysis was the HopZ1a^{C216A}-associating protein complex, and it was unfortunately found to have PSR2 contamination in its mass spec dataset, which made the experimental

and the control dataset incomparable. Although it was difficult to conclude whether these RNA-related regulators were the background signals of RNA silencing-induced 16c plants, or they did specifically associate with PSR2 and PP2A, I decided to use a targeted approach for examining the involvement of argonaute proteins in the PSR2/PP2A complex.

A.2 Argonautes as potential substrates of PSR2/PP2A holoenzyme for RNA silencing regulation

Members of the AGO protein family are key players in small RNA-induced gene silencing (Meister, 2013). AGO proteins are highly specialized in binding to small RNA species and mediating downstream repression of specific target RNAs by either degradation of translational inhibition. The number of AGOs that are present in different species varies. Arabidopsis has ten AGOs, divided into three clades: the AGO1/AGO5/AGO10 clade, the AGO2/AGO3/AGO7 clade, and the AGO4/AGO6/AGO8/AGO9 clade (Vaucheret, 2008).

Interestingly, mass spectrometry analyses of the 16c system identified AGO1 and AGO4 as possible candidates associated with PSR2/RCN1 protein complexes (**Tables 3.4** and **3.5**). Therefore, I aimed to examine whether AGOs could be the substrates of PP2A. In animals, the post-translational phosphorylation modification had been found on AGO regulation. Phosphorylation of AGO2 enhances its localization to P-bodies where the miRNA- and siRNA-mediated RNA silencing occurs (Heo & Kim, 2009); phosphorylation of human AGO also suggests an enhanced small RNA binding ability

(Meister, 2013, Rudel et al., 2011, Zeng et al., 2008). However, whether phosphorylation regulation occurs on plant AGOs to affect their activity and localization is unknown. To examine whether PSR2/PP2A suppress phasiRNA biogenesis via regulating AGOs, the physical protein interactions between AGOs and PSR2/PP2As were examined using Y2H, co-IP, and BiFC experiments.

A.3 AGOs did not physically interact with either PSR2 or PP2A

Firstly, the Y2H experiment was performed to test protein interactions of PSR2 and diverse PP2A subunits with various AGOs. Four Arabidopsis AGOs (AGO1, AGO4, AGO9, and AGO10) were cloned into the Y2H AD vectors (AD-AGO4, AD-AGO9, and AD-AGO10 were cloned by Dr. Yingnan Hou). None of these AGOs interacted with BD-PSR2 nor BD-RCN1 (**Figure A.1**). Instead of using full-length proteins for Y2H, specific domains of AGO were also cloned into the Y2H BD vector, including the N′-terminal region (N100), the PAZ domain, the MID domain, and the PIWI domain. Similar to the previous result of intact AGO proteins, none of AGO domains interacted with AD-PSR2 (**Figure A.2**). The negative interactions between AGO and the A and C subunits of PP2A (AD-RCN1, AD-PDF1, and AD-PP2AC4) were also confirmed in this Y2H assay (**Figure A.3**).

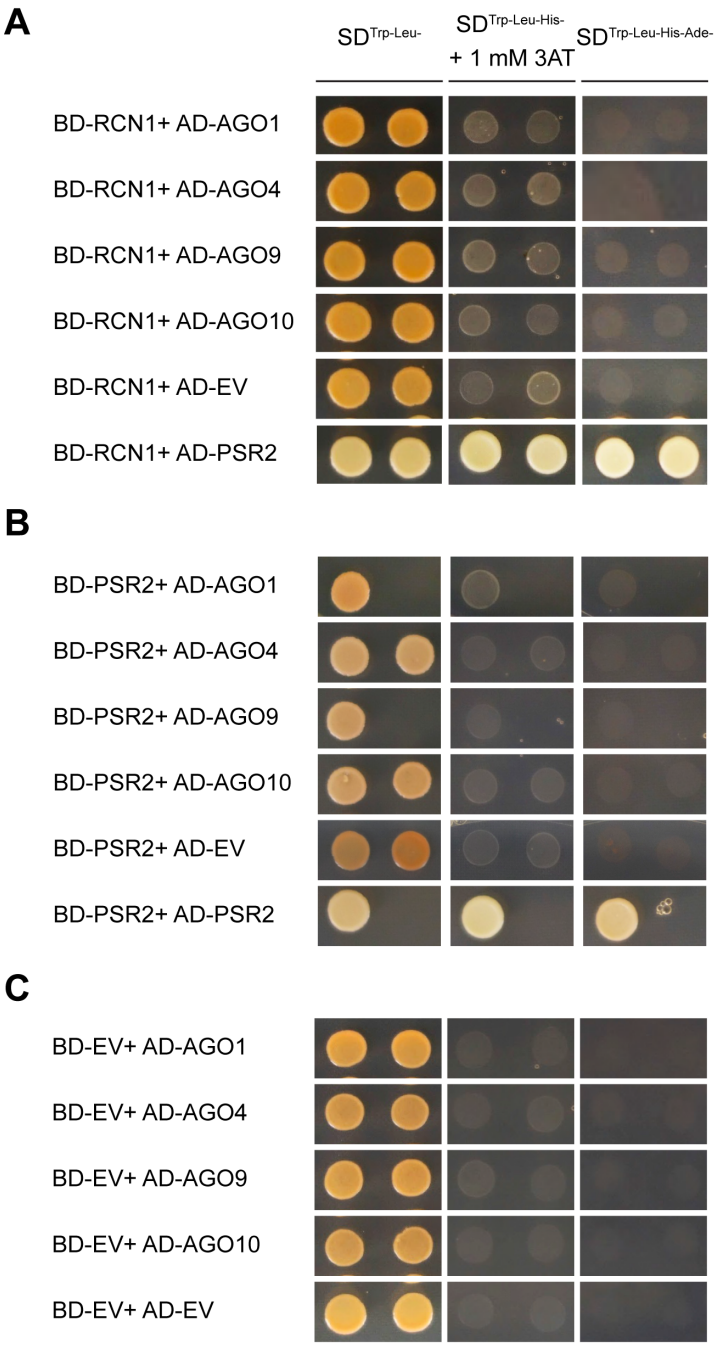
A
SD Trp-Leu-
SD Trp-Leu-His- + 1 mM 3AT
SD Trp-Leu-His-Ade-
BD-RCN1+ AD-AGO1
BD-RCN1+ AD-AGO4
BD-RCN1+ AD-AGO9
BD-RCN1+ AD-AGO10
BD-RCN1+ AD-EV
BD-RCN1+ AD-PSR2
B
BD-PSR2+ AD-AGO1
BD-PSR2+ AD-AGO4
BD-PSR2+ AD-AGO9
BD-PSR2+ AD-AGO10
BD-PSR2+ AD-EV
BD-PSR2+ AD-PSR2
C
BD-EV+ AD-AGO1
BD-EV+ AD-AGO4
BD-EV+ AD-AGO9
BD-EV+ AD-AGO10
BD-EV+ AD-EV

Figure A.1. Arabidopsis AGO proteins did not interact with either RCN1 or PSR2 in Y2H assays. Four different Arabidopsis AGOs (AGO1, AGO4, AGO9 and AGO10) was examined and did not show interaction with either RCN1 **(A)** or PSR2 **(B)**. The protein interactions in Y2H assay were selected by the nutrient-deficient SD media, $SD^{Trp-Leu-His-}$ and $SD^{Trp-Leu-His-Ade-}$. BD empty vector controls were shown in **(C)**.

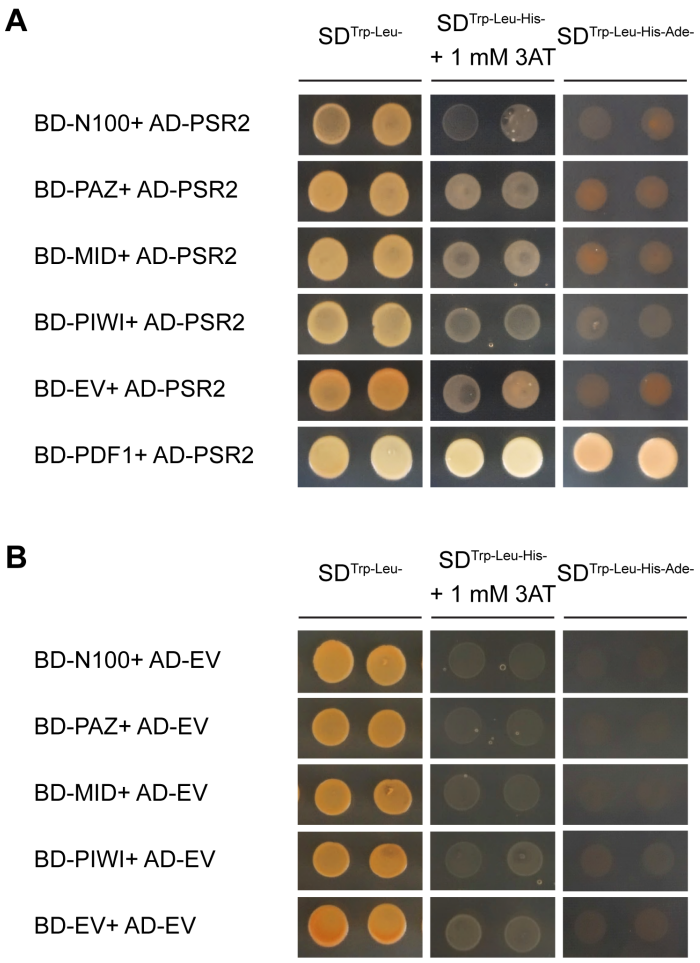

Figure A.2. AGO1 domains did not interact with PSR2 in Y2H assays. (A) The protein interactions in Y2H assay were selected by the nutrient-deficient SD media, $SD^{Trp–Leu–His–}$ and $SD^{Trp–Leu–His–Ade–}$. Results showed that four different domains of AGO1 protein (N100, PAZ, MID and PIWI) did not show interaction with PSR2. The mild self-activation seen on $SD^{Trp–Leu–His–}$ plates in (A) might be cause by the AD-PSR2 construct. **(B)** AD empty vector controls. Constructs of BD-AGO1 domains were kindly provided by Dr. Bailong Zhang in Dr. Xuemei Chen's lab at UC Riverside.

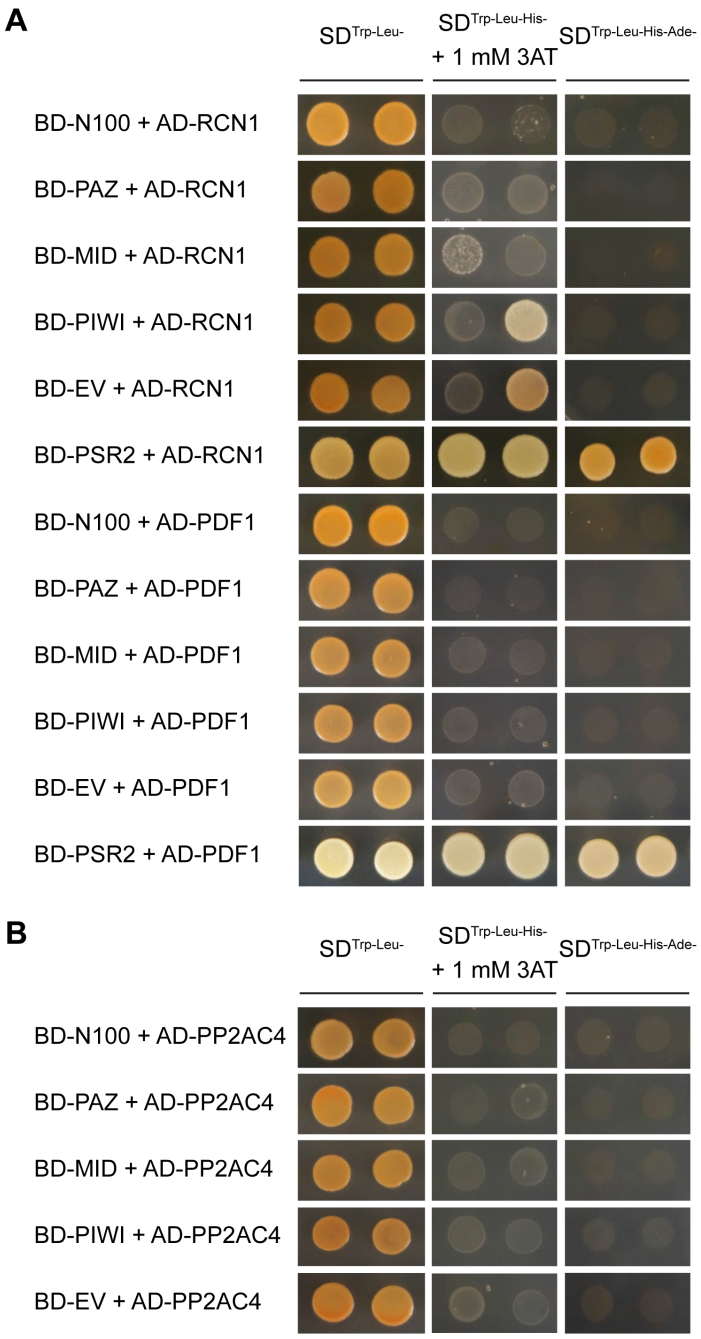
A
SD Trp-Leu-
SD Trp-Leu-His- + 1 mM 3AT
SD Trp-Leu-His-Ade-
BD-N100 + AD-RCN1
BD-PAZ + AD-RCN1
BD-MID + AD-RCN1
BD-PIWI + AD-RCN1
BD-EV + AD-RCN1
BD-PSR2 + AD-RCN1
BD-N100 + AD-PDF1
BD-PAZ + AD-PDF1
BD-MID + AD-PDF1
BD-PIWI + AD-PDF1
BD-EV + AD-PDF1
BD-PSR2 + AD-PDF1
B
SD Trp-Leu-
SD Trp-Leu-His- + 1 mM 3AT
SD Trp-Leu-His-Ade-
BD-N100 + AD-PP2AC4
BD-PAZ + AD-PP2AC4
BD-MID + AD-PP2AC4
BD-PIWI + AD-PP2AC4
BD-EV + AD-PP2AC4

Figure A.3. AGO1 domains did not interact with either PP2A A or C subunits in Y2H assays. None of AGO1 domains (N100, PAZ, MID and PIWI) showed interaction with PP2A A subunits (RCN1 and PDF1) **(A)** or C4 subunits. **(B)** The protein interactions in Y2H assay were selected by the nutrient-deficient SD media, $SD^{Trp-Leu-His-}$ and $SD^{Trp-Leu-His-Ade-}$.

Next, a comprehensive protein-protein interaction between Arabidopsis AGO1 and PP2As was examined using BiFC assay. All three PP2A A subunits (RCN1, PDF1, and PDF2) and four C subunits (PP2AC2, PP2AC3, PP2AC4, PP2AC5) were cloned into the pVYCE BiFC vector for expressing PP2A-cVenus fusion proteins. Likewise, Arabidopsis AGO1 was also cloned in to the pVYNE BiFC vector for expressing AGO1-nVenus fusion protein. Since PP2As play roles in the regulation of RNA silencing suppression induced by PSR2, I examined PP2A-AGO1 protein interactions with the presence of PSR2. To do so, PP2A-cVenus, AGO1-nVenus and 3×Flag-PSR2 were co-expressed in *N. benthamiana* leaf cells, and the protein interactions were visualized using confocal microscopy. BiFC results suggested that AGO1 did not interact with any of the A or C subunits of PP2A (**Figure A.4**).

Since AGOs were identified by the mass spectrometry-based IP experiments, the co-IP assay was also used to examine the interaction of PSR2/PP2A and AGO. Previous mass spectrometry data showed that AGO1 presented in both PSR2- and RCN1-associating protein complexes. Therefore, I firstly used 3×Flag-tagged PSR2 as the bait to immunoprecipitate AGO1 from plant protein extracts. The HA-tagged PP2A A subunits (RCN1, PDF1, and PDF2) were also expressed in the same plant protein extracts to serve as the positive controls. In the IP products, AGO1 could not be detected by western blot using AtAGO1-specific antibody; however, the positive controls (HA-RCN1, HA-PDF1, and HA-PDF2) could be detected (**Figure A.5A**). Furthermore, I tried using 3×Flag-tagged RCN1 to immunoprecipitate AGO1 with c-Myc-tagged PSR2 as a positive control. Again, 3×Flag-RCN1 successfully immunoprecipitated PSR2-c-Myc but failed

to immunoprecipitate AGO1 (**Figure A.5B**). All above co-IP data suggested that AGO1 was not associated with the PSR2/PP2A holoenzyme. The association of AGOs with PSR2/PP2A holoenzyme might be the false positive result of mass spectrometry analyses since the Mascot ranking and Mascot score of AGOs were very low. AGOs might be the background signal of the RNA silencing-induced 16c plants, or AGOs might have fast and weak physical interaction (phosphorylation/de-phosphorylaton events) with PSR2/PP2A holoenzyme, which could not be identified by the co-IP western blot. A further systematic phosphoproteome analysis (e.g. the TiO2-based phosphoproteome screening) to identify potential substrates of the PSR2/PP2A holoenzyme will be needed to confirm whether PSR2/PP2A can post-translationally modify.

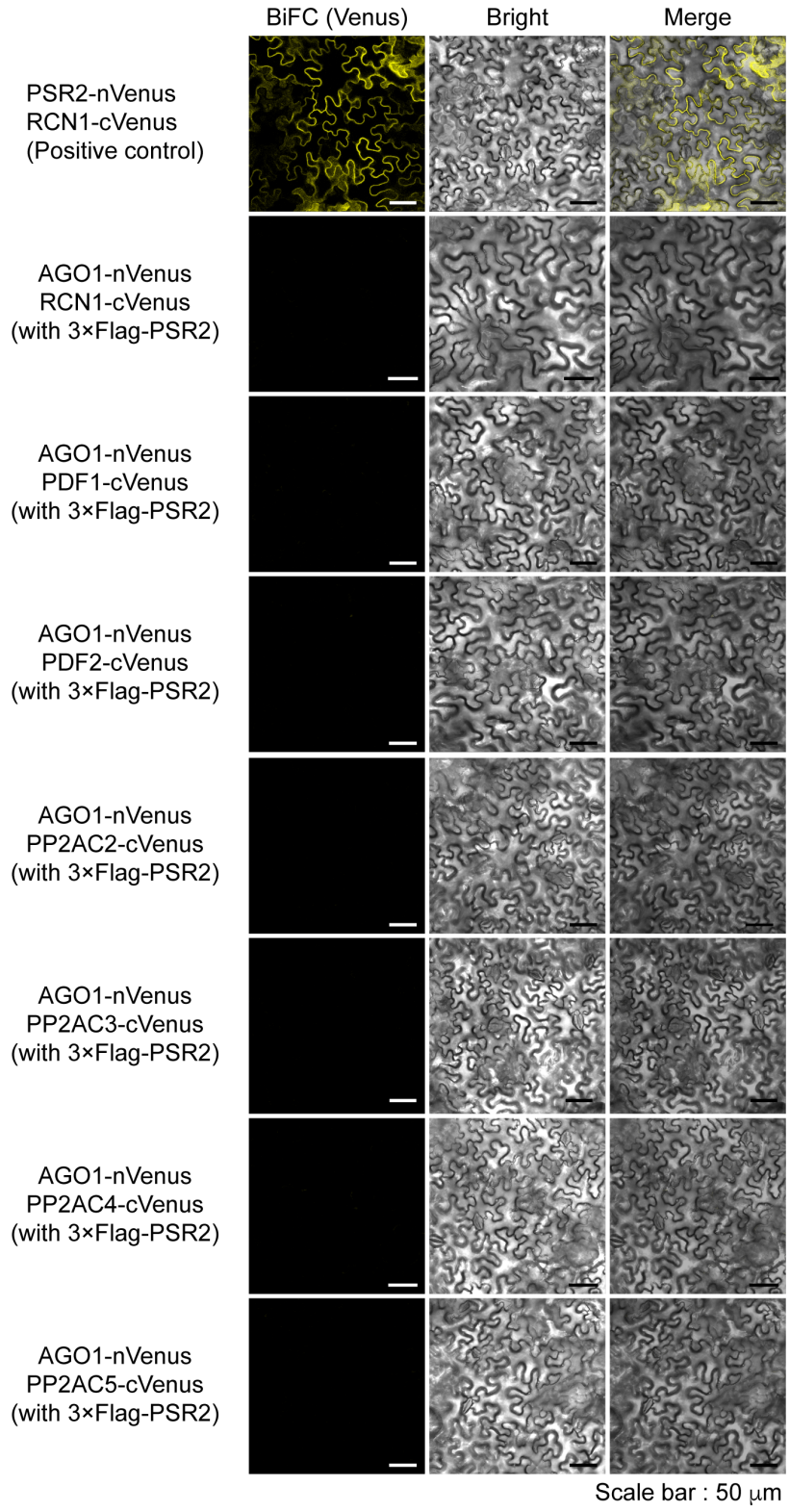
BiFC (Venus)
Bright
Merge
PSR2-nVenus
RCN1-cVenus
(Positive control)
AGO1-nVenus
RCN1-cVenus
(with 3×Flag-PSR2)
AGO1-nVenus
PDF1-cVenus
(with 3×Flag-PSR2)
AGO1-nVenus
PDF2-cVenus
(with 3×Flag-PSR2)
AGO1-nVenus
PP2AC2-cVenus
(with 3×Flag-PSR2)
AGO1-nVenus
PP2AC3-cVenus
(with 3×Flag-PSR2)
AGO1-nVenus
PP2AC4-cVenus
(with 3×Flag-PSR2)
AGO1-nVenus
PP2AC5-cVenus
(with 3×Flag-PSR2)
Scale bar : 50 μm

Figure A.4. Arabidopsis AGO1 did not associate with PP2A A or C subunits in bimolecular fluorescence complementation (BiFC) assay. *N. benthamiana* leaves were infiltrated with Agrobacteria carrying indicated constructs. Note that 3×Flag-PSR2 was also present in *N. benthamiana* leaves. No fluorescence was detected in the samples of AGO1 and A/C subunits. Sample of PSR2-nVenus/RCN1-cVenus was a positive control for this BiFC assay. Scale bar = 50 μm.

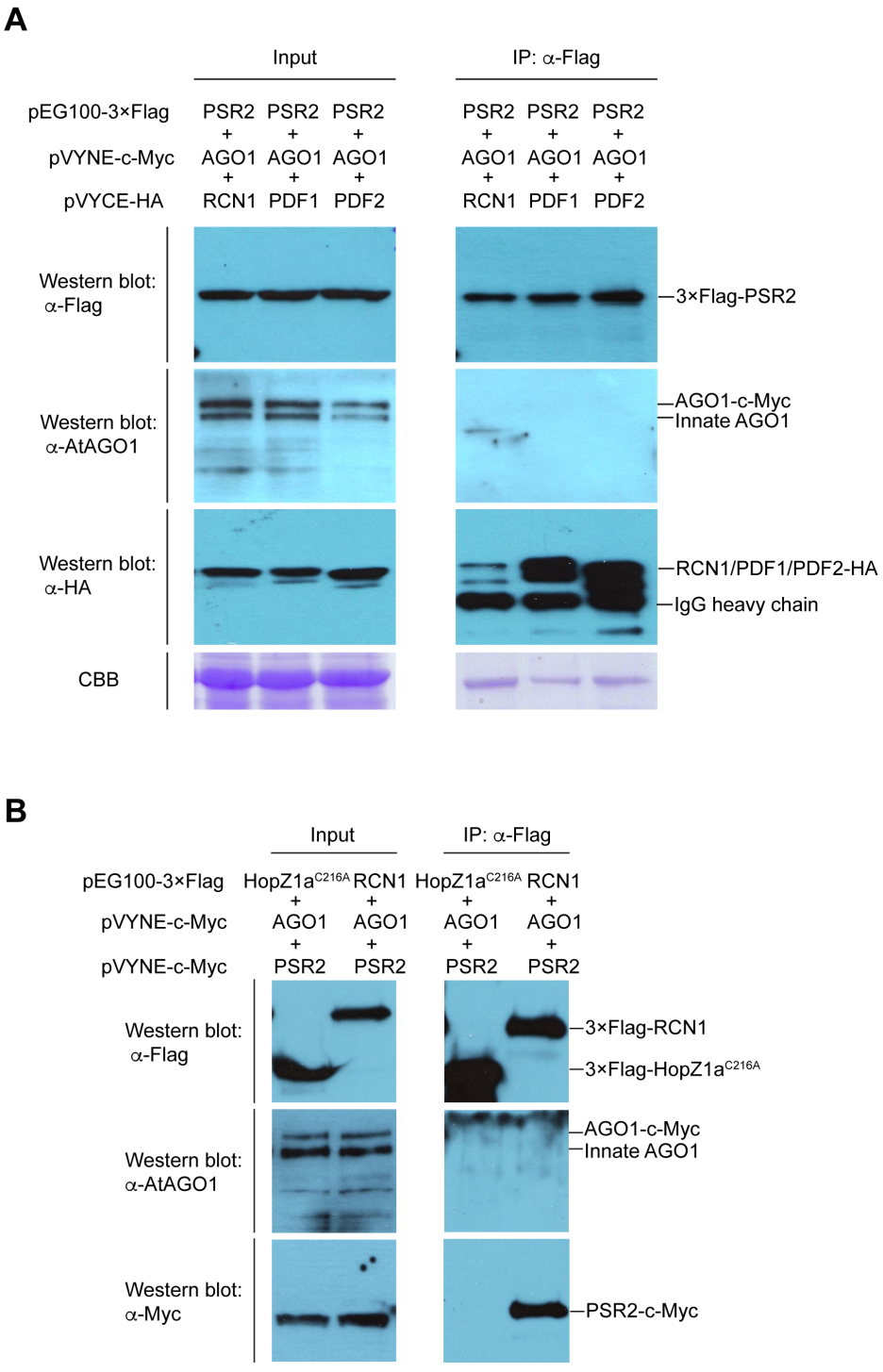
A
Input
IP: α-Flag
pEG100-3×Flag
pVYNE-c-Myc
pVYCE-HA
PSR2 + AGO1 + RCN1
PSR2 + AGO1 + PDF1
PSR2 + AGO1 + PDF2
Western blot: α-Flag
Western blot: α-AtAGO1
Western blot: α-HA
CBB
3×Flag-PSR2
AGO1-c-Myc
Innate AGO1
RCN1/PDF1/PDF2-HA
IgG heavy chain
B
Input
IP: α-Flag
pEG100-3×Flag
pVYNE-c-Myc
pVYNE-c-Myc
HopZ1a^C216A + AGO1 + PSR2
RCN1 + AGO1 + PSR2
Western blot: α-Flag
Western blot: α-AtAGO1
Western blot: α-Myc
3×Flag-RCN1
3×Flag-HopZ1a^C216A
AGO1-c-Myc
Innate AGO1
PSR2-c-Myc

Figure A.5. PSR2/PP2A complex did not associate with Arabidopsis AGO1 *in planta*. (A) 3×Flag-PSR2 was co-expressed with c-Myc-AGO1 and three different HA-tagged PP2A A subunits (RCN1, PDF1, and PDF2) in *N. benthamiana* and the total protein extracts were subjected to a co-IP assay using anti-Flag resin. Immunoprecipitates were detected by western blotting. c-Myc-AGO1 was not present in the 3×Flag-PSR2 immunocomplexes, however, the PP2A A subunits (positive control) were associated with PSR2. CBB staining was used as a loading control. **(B)** 3×Flag-RCN1 was co-expressed with both c-Myc-AGO1 and c-Myc-PSR2 in *N. benthamiana* for the anti-Flag co-IP assay followed by western blot analyses. 3×Flag-RCN1 was not associated with c-Myc-AGO1, but it had interaction with c-Myc-PSR2 (positive control). 3×Flag-HopZ1a^{C216A} was a non-interacting protein of PSR2 which served as a negative control.

REFERENCES

Agrios GN, 2005. *Plant pathology*. Amsterdam ; Boston: Elsevier Academic Press.

Barrangou R, Fremaux C, Deveau H, *et al*., 2007. CRISPR provides acquired resistance against viruses in prokaryotes. *Science* **315**, 1709-12.

Bart R, Cohn M, Kassen A, *et al*., 2012. High-throughput genomic sequencing of cassava bacterial blight strains identifies conserved effectors to target for durable resistance. *Proc Natl Acad Sci U S A* **109**, E1972-9.

Bittner-Eddy PD, Crute IR, Holub EB, Beynon JL, 2000. RPP13 is a simple locus in Arabidopsis thaliana for alleles that specify downy mildew resistance to different avirulence determinants in Peronospora parasitica. *Plant J* **21**, 177-88.

Blakeslee JJ, Zhou HW, Heath JT, *et al*., 2008. Specificity of RCN1-mediated protein phosphatase 2A regulation in meristem organization and stress response in roots. *Plant Physiol* **146**, 539-53.

Bos JI, Armstrong MR, Gilroy EM, *et al*., 2010. Phytophthora infestans effector AVR3a is essential for virulence and manipulates plant immunity by stabilizing host E3 ligase CMPG1. *Proc Natl Acad Sci U S A* **107**, 9909-14.

Boutemy LS, King SR, Win J, *et al*., 2011. Structures of Phytophthora RXLR effector proteins: a conserved but adaptable fold underpins functional diversity. *J Biol Chem* **286**, 35834-42.

Cai Q, Qiao L, Wang M, *et al*., 2018. Plants send small RNAs in extracellular vesicles to fungal pathogen to silence virulence genes. *Science* **360**, 1126-9.

Cao M, Du P, Wang X, *et al*., 2014. Virus infection triggers widespread silencing of host genes by a distinct class of endogenous siRNAs in Arabidopsis. *Proc Natl Acad Sci U S A* **111**, 14613-8.

Chen Y, Xu Y, Bao Q, *et al*., 2007. Structural and biochemical insights into the regulation of protein phosphatase 2A by small t antigen of SV40. *Nat Struct Mol Biol* **14**, 527-34.

Cho US, Morrone S, Sablina AA, Arroyo JD, Hahn WC, Xu W, 2007. Structural basis of PP2A inhibition by small t antigen. *PLoS Biol* **5**, e202.

Clough SJ, Bent AF, 1998. Floral dip: a simplified method for Agrobacterium-mediated transformation of Arabidopsis thaliana. *Plant J* **16**, 735-43.

Dangl JL, Horvath DM, Staskawicz BJ, 2013. Pivoting the plant immune system from dissection to deployment. *Science* **341**, 746-51.

Deyoung BJ, Innes RW, 2006. Plant NBS-LRR proteins in pathogen sensing and host defense. *Nat Immunol* **7**, 1243-9.

Ding SW, 2010. RNA-based antiviral immunity. *Nat Rev Immunol* **10**, 632-44.
Doehlemann G, Hemetsberger C, 2013. Apoplastic immunity and its suppression by filamentous plant pathogens. *New Phytol* **198**, 1001-16.

Eitas TK, Dangl JL, 2010. NB-LRR proteins: pairs, pieces, perception, partners, and pathways. *Curr Opin Plant Biol* **13**, 472-7.

Erwin DC, Ribeiro OK, 1996. *Phytophthora diseases worldwide*. St. Paul, Minn.: APS Press.

Farkas I, Dombradi V, Miskei M, Szabados L, Koncz C, 2007. Arabidopsis PPP family of serine/threonine phosphatases. *Trends Plant Sci* **12**, 169-76.

Fawke S, Doumane M, Schornack S, 2015. Oomycete interactions with plants: infection strategies and resistance principles. *Microbiol Mol Biol Rev* **79**, 263-80.

Fei Q, Xia R, Meyers BC, 2013. Phased, secondary, small interfering RNAs in posttranscriptional regulatory networks. *Plant Cell* **25**, 2400-15.

Grunwald NJ, 2012. Genome sequences of Phytophthora enable translational plant disease management and accelerate research. *Canadian Journal of Plant Pathology-Revue Canadienne De Phytopathologie* **34**, 13-9.

Haas BJ, Kamoun S, Zody MC*, et al*., 2009. Genome sequence and analysis of the Irish potato famine pathogen Phytophthora infestans. *Nature* **461**, 393-8.

Haverkort AJ, Boonekamp PM, Hutten R, *et al*., 2008. Societal costs of late blight in potato and prospects of durable resistance through sisgenic modification. *Potato Research* **51**, 47-57.

He X, Anderson JC, Del Pozo O, Gu YQ, Tang X, Martin GB, 2004. Silencing of subfamily I of protein phosphatase 2A catalytic subunits results in activation of plant defense responses and localized cell death. *Plant J* **38**, 563-77.

Heo I, Kim VN, 2009. Regulating the regulators: posttranslational modifications of RNA silencing factors. *Cell* **139**, 28-31.

Janssens V, Goris J, 2001. Protein phosphatase 2A: a highly regulated family of serine/threonine phosphatases implicated in cell growth and signalling. *Biochem J* **353**, 417-39.

Jiang RH, Tyler BM, 2012. Mechanisms and evolution of virulence in oomycetes. *Annu Rev Phytopathol* **50**, 295-318.

Jones JD, Dangl JL, 2006. The plant immune system. *Nature* **444**, 323-9.
Judelson HS, Blanco FA, 2005. The spores of Phytophthora: weapons of the plant destroyer. *Nat Rev Microbiol* **3**, 47-58.

Kale SD, Gu B, Capelluto DG, *et al*., 2010. External lipid PI3P mediates entry of eukaryotic pathogen effectors into plant and animal host cells. *Cell* **142**, 284-95.

Kamoun S, 2006. A catalogue of the effector secretome of plant pathogenic oomycetes. *Annu Rev Phytopathol* **44**, 41-60.

Kamoun S, Furzer O, Jones JD, *et al*., 2015. The Top 10 oomycete pathogens in molecular plant pathology. *Mol Plant Pathol* **16**, 413-34.

Katiyar-Agarwal S, Jin H, 2010. Role of small RNAs in host-microbe interactions. *Annu Rev Phytopathol* **48**, 225-46.

Kremmer E, Ohst K, Kiefer J, Brewis N, Walter G, 1997. Separation of PP2A core enzyme and holoenzyme with monoclonal antibodies against the regulatory A subunit: abundant expression of both forms in cells. *Mol Cell Biol* **17**, 1692-701.

Kuan T, Zhai Y, Ma W, 2016. Small RNAs regulate plant responses to filamentous pathogens. *Semin Cell Dev Biol* **56**, 190-200.

Lee SJ, Rose JK, 2010. Mediation of the transition from biotrophy to necrotrophy in hemibiotrophic plant pathogens by secreted effector proteins. *Plant Signal Behav* **5**, 769-72.

Li C, Zamore PD, 2018. Analysis of Small RNAs by Northern Hybridization. *Cold Spring Harb Protoc* **2018**, pdb prot097493.

Li X, Kapos P, Zhang Y, 2015. NLRs in plants. *Curr Opin Immunol* **32**, 114-21.
Mchale L, Tan X, Koehl P, Michelmore RW, 2006. Plant NBS-LRR proteins: adaptable guards. *Genome Biol* **7**, 212.

Meister G, 2013. Argonaute proteins: functional insights and emerging roles. *Nat Rev Genet* **14**, 447-59.

Molnar A, Melnyk C, Baulcombe DC, 2011. Silencing signals in plants: a long journey for small RNAs. *Genome Biol* **12**, 215.

Morgan W, Kamoun S, 2007. RXLR effectors of plant pathogenic oomycetes. *Curr Opin Microbiol* **10**, 332-8.

Nakahara KS, Masuta C, 2014. Interaction between viral RNA silencing suppressors and host factors in plant immunity. *Curr Opin Plant Biol* **20**, 88-95.

Navarro L, Dunoyer P, Jay F, *et al*., 2006. A plant miRNA contributes to antibacterial resistance by repressing auxin signaling. *Science* **312**, 436-9.

Navarro L, Jay F, Nomura K, He SY, Voinnet O, 2008. Suppression of the microRNA pathway by bacterial effector proteins. *Science* **321**, 964-7.

Pall GS, Hamilton AJ, 2008. Improved northern blot method for enhanced detection of small RNA. *Nat Protoc* **3**, 1077-84.

Pallas DC, Shahrik LK, Martin BL, *et al*., 1990. Polyoma small and middle T antigens and SV40 small t antigen form stable complexes with protein phosphatase 2A. *Cell* **60**, 167-76.

Panstruga R, Dodds PN, 2009. Terrific protein traffic: the mystery of effector protein delivery by filamentous plant pathogens. *Science* **324**, 748-50.

Pumplin N, Voinnet O, 2013. RNA silencing suppression by plant pathogens: defence, counter-defence and counter-counter-defence. *Nat Rev Microbiol* **11**, 745-60.

Qiao Y, Liu L, Xiong Q, *et al*., 2013. Oomycete pathogens encode RNA silencing suppressors. *Nat Genet* **45**, 330-3.

Richards TA, Talbot NJ, 2007. Plant parasitic oomycetes such as phytophthora species contain genes derived from three eukaryotic lineages. *Plant Signal Behav* **2**, 112-4.

Rudel S, Wang Y, Lenobel R, *et al*., 2011. Phosphorylation of human Argonaute proteins affects small RNA binding. *Nucleic Acids Res* **39**, 2330-43.

Ruediger R, Hentz M, Fait J, Mumby M, Walter G, 1994. Molecular model of the A subunit of protein phosphatase 2A: interaction with other subunits and tumor antigens. *J Virol* **68**, 123-9.

Ruediger R, Roeckel D, Fait J, Bergqvist A, Magnusson G, Walter G, 1992. Identification of binding sites on the regulatory A subunit of protein phosphatase 2A for the catalytic C subunit and for tumor antigens of simian virus 40 and polyomavirus. *Mol Cell Biol* **12**, 4872-82.

Segonzac C, Macho AP, Sanmartin M, Ntoukakis V, Sanchez-Serrano JJ, Zipfel C, 2014. Negative control of BAK1 by protein phosphatase 2A during plant innate immunity. *EMBO J* **33**, 2069-79.

Shi Y, 2009. Serine/threonine phosphatases: mechanism through structure. *Cell* **139**, 468-84.

Tamura K, Stecher G, Peterson D, Filipski A, Kumar S, 2013. MEGA6: Molecular Evolutionary Genetics Analysis version 6.0. *Mol Biol Evol* **30**, 2725-9.

Thomma BP, Nurnberger T, Joosten MH, 2011. Of PAMPs and effectors: the blurred PTI-ETI dichotomy. *Plant Cell* **23**, 4-15.

Torto-Alalibo T, Collmer CW, Gwinn-Giglio M, 2009. The Plant-Associated Microbe Gene Ontology (PAMGO) Consortium: community development of new Gene Ontology terms describing biological processes involved in microbe-host interactions. *BMC Microbiol* **9 Suppl 1**, S1.

Tyler BM, 2007. Phytophthora sojae: root rot pathogen of soybean and model oomycete. *Mol Plant Pathol* **8**, 1-8.

Tyler BM, Tripathy S, Zhang X, *et al*., 2006. Phytophthora genome sequences uncover evolutionary origins and mechanisms of pathogenesis. *Science* **313**, 1261-6.

Uhrig RG, Labandera AM, Moorhead GB, 2013. Arabidopsis PPP family of serine/threonine protein phosphatases: many targets but few engines. *Trends Plant Sci* **18**, 505-13.

Vaucheret H, 2008. Plant ARGONAUTES. *Trends Plant Sci* **13**, 350-8.

Waadt R, Schmidt LK, Lohse M, Hashimoto K, Bock R, Kudla J, 2008. Multicolor bimolecular fluorescence complementation reveals simultaneous formation of alternative CBL/CIPK complexes in planta. *Plant J* **56**, 505-16.

Wang Y, Bouwmeester K, Van De Mortel JE, Shan W, Govers F, 2013. A novel Arabidopsis-oomycete pathosystem: differential interactions with Phytophthora capsici reveal a role for camalexin, indole glucosinolates and salicylic acid in defence. *Plant Cell Environ* **36**, 1192-203.

Weiberg A, Wang M, Lin FM, *et al*., 2013. Fungal small RNAs suppress plant immunity by hijacking host RNA interference pathways. *Science* **342**, 118-23.

Whisson SC, Boevink PC, Moleleki L, *et al*., 2007. A translocation signal for delivery of oomycete effector proteins into host plant cells. *Nature* **450**, 115-8.

Win J, Morgan W, Bos J, *et al*., 2007. Adaptive evolution has targeted the C-terminal domain of the RXLR effectors of plant pathogenic oomycetes. *Plant Cell* **19**, 2349-69.

Wong J, Gao L, Yang Y, *et al*., 2014. Roles of small RNAs in soybean defense against Phytophthora sojae infection. *Plant J* **79**, 928-40.

Wrather JA, Koenning SR, 2006. Estimates of disease effects on soybean yields in the United States 2003 to 2005. *J Nematol* **38**, 173-80.

Wu CH, Abd-El-Haliem A, Bozkurt TO*, et al*., 2017. NLR network mediates immunity to diverse plant pathogens. *Proc Natl Acad Sci U S A* **114**, 8113-8.

Wu CH, Belhaj K, Bozkurt TO, Birk MS, Kamoun S, 2016. Helper NLR proteins NRC2a/b and NRC3 but not NRC1 are required for Pto-mediated cell death and resistance in Nicotiana benthamiana. *New Phytol* **209**, 1344-52.

Xiong Q, Ye W, Choi D*, et al*., 2014. Phytophthora suppressor of RNA silencing 2 is a conserved RxLR effector that promotes infection in soybean and Arabidopsis thaliana. *Mol Plant Microbe Interact* **27**, 1379-89.

Yan L, Wei S, Wu Y*, et al*., 2015. High-efficiency genome editing in Arabidopsis using YAO promoter-driven CRISPR/Cas9 system. *Mol Plant* **8**, 1820-3.

Yang L, Huang H, 2014. Roles of small RNAs in plant disease resistance. *J Integr Plant Biol* **56**, 962-70.

Ye W, Ma W, 2016. Filamentous pathogen effectors interfering with small RNA silencing in plant hosts. *Curr Opin Microbiol* **32**, 1-6.

Yoshikawa M, Peragine A, Park MY, Poethig RS, 2005. A pathway for the biogenesis of trans-acting siRNAs in Arabidopsis. *Genes Dev* **19**, 2164-75.

Yu A, Lepere G, Jay F*, et al*., 2013. Dynamics and biological relevance of DNA demethylation in Arabidopsis antibacterial defense. *Proc Natl Acad Sci U S A* **110**, 2389-94.

Zeng Y, Sankala H, Zhang X, Graves PR, 2008. Phosphorylation of Argonaute 2 at serine-387 facilitates its localization to processing bodies. *Biochem J* **413**, 429-36.

Zhang T, Zhao YL, Zhao JH*, et al*., 2016. Cotton plants export microRNAs to inhibit virulence gene expression in a fungal pathogen. *Nat Plants* **2**, 16153.

Zhang X, Zhao H, Gao S, *et al*., 2011. Arabidopsis Argonaute 2 regulates innate immunity via miRNA393(*)-mediated silencing of a Golgi-localized SNARE gene, MEMB12. *Mol Cell* **42**, 356-66.

Zhou HW, Nussbaumer C, Chao Y, Delong A, 2004. Disparate roles for the regulatory A subunit isoforms in Arabidopsis protein phosphatase 2A. *Plant Cell* **16**, 709-22.